PREFACE

We would like to offer the readers the scientific activity report of the Frank Laboratory of Neutron Physics for 2017. The first part of the report presents a brief review of the experimental and theoretical results achieved in the main scientific directions – condensed matter physics, neutron nuclear physics, applied research and development and creation of elements of neutron spectrometers for condensed matter investigations. The second part includes the reports on the operation of the modernized IBR-2 pulsed reactor, the development of the IREN neutron source and researches carried out on EG-5 facility. A list of publications for 2016, the information regarding the seminars and conferences organized in FLNP and a statistical view on the FLNP personnel structure are presented as well.

In 2017 the main achievements of the Laboratory were:

- successful fulfillment of the user program at the IBR-2 spectrometers;
- development of spectrometer complex at the IBR-2 reactor;
- development of IREN facility.

In 2017 the IBR-2 reactor operated for physical experiments for 2471 hours, the IREN facility 1049 hours and EG - 515 hours.

FLNP has cooperation agreements in the field of neutron investigations with almost 200 scientific institutes and universities from more than 40 countries from all over the world. A significant contribution to this cooperation is made by the JINR Member States.

The FLNP staff consists of more than 500 employees in this about 30 % younger than 35 years of age. The scientific staff includes 106 Ph.D. and 24 D.Sc. researchers and more then 100 researchers and specialists from 18 of the JINR Member States (besides the Russian Federation) and associated members.

The organization of annual conferences and schools covering all FLNP research fields helps to recruit young specialists — one of the top priority tasks of the FLNP Directorate.

In 2017 FLNP celebrated its 60th anniversary. Our history is full of outstanding achievements, names of talented scientists, engineers and employees JINR is rightly proud of. The establishment of the Laboratory is connected with such prominent physicists as D.I.Blokhintsev, I.M.Frank, F.L.Shapiro. The constellation of pulsed neutron sources of IBR, IBR-30, IBR-2 developed by FLNP researchers provided JINR with leading positions in the field of neutron research and gave an opportunity to implement a series of contributions that went down to history forever.

V.N. Shvetsov

Director

Members of the Directorate of the Frank Laboratory of Neutron Physics:

SHVETSOV
Valeryi
Nikolaevich
Director
since 2013

Deputy Directors for Science

CULICOV
Otilia
Ana
since 2013

LYCHAGIN
Egor
Valerievich
since 2013

KUČERKA
Norbert
since 2014

KOZENKOV
Sergey
Vyacheslavovich
Deputy Director
for General Issues
since 1989

VINOGRADOV
Alexander
Vital'evich
Chief Engineer
since 2007

CHUDOBA
Dorota
Marta
Scientific secretary
since 2013

SCIENTIFIC HIGHLIGHTS

1. CONDENSED MATTER PHYSICS

The main objectives of research in the framework of the theme involved the application of neutron scattering techniques and complementary methods to investigate the structure, dynamics and microscopic properties of nanosystems and novel materials, which are of great importance for the development of nanotechnologies in the fields of electronics, pharmacology, medicine, chemistry, modern condensed matter physics and interdisciplinary sciences.

The greater part of experimental research was carried out on the spectrometers of the modernized IBR-2 reactor in accordance with the Topical Plan for JINR Research and International Cooperation and FLNP User Program. A number of scientific experiments were performed in neutron and synchrotron centers in Russia and abroad under the existing cooperation agreements and accepted beam time application proposals. Also, the activities on the modernization of the available spectrometers and the development of new instruments were carried out in accordance with the development program plan for the IBR-2 spectrometers.

Within the framework of investigations under the theme the employees of the FLNP Department of Neutron Investigations of Condensed Matter (NICM) maintained broad cooperation with many scientific organizations in Russia and abroad. The cooperation, as a rule, was documented by joint protocols or agreements. In Russia, especially active collaboration was with the thematically-close organizations, such as RRC KI, PNPI, MSU, IMP UB RAS, IC RAS, INR RAS and others.

A list of the main scientific topics studied by the employees of the NICM Department includes:

- Investigation of the structure and properties of novel functional materials;
- Investigation of the structure and properties of materials under extreme conditions;
- Investigation of fundamental regularities of real-time processes in condensed matter;
- Investigation of atomic dynamics of materials for nuclear power engineering;
- Computer simulation of physical and chemical properties of novel crystalline and nanostructured materials;
- Investigation of magnetic properties of layered nanostructures;
- Investigation of structural characteristics of carbon- and silicon-containing nanomaterials;
- Investigation of molecular dynamics of nanomaterials;
- Investigation of magnetic colloidal systems in bulk and at interfaces;
- Structural analysis of polymer nanodispersed materials;
- Investigation of supramolecular structure and functional characteristics of biological materials;
- Investigation of structure and properties of lipid membranes and lipid complexes;
- Investigation of texture and physical properties of Earth's rocks, minerals and engineering materials;
- Non-destructive control of internal stresses in industrial products and engineering materials;
- Introscopy of internal structure and processes in industrial products, rocks and natural heritage objects.

Structure investigations of novel oxide, intermetallic and nanostructured materials

Binary copper oxide CuO is one of the most structurally simple improper multiferroics in which spontaneous ferroelectric polarization arises as a result of symmetry inversion violation by the modulated antiferromagnetic (AFM) ordering formed in the intermediate phase in the temperature range T_{N1} - T_N 213-230 K. Theoretical calculations predicted the existence of such a phase at room temperature at high pressures of 20-40 GPa and the extension of its temperature range up to 0 K. To verify this assumption, the atomic and magnetic structures of CuO were studied by neutron and X-ray diffraction, **Fig. 1-1** [1]. It was revealed that the crystal lattice compressibility of the monoclinic CuO structure exibits an anomalous behavior; it is accompanied first by an increase in the lattice parameter *a* in the pressure range of up to 13 GPa, and then by its decrease (with a subsequent growth in pressure up to 40 GPa) down to the value approximately equal to the value at normal pressure. No anomalies in the behavior of other lattice parameters were observed. The Néel temperature in the pressure range of up to 11 GPa increases up to 250 K. The region of existence of the incommensurate AFM phase with ferroelectric polarization at high pressures was determined using temperature dependences of the monoclinic angle of the crystal lattice for which the anomalies at the points of magnetic transitions, T_N and T_{N1}, are observed (**Fig. 1**). The temperature range of its stability extends under pressure.

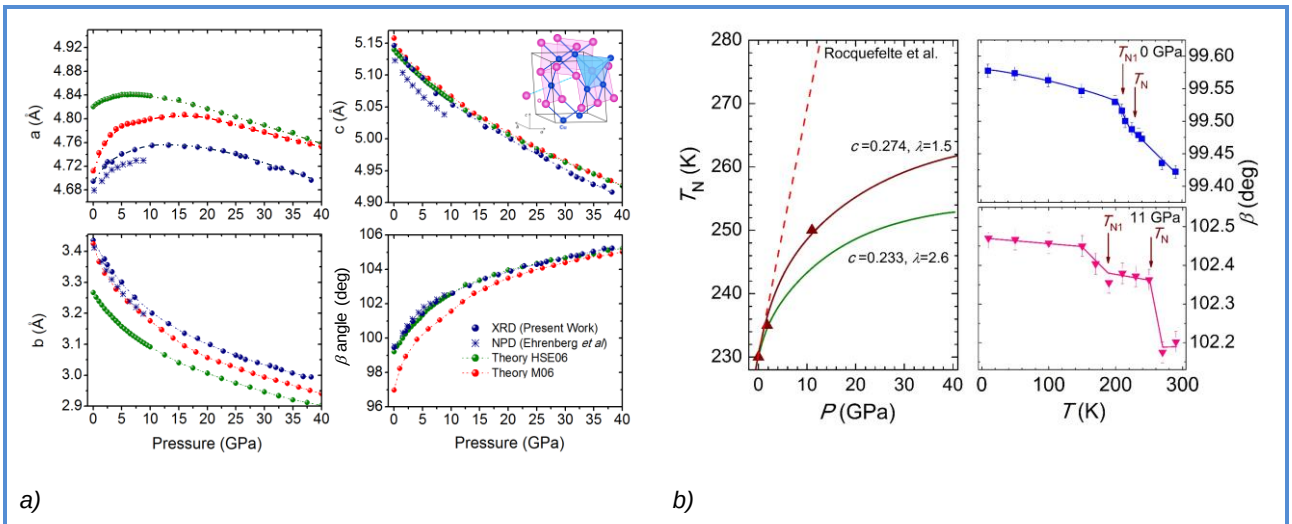

a) *b)*

Fig. 1-1. *Pressure dependences of unit cell parameters of CuO (a). Experimental points, results of theoretical DFT calculations using hybrid functionals HSE06, M06 and results of previous neutron studies are shown. Experimental and calculated pressure dependences of Néel temperature and temperature dependences of monoclinic angle of CuO crystal lattice at a pressure of 0 and 11 GPa (b).*

The estimates based on the experimental data showed that at a pressure range of up to 40 GPa the Néel temperature increases up to about 265 K, which is much below room temperature. To explain the observed anomalies in the structural behavior of CuO under pressure, theoretical first principles calculations were carried out and successfully reproduced the pressure dependences for the structural parameters.

SCIENTIFIC HIGHLIGHTS

Another simple binary oxide, Cr_2O_3 (escoilite), is one of the first known magnetoelectric materials, in which the occurrence of spontaneous ferroelectric polarization under external magnetic fields was found. In the previous high-pressure studies of Cr_2O_3 by second harmonic optical spectroscopy, it was suggested that a magnetic phase transition occurs at P ~ 20 GPa, which can result in the suppression of the magnetoelectric effect. The stability of the initial magnetic structure and the absence of magnetic phase transitions at pressures up to 35 GPa were established in the neutron diffraction studies of Cr_2O_3 [2] performed in the temperature range of 4-300 K at the DN-6 diffractometer, **Fig. 1-2**. At the same time, the Néel temperature (T_N = 307 K at P = 0) rises under compression with the positive pressure coefficient dT_N/dP = 2.8 K/GPa.

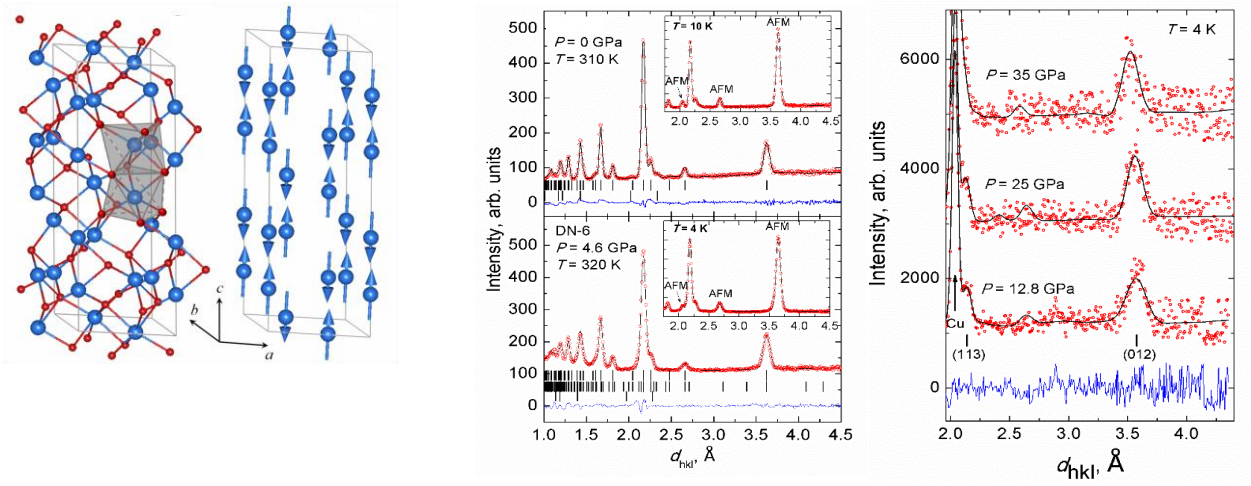

a) *b)*

Fig. 1-2. *Rhombohedral crystal structure with $R\bar{3}c$ symmetry and AFM structure of Cr_2O_3 (a). Neutron diffraction spectra of Cr_2O_3 at various temperatures and pressures in the range of up to 35 GPa refined by the Rietveld method (b).*

An anomalous structural phase separation observed in layered electrode materials of lithium-ion batteries at first charging and disappearing during their subsequent operation, was investigated. The study was carried out for $Li_xNi_{0.8}Co_{0.15}Al_{0.05}O_2$ (NCA) prepared at different calendering levels (high-temperature rolling to reduce electrode bulk density). A specialized electrochemical cell with a new design was used in the neutron experiment. The in operando/in situ studies were performed at the HRFD diffractometer. The presented illustrations (**Fig. 1-3**) clearly show a splitting of the diffraction peak (003) because of the formation of a two-phase state in the cathode material. The analysis of the obtained results revealed [3] that the phase-separation state in NCA in the first electrochemical cycle observed by diffraction is not caused by the properties of atomic and electronic structures of NCA but determined by the peculiarities of the microstructure of material in use.

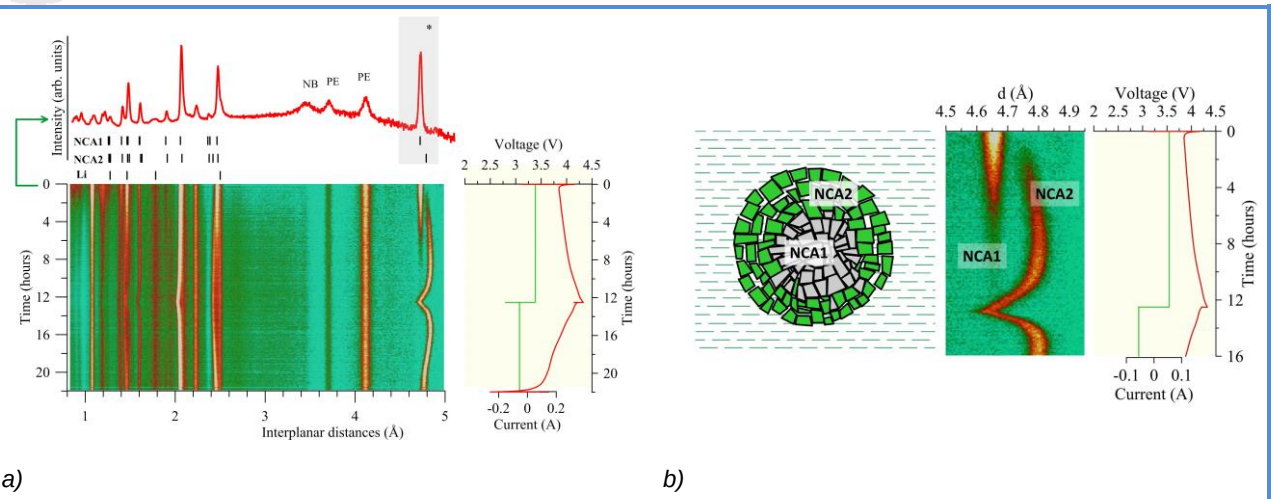

a) *b)*

Fig. 1-3. *(a) Evolution of diffraction peaks from NCA electrode material during electrochemical cycling. Measurements were made with a specialized electrochemical cell. At the top, diffraction spectrum for the initial state of NCA is given. In addition to the peaks from anode and cathode, peaks from boron nitride (NB) and a separator (PE) can be seen. The asterisk denotes the area of peak (003) from NCA, which was used in the analysis of the phase separation, manifesting as a splitting at a certain level of charge. (b) Evolution of peak 003 from NCA material during first charging. Model representation of the process shows a spherical conglomerate of primary NCA particles during electrochemical cycling. The gray area corresponds to the NCA1 phase which does not satisfactory contact with electrolyte. The green-colored particles correspond to the NCA2 phase already in contact with electrolyte (at the left).*

Iron manganese alloys are well known as functional materials exhibiting the shape-memory effect and possessing high internal friction and other interesting physical properties. Despite the fact that the mechanism of the shape-memory effect in these alloys, which is based on the martensitic transformation fcc ↔ hcp ($\gamma \leftrightarrow \varepsilon$), is generally well studied, there remain unanswered questions related to the influence of preliminary heat treatment of the alloy on its microstructure, temperature and kinetics of structural transitions. To clarify these questions, a martensitic transition in two samples with composition Fe-22% Mn-3% Si was studied by neutron diffraction [4]. The two samples were subjected to a different number of heating-cooling cycles, namely the first sample (S1) underwent 1 cycle and the second sample (S12) – 12 cycles. The measurements were carried out at the HRFD diffractometer in two modes (high intensity and high resolution). Diffraction spectra during heating-cooling cycles (rate of temperature change of about 2 K/min) were measured in situ with an exposure time ts = 1 min, which made it possible to analyze the kinetics of structural transitions and accompanying effects. The microstructural parameters were obtained from the diffraction spectra measured with high resolution ($\Delta d/d \approx 0.002$). In both samples, there was a mixture of phases A1 (γ, fcc, sp. gr. Fm3m; $a \approx 3.693$ Å) and A3 (ε, hcp, sp. gr. P63/mmc; $a \approx 2.534$ Å, $c \approx 4.103$ Å) (**Fig. 1-4**). The amount of phase A3 in sample S2 was several times greater than in sample S1, which is evident from the ratio of intensities of peaks (002)A3 and (111)A1. When heating, the structural transition occurred at about 200°C, which can be seen from the behavior of intensities of characteristic diffraction peaks (**Fig. 1-4**). In sample S1, the transition A1 + A3 → A1 was completed at $T \approx 190$°C, whereas in sample S12 it occurred at $T \approx 220$°C. When cooling, the transition A1 → A1 + A3 occurred at $T \approx 120$°C and $T \approx 100$°C for S1 and S12, respectively. These temperatures of the reversible non-diffusion transition $\varepsilon \leftrightarrow \gamma$ are in good agreement with the data

obtained by other methods (DSC and TDIF). The comparison of the phase transition kinetics in the samples under study has shown that the shift in the transition temperature in S1 and S12 (defined as the temperature at which the fraction of phase A3 decreases by a factor of two) is about 34°C. In addition, the transition kinetics in S12 is somewhat slower than in S1.

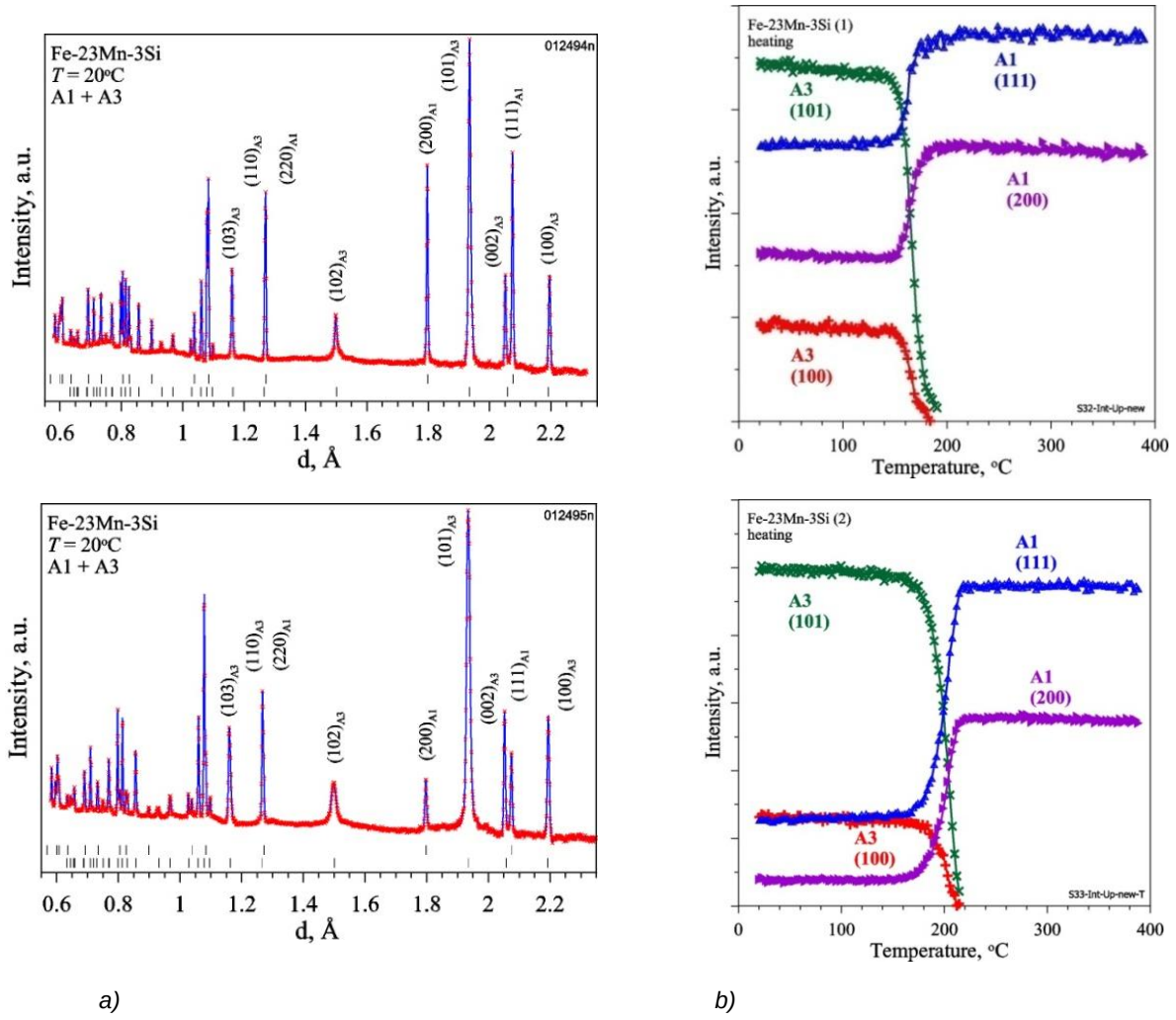

Fig. 1-4. (a) Neutron diffraction spectra of samples S1 (top) and S12 (bottom) in the initial state. All peaks correspond to either phase A1 (Fm3m) or phase A3 (P63/mmc). (b) Temperature dependences for intensities of characteristic diffraction peaks for A1 and A3 phases in samples S1 (top) and S12 (bottom).

Catalytic materials (copper-containing spinel oxides CuB_2O_4 (B = Me^{3+}) were studied. One of the effective methods for regulating physicochemical properties and controlled synthesis of spinels with defined properties is a variation of chemical composition and ratio of components. The structural characteristics of nanodispersed powders of spinels $CuFe_{2-x}Cr_xO_4$ (x = 0 ÷ 2) were determined by neutron diffraction. The interval of Fe/Cr ratio that ensures the existence of cubic and tetragonal spinel modifications was refined. The cation distribution between octa- and tetrahedral positions was estimated. A correlation was found between the distribution of catalytically active Cu^{2+} cations in the

spinel structure and the activation energy of the low-temperature CO vapour conversion reaction. The variation of the chemical nature and ratio of Me^{3+} cations make it possible to regulate the activation energy of the model catalytic reaction of CO vapour conversion, which is an important energy characteristic of copper as a catalytically active component of catalysts.

Investigation of magnetic fluids and nanoparticles

The structural organization of layers of gold nanoparticles deposited from aqueous solutions on silicon substrate and functionalized with a molecular layer of 1.9-nonanedithiol (promising systems for nanoelectronic devices due to their specific optical properties) was studied. For a full description of the system, data of neutron reflectometry, atomic force microscopy, X-ray reflectometry and diffraction were used. On the basis of neutron reflectometry data (GRAINS reflectometer) the structure profile of gold nanoparticle layers was determined and used to estimate the layer thickness and particle packing density (**Fig. 1-5**). The presence of water molecules in the adsorbed layers of gold nanoparticles was established. The obtained results were used in the complex approach, which allowed us to reliably and unambiguously describe the surface packing of nanoparticles [5]. The study was performed in cooperation with the Chuiko Institute of Surface Chemistry NASU, Institute of Physics NASU, Faculty of Physics of Taras Shevchenko National University of Kyiv (Kiev, Ukraine).

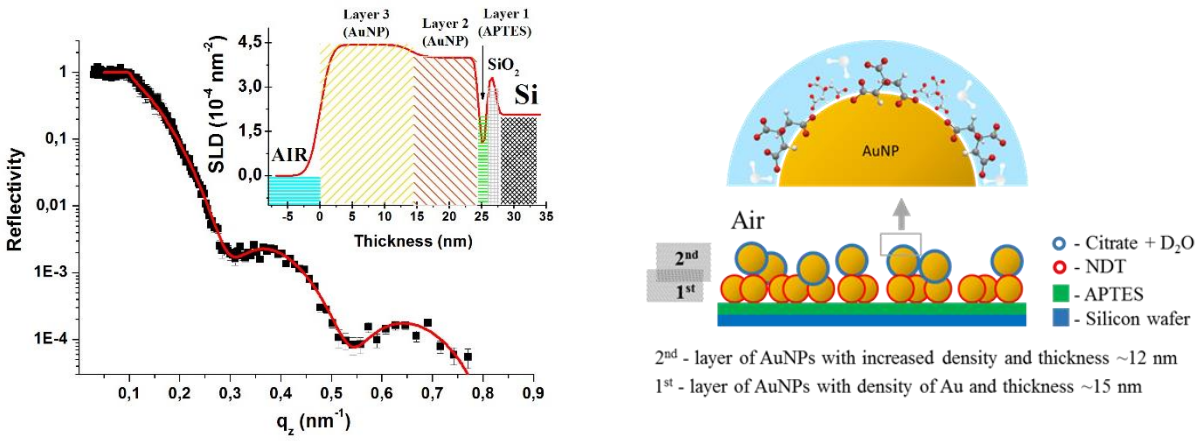

a) *b)*

Fig. 1-5. *Layers of functionalized gold nanoparticles on silicon substrate: neutron reflectometry data with the corresponding SLD profile and a model suggested for structural organization of gold particles on the surface.*

In the framework of the studies of aqueous magnetic fluids for biomedical purposes, combined experiments on small-angle neutron scattering and synchrotron radiation were performed for nanoparticles of various compositions in dry powders and in a liquid carrier [6,7]. The structural peculiarities of the systems with nanoparticles of magnetite, cobalt ferrite, and composite magnetite/cobalt ferrite nanoparticles with a core-shell structure were determined and analyzed. A specific feature of the systems under study is the use of biocompatible surfactants (including polysorbate-80, polyethylene glycol, etc.) in the stabilizing coating of magnetic particles. The

experiments were conducted on the YuMO small-angle scattering spectrometer at the IBR-2 reactor of JINR (Dubna, Russia), as well as on the DIKSI small-angle scattering station at the synchrotron source of the NRC "Kurchatov Institute" (Moscow, Russia). The study was performed in cooperation with the Vernadsky Institute of General and Inorganic Chemistry NASU (Kiev, Ukraine) and the Faculty of Physics of Taras Shevchenko National University of Kyiv (Kiev, Ukraine).

Investigation of carbon nanomaterials

In the framework of research of biological activity of fullerenes, the effects of inhibition and depolymerization of amyloid fibrils (lysozyme, insulin) in aqueous solutions of C60 and C70 fullerenes (synthesized by various methods) were considered [8,9]. The approach combining the analysis of small-angle neutron scattering (YuMO spectrometer), atomic force microscopy and Thioflavin T fluorescence was applied. Thus, out of the two types of solutions under study (solutions prepared by solvent replacement and dilute solutions based on N-methylpyrrolidone (NMP)), C60 and C70 solutions prepared using NMP exhibited a noticeable inhibitory and depolymerizing activity (**Fig. 1-6**). In order to exclude the effect of a moderately toxic NMP solvent on amyloids, additional experiments were performed with a pure solvent containing the same fullerene amount as in the mixtures. The results of these experiments revealed no effect of the solvent on amyloids. Thus, the residual concentration of the primary NMP solvent in aqueous solutions of fullerenes is not the cause of the effects of depolymerization/inhibition of amyloid fibrilization. The analysis of the small-angle scattering data revealed several stages of amyloid depolymerization. The study was performed in cooperation with the Institute of Experimental Physics of the Slovak Academy of Sciences (Košice, Slovakia) and the Faculty of Physics of Taras Shevchenko National University of Kyiv (Kiev, Ukraine).

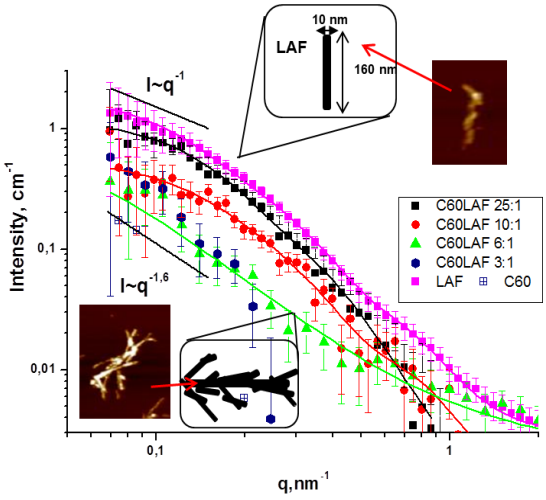

Fig. 1-6. SANS data for mixtures of amyloid fibrils of lysozyme with aqueous fullerene solution NMP/nC60 in different proportions.

In the framework of the study of kinetic effects in fullerene solutions, a method was suggested for calculating the evolution of the size distribution functions of C60 fullerene clusters in polar solvents [10, 11]. This method makes it possible to calculate the distribution function f(r,t) at

an arbitrary point of time for any given system parameters (**Fig. 1-7**). A theoretical description of the critical effect of dilution of polar solutions of C60 fullerene with water was proposed as well. This effect (found experimentally in the solutions of C60 in N-methylpyrrolidone) consists in an abrupt decrease in the fullerene aggregate size when the volume fraction of added water exceeds ~ 40%.

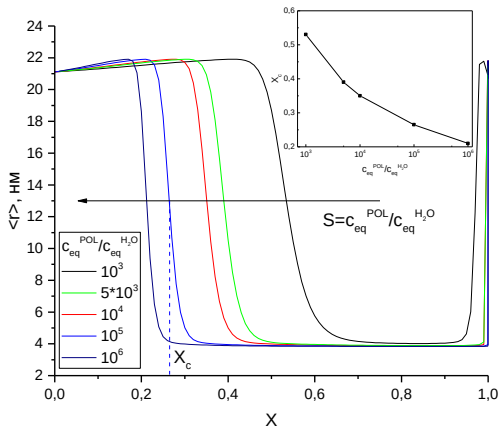

Fig. 1-7. Dependence of the average cluster size in the C60/NMP solution after dilution with water at the time t = 1 on the degree of dilution, X, for different values of the ratio S = c^{POL}/c^{H2O} = 10^3, $5*10^3$, 10^4, 10^5, 10^6 (curves from right to left). The inset shows the dependence of the critical value of the dilution factor, X_c, on S.

The effect was explained using a special dependence of saturation concentration of the system, which takes account of solubilization properties of the solvent with respect to fullerenes: $c_{eq}^{MIX} = c_{eq}^{H_2O} 10^{X\left(\lg c_{eq}^{POL} - \lg c_{eq}^{H_2O}\right)}$, where X is the model parameter characterizing the degree of dilution; $c_{eq}^{H_2O}$ is the equilibrium concentration of complexes in water; and c_{eq}^{POL} is the equilibrium concentration of complexes in a polar solvent.

Investigation of layered nanostructures and electrochemical interfaces

In the framework of structural studies of electrochemical interfaces [12], neutron reflectometry experiments (GRAINS reflectometer) were conducted on model planar systems 'solid electrode-liquid electrolyte' with changing contrast between the electrode and electrolyte [13]. We tested specialized cells that allow experiments with anhydrous electrolytes based on organic solvents, which are actively used today in lithium-ion batteries and supercapacitors. The sensitivity of neutron reflectometry (implemented on a time-of-flight reflectometer at the IBR-2 reactor) to the formation of the solid electrolyte interphase (SEI) on the surface of a thin-film metal electrode in in-operando conditions, was studied (**Fig. 1-8**).

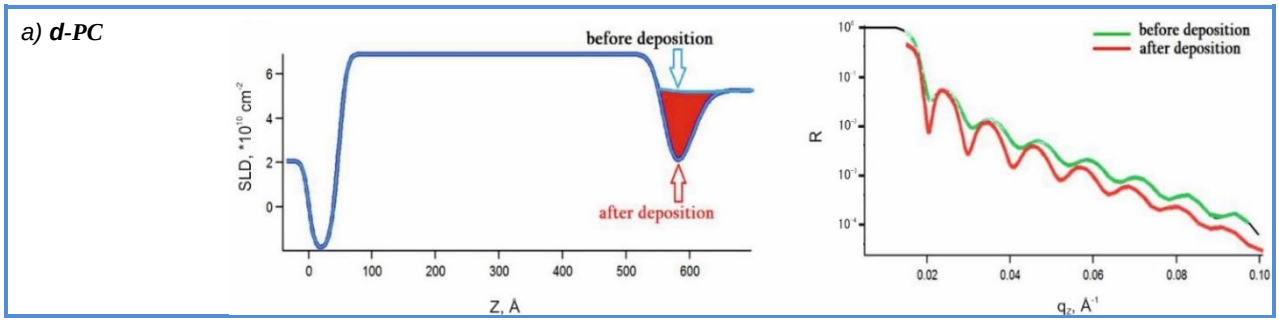

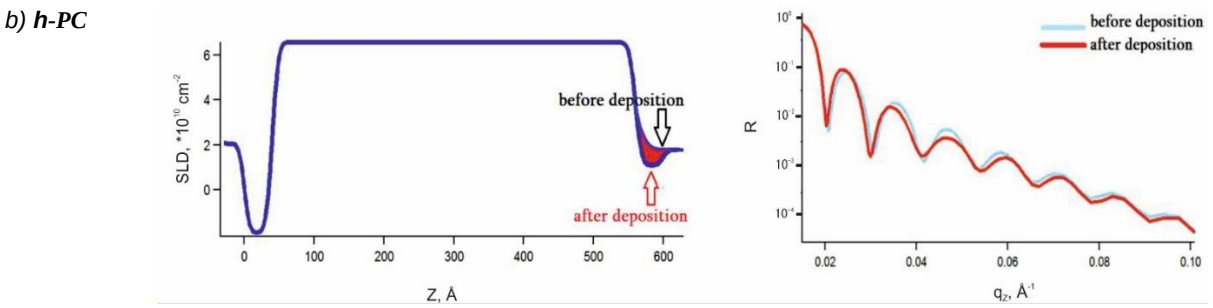

Fig. 1-8. *Effect of the formation of solid electrolyte interphase (SEI) on the reflectivity curves from the interface of a metal electrode (Cu on Si) in contact with a liquid electrolyte (0.1 M $LiClO_4$ solution in propylene carbonate, PC) based on deuterated (a) and protonated (b) solvents. The obtained scattering-length density (SLD) profiles and corresponding reflectivity curves before and after SEI layer formation.*

The study was performed in cooperation with the Faculty of Chemistry, Moscow State University (Moscow, Russia), Dubna University (Dubna, Russia) and Engineering Incubator Ltd. (Dubna, Russia).

The magnetic states of layered ferromagnetic-superconducting nanostructures Nb(70nm)/Ni(65%)Cu(35%)(7nm)/Si were studied by polarized neutron reflectometry. The dependences of the intensity of specularly reflected neutrons from this structure under various conditions are shown in **Fig. 1-9a,b**. The black curve corresponds to the magnetic field of 25 Oe, the red one – to the field of 25 Oe, but the system was pre-magnetized in the field of 500 Oe, the blue one – to the field of 200 Oe. As one can see, the state formed at 9 K is also repeated at 4 K.

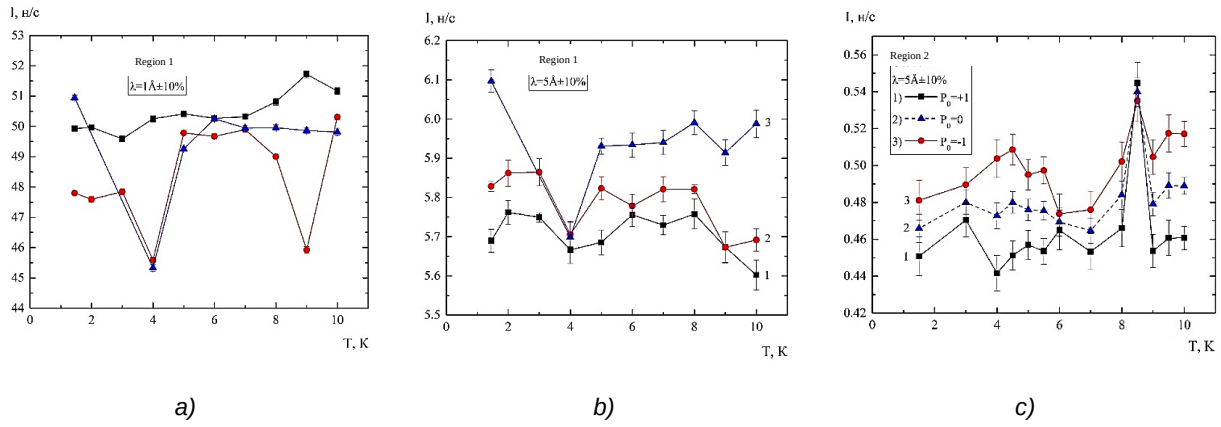

a) *b)* *c)*

Fig. 1-9. *Intensity of specularly reflected beam from nanostructure Nb(70nm)/Ni(65%)Cu(35%)(7nm)/Si at λ = 1 Å (a) and λ = 5 Å (b). Scattering into the region outside the specularly reflected beam (c).*

The analysis shows that the scattering occurs from a domain lattice structure with interplanar spacing in the range of 0.3-2 nm, which can be identified as cryptoferromagnetic. **Figure 1-9c** shows the neutron scattered intensity in the region around the specular beam. The scattering occurs from a lattice of clusters with magnetic moments directed against the magnetic field. The lattice spacing is 3.5 nm. It can be seen that the two types of scattering are correlated. It may be suggested that the crypto-state occures in the space between the clusters, where the external field is compensated by the field scattered from the clusters.

To explain the reversibility of magnetic lattice formation, two models were proposed. In the first model, at T ≈ Tc the structures are formed due to the proximity effect when the superconductor is in contact with the surface layer of a ferromagnet. At T = 4 K the entire ferromagnetic layer becomes superconducting. In the second model, the wave vector of the superconducting pair (proportional to the energy of the exchange interaction of localized magnetic moments with the pair) meets the conditions kf(Tc) df=2π, kf(4K) df=4π. As a result, when the pair passes through the ferromagnetic layer, due to the interference of pair reflections from the boundaries of the ferromagnetic layer, equal conditions for the crypto-state are created.

Investigation of biological nanosystems, lipid membranes and lipid complexes

The supramolecular organization of visual pigment rhodopsin in the photoreceptor membrane was studied by small-angle neutron scattering with contrast variation. Visual pigment rhodopsin is a typical representative of a large family of G-protein-coupled receptors (GPCRs). GPCRs function in the dimeric or oligomeric states in membranes. However, the functional role of the dimeric state of rhodopsin and the whole class A of rhodopsin-like GPCRs has not yet been established. The supramolecular organization of rhodopsin in photoreceptor membranes is currently the subject of contentious debates. For many years, it has been generally accepted that rhodopsin functions in the monomeric state. The standpoint was based on the study of the lateral diffusion of rhodopsin in photoreceptor membranes. At the same time, on the basis of photoreceptor membrane images obtained using atomic force microscopy, it was suggested that rhodopsin molecules in this membrane have a dimeric organization. The investigation of the crystal structure of the deprotonated form of photoactivated rhodopsin also revealed its dimeric state, which led to the conclusion that the rhodopsin dimer is a functional unit. Recently, however, a number of papers have been published that support the original idea of the supramolecular organization of rhodopsin as a monomer in photoreceptor membranes. The samples under study were ‘disk’ membranes with rhodopsin isolated from fragments of rods, as well as rod fragments themselves. On the basis of the results of the experiments on small-angle neutron scattering with contrast variation (YuMO spectrometer, IBR-2) and small-angle X-ray scattering (Rigaku spectrometer, MIPT, Dolgoprudny, Russia and BM-29 BioSAXS facility, ESRF, Grenoble, France), layered structures with the dimensions corresponding to the transverse dimension of the disks were revealed in the rod fragments. It was also shown that rhodopsin is uniformly distributed in the membrane, as in the case of the samples of "disks" isolated from the rod fragments.

Small-angle neutron scattering was used to determine the structural organization of nanodrug doxolip (**Fig. 1-10**). Doxolip (doxorubicin embedded in the lipid bilayer of soybean phospholipids) is a critically small vesicle. The structure of doxolip is stable with respect to its concentration in water (5-25%) and temperature variation (20-37°C).

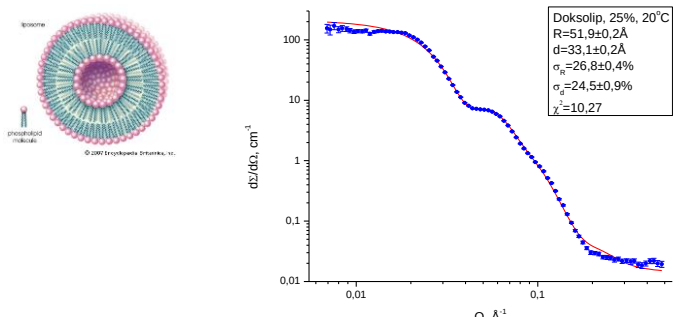

Fig. 1-10. Structural model and small-angle scattering curve of doxolip.

Polymeric materials

Neutron reflectivity curves (GRAINS reflectometer) for thin-film polymer nanocomposites based on polystyrene (or its deuterated analogue) with an addition of C_{60} and C_{70} fullerenes were obtained. Simultaneously with neutron experiments, the samples were studied using atomic force microscopy in cooperation with FLNR JINR (A. Oleinichak). Since the literature data on the organization of fullerene C_{60} in thin polystyrene films are controversal, for the first-time investigations were extended to include systems with fullerene C_{70}. The temperature dependence of reflectivity curves of nanocomposite films with fullerene C_{60} in the vicinity of the glass transition temperature was obtained and analyzed. The approximations of the curves when determining the scattering length density profile from the reflectometry data were compared for the cases with the absence and presence of an oxide layer on the substrate (float glass) (**Fig. 1-11**).

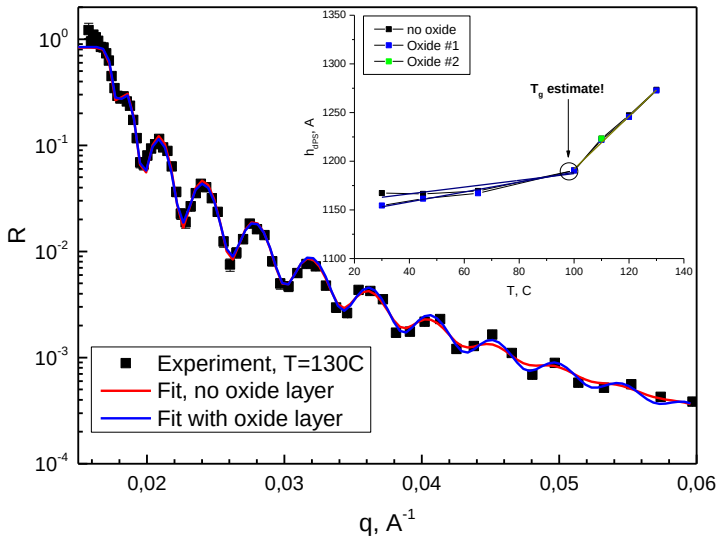

Fig. 1-11. Neutron reflectivity curve from dPS/C60 nanocomposite film at T = 130°C. The inset shows the temperature dependence of film thickness obtained from reflectometry data; the break in the dependence corresponds to the glass transition temperature of the material, T_g.

It was found that the glass transition temperature of composite films depends strongly on the disperse state of fullerene in the initial solution used in the preparation of the nanocomposite. Thus, the formation of fullerene aggregates in this solution shifts the glass transition temperature of the final system by approximately 10°C towards higher values. At present, the possibilities are considered of applying the latest developments in the theory of glass transition of polymers [14, 15] to composites.

In a series of experiments on small-angle neutron scattering performed on YuMO (Dubna, Russia), MAUD (Řež, Czech Republic), KWS-3 (Garching, Germany), the formation of silicate (silicon dioxide) clusters in water-alcohol solutions of tetraethoxysilane (TEOS), $Si(OC_2H_5)_4$, was studied. The cluster formation was initiated by sol-gel polymerization of TEOS under alkaline conditions (pH ~ 10.5). To clarify the structural aspects of two-stage clusterization (first, -SiOH functional groups are generated by hydrolysis of alkoxide groups, then these groups undergo condensation to form a silicate polymer through the formation of Si-O-Si bonds), the contrast variation method was applied with a change in the fraction of the deuterated component in both water and alcohol fractions of the initial solution [16]. Two types of experiments for different molar ratios of H_2O/TEOS in the solution showed (**Fig. 1-12**) that the cluster structure contains neither residual hydroxyl groups nor unhydrolyzed alcohol groups. This result contradicts theoretical models which employ the idea of unhydrolyzed ("poisoned") alcohol groups to explain the dependence of the cluster structure on the H_2O/TEOS ratio. Apparently, there is a large conformational variety of

polymeric structures (formed from hydrolyzed tetraethoxysilane in alkaline solutions) which are sensitive to the hydrolysis rate determined by the amount of water in the solution. The study was performed in collaboration with the Faculty of Physics of Taras Shevchenko National University of Kyiv (Kiev, Ukraine).

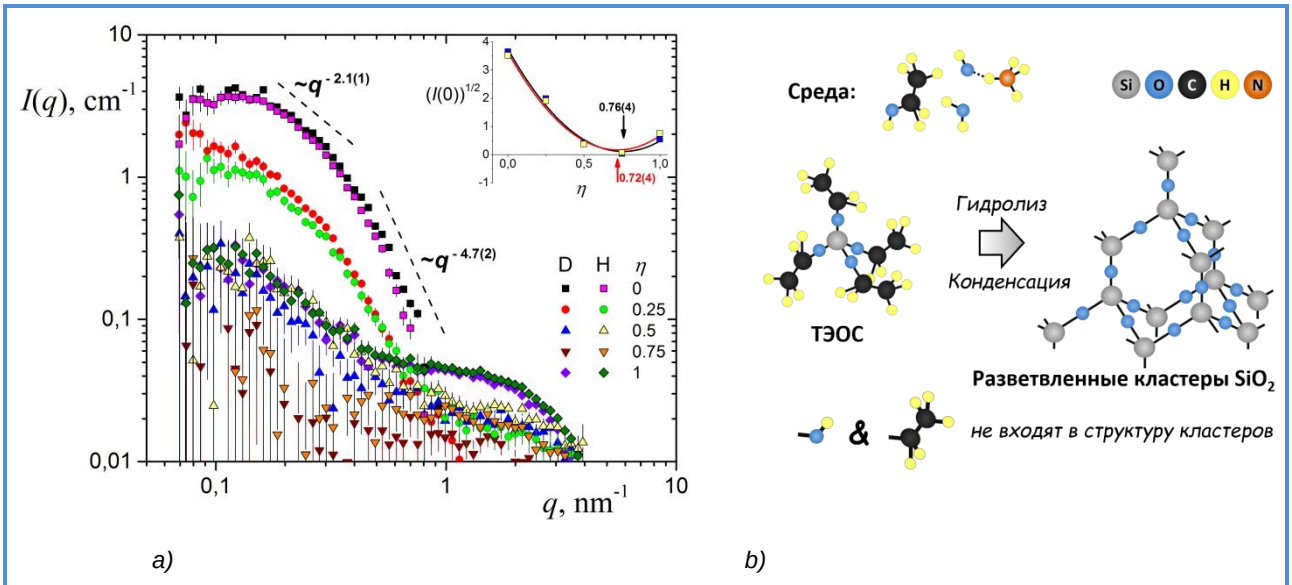

Fig. 1-12. *(a) Contrast variation in the SANS experiments on two (light and heavy water) types of water-alcohol solutions of silicate clusters of hydrolyzed TEOS. The inset shows the experimentally obtained values of forward scattered intensity, $I(0)^{1/2}$, as a function of volume fraction of D-ethanol, η, together with parabolic approximations and corresponding match points. (b) Molecular models of the components of the initial solution and those obtained in the course of hydrolysis/condensation of silicon dioxide clusters.*

In the framework of the studies of mixed solutions of polymers and surfactants, the effect of polymers (polyethylene glycol) on the formation of micellar aggregates of sodium oleate [17] and dodecylbenzenesulfonic acid [18] was considered. This study was aimed at clarifying the equilibrium structural features of aqueous magnetic fluids for biomedical purposes, where one of the surfactants under study (sodium oleate) is used as a stabilizer of magnetic particles, and the polymer is added to enhance the biocompatibility of the system. Small-angle neutron scattering (SANS) was used to determine the structural parameters of micelles in solutions with different surfactant concentrations in the absence and presence of polyethylene glycol. The results of the SANS analysis were complemented by the experiments on the measurement of surface tension to determine the surface properties of mixed solutions. A number of qualitative changes in the behavior of micelle parameters (aggregation number, mean radius, degree of ionization, anisotropy, surface potential) were detected when increasing the surfactant concentration for different surfactant/polymer ratios, which is indicative of the interaction of polymer chains with micelles. The study was performed in collaboration with the Wigner Research Center for Physics of the Hungarian Academy of Sciences (Budapest, Hungary) and the Faculty of Physics of Taras Shevchenko National University of Kyiv (Kiev, Ukraine).

Atomic and molecular dynamics

Organic conjugates of the donor-acceptor type that can be used as synthons of specific molecular configurations in the crystal structure are of current interest in the field of structural design of new functional materials for electronic technologies. The structure and dynamics of molecular complexes of bromoaniline and chloroanilinic acids (BrA and ClA) with picolines (2-MP, 3-MP) were studied, **Fig. 1-13** [19]. From X-ray diffraction experiments on single crystals at T = 100 K, it was found that in the systems under study the synthons of types B:XA:XA:B, :(B:XA:B):XA, and B:XA:B, where XA and B correspond to molecular groups of acids and picolines, respectively, are formed.

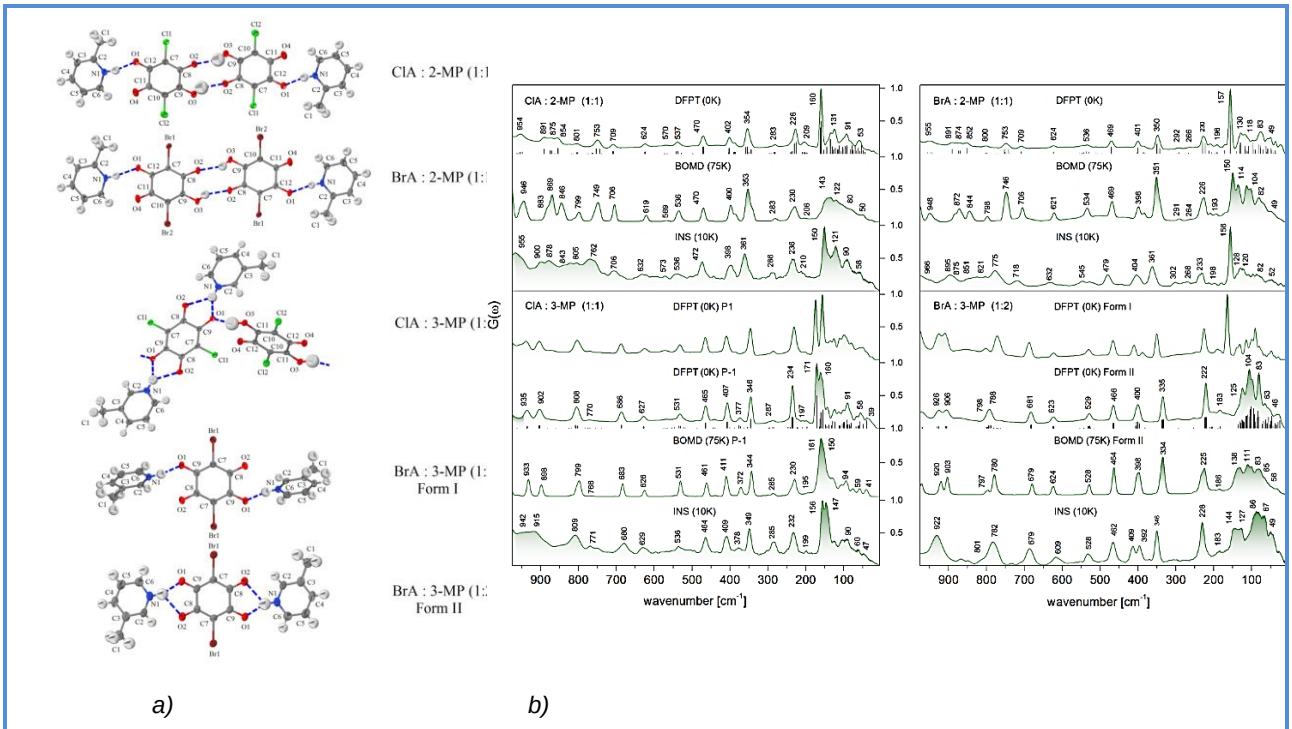

Fig. 1-13. Structure of molecular complexes of bromoaniline and chloroanilinoic acids with picolines according to X-ray diffraction data (a). Experimental spectra of inelastic neutron scattering from complexes under study and results of theoretical DFPT calculations (b).

The structural studies were complemented by investigations of vibrational dynamics of molecular groups by NMR, optical and neutron spectroscopy and other methods. To analyze the experimental data, we performed theoretical calculations within the DFPT approximation. The role of structural aspects, intermolecular forces, proton transfer, dipole interactions in the formation of the observed spectral features was analyzed.

The vibrational dynamics of glass-forming polar alcohols with a single phenyl ring and inclusions of fluorine atoms (2TFMP, 4TFMP and BEP) in glass (obtained from isotropic liquid) and ordered crystalline (obtained by cold crystallization of a metastable supercooled state) states was studied by incoherent inelastic neutron scattering and infrared spectroscopy, **Fig. 1-14** [20]. It was shown that the strength of hydrogen bonds in fluorinated materials is approximately the same. This means that the functional group CF_3 has no profound effect on intermolecular interactions, while

sterical conditions are of importance, especially in the formation of the cluster structure closely related to the changes in the dynamics of fluorinated compounds.

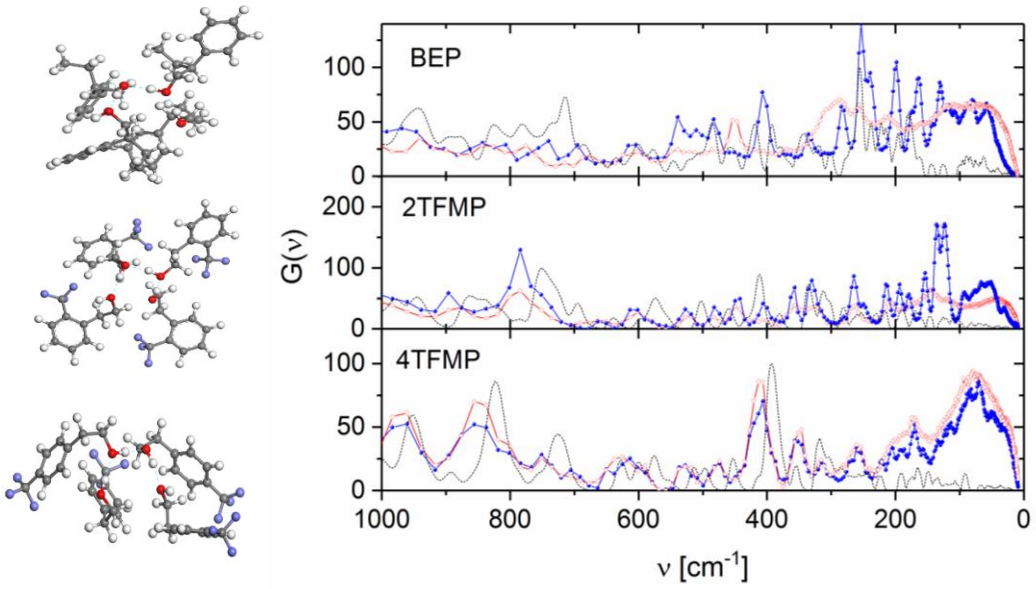

Fig. 1-14. *Structure of molecular groups (left) and generalized vibrational density of states (right) in solid phases of crystalline state (blue) and glass state (red) at T = 5 K for BEP, 2TFMP and 4TFMP. Dashed lines show the results of theoretical calculations for tetrameric clusters.*

Temperature studies of vibrational modes revealed the important role of hydrogen bonds in molecular interactions. In fluorinated compounds, splitting or asymmetry of the OH stretching mode is observed in the low-temperature region, which demonstrates the existence of different configurations of frozen molecular clusters. Theoretical DFT calculations for tetrameric molecular clusters are in good agreement with the experimental data. When comparing the generalized vibrational density of states of the ordered crystalline phase and the glass phase obtained from an isotropic liquid, one can notice some broadening of the vibrational modes associated with the rotational and translational molecular disorder frozen in the glass state (**Fig. 1-14**). The difference in the region below 40 cm^{-1} is indicative of the existence of excitations in the glass phase of localized and anharmonic character, which differ from collective phonon excitations propagating in the crystal with a long-range molecular order. The low-energy barrier for torsional motions of CH3-CH2-CH- and OH-C2-CH functional groups connected to the phenyl ring is also observed in the spectra of inelastic neutron scattering in the region of lattice vibrations. The study was performed by the group from Institute of Nuclear Physics Polish Academy of Sciences (Krakow, Poland).

Applied research

At the FSD diffractometer, studies of mechanical properties and basic microstructure parameters of TRIP-composites with austenite matrix and strengthening phase of partially stabilized zirconium dioxide ZrO_2 were continued (**Fig. 1-15**) in collaboration with the Institute of Metal Forming (Freiberg University of Mining and Technology, Germany). The advantage of these materials is the

ability of both composite components to undergo significant plastic deformations without destruction due to related martensitic transformation mechanisms (TRIP-effect). The purpose of this work was to investigate the effect of plastic deformation on the properties of a new powder composite TRIP-material based on the patented high-alloy austenitic steel and partially stabilized zirconium dioxide ZrO_2. Both structural components have a potential for phase transformation under external stresses. For neutron experiments, a series of TRIP-composites with austenite matrix and strengthening phase of zirconium dioxide ZrO_2 partially stabilized by yttrium oxide (Y-PSZ, series 2) were fabricated by powder metallurgy using hot pressing. In each series, the content of the ceramic phase ZrO_2 was 0, 10, 20, 30, and 100 wt%.

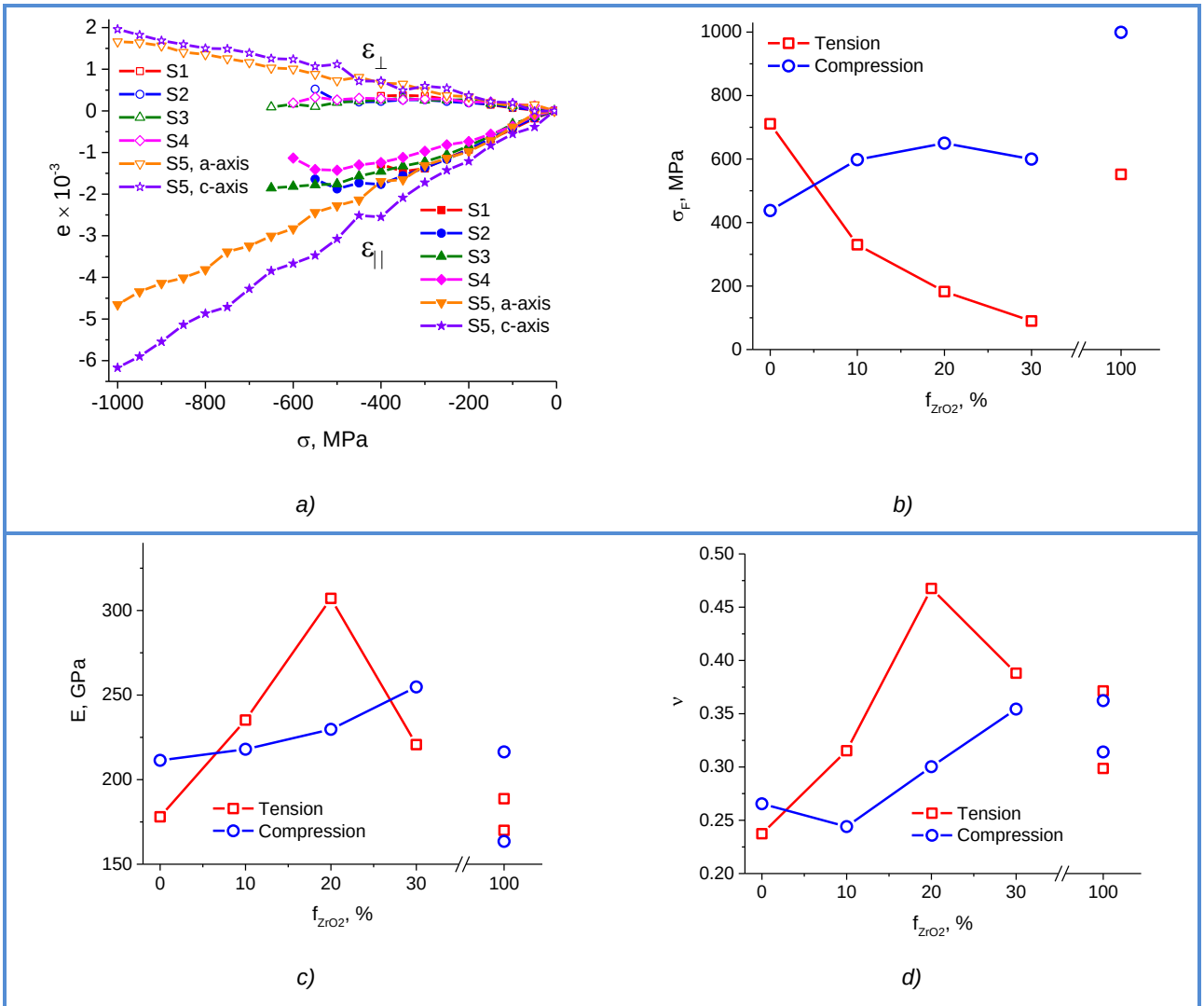

Fig. 1-15. *a) Deformation curves ε(σ) for austenite matrix of samples S1-S4 and sample S5. Ultimate strength of TRIP-composite (b), Young's modulus (c) and Poisson's ratio (d) for austenite phase in the matrix and sample S5 depending on ZrO_2 content.*

The process of formation of martensitic phases in sample S1 began at stresses of 350 MPa and higher, while for samples S2-S4 practically no martensite phases were observed. Apparently, the reason for this behavior is the redistribution of stresses between the phases of austenite and ZrO_2

ceramics, as well as the formation of microcracks along interphase boundaries. Consequently, the stress level in the austenite matrix did not reach the values sufficient for phase transformations. In the ceramic sample S5 from pure zirconium dioxide (100% ZrO_2), there was only one tetragonal phase in the entire stress range (up to 1000 MPa); no phase transformations were observed.

The obtained ultimate strength values of the material depend on the ZrO_2 content. In addition, there is a significant difference in the strength properties of the material under compression and stretching. The Young's moduli and Poisson's coefficients determined in the elastic region from the linear dependences of ε(σ) also depend on the content of zirconium dioxide and, in addition, significantly differ in magnitude for compression and stretching. Apparently, the main factor explaining this behavior of the material is the formation of microcracks along interphase boundaries in the process of deformation. The fracture surface appearance characteristic for brittle fracture counts in favour of this assumption. In addition, it is confirmed by small stress jumps due to microcracking observed in the deformation curves ε(σ). The microcracks are most likely localized on the residual pores of the ceramic phase, which results in further elastic deformation of the composite.

In collaboration with MEPhI, first experiments on physical and mechanical destruction tests of steel X18H10T were conducted. The data of two methods (scanning contact potentiometry and thermal neutron diffraction) were recorded synchronously (**Fig. 1-16**). In the course of the experiment, the sample was subjected to an external uniaxial tensile stress in the range of 100 ÷ 750 MPa *in situ* in a neutron beam using an LM-29 testing machine. At stresses above 400 MPa, the deformation of the material was of a plastic nature and manifested itself in a noticeable broadening of diffraction peaks due to an increase in the dislocation density in the material. In addition, the formation of α'-martensite phase was observed in the austenite matrix in the region of plastic deformations at stress rates higher than 650 MPa. At applied stresses above 700 MPa, the formation of a neck in the right part of the specimen was visually observed, which pointed to the localization of plastic deformation in this region and the termination of plastic deformation in the remaining volume of the sample.

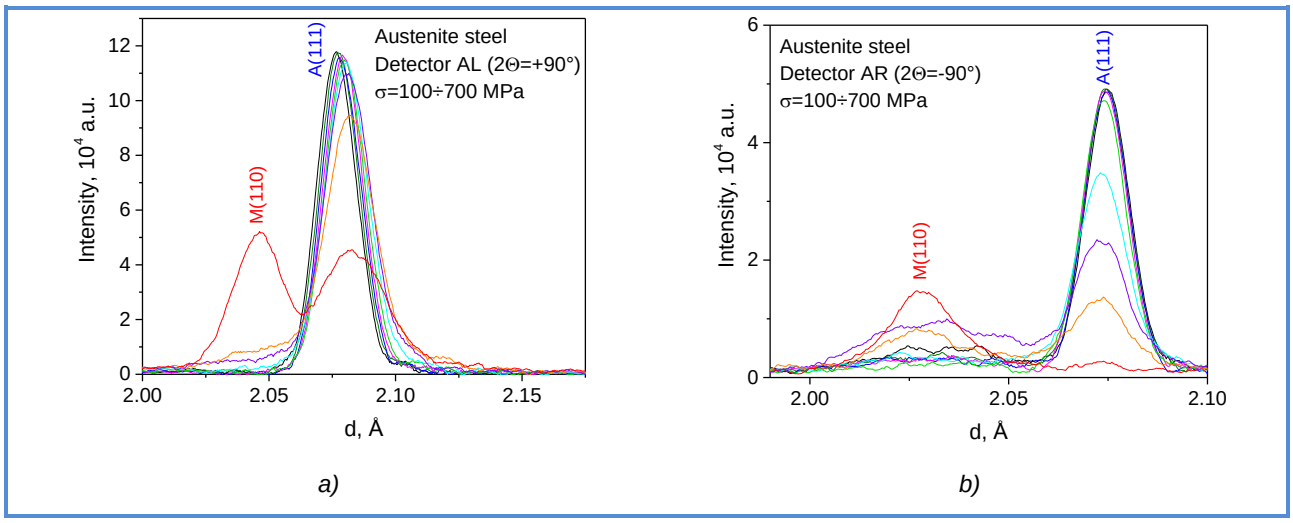

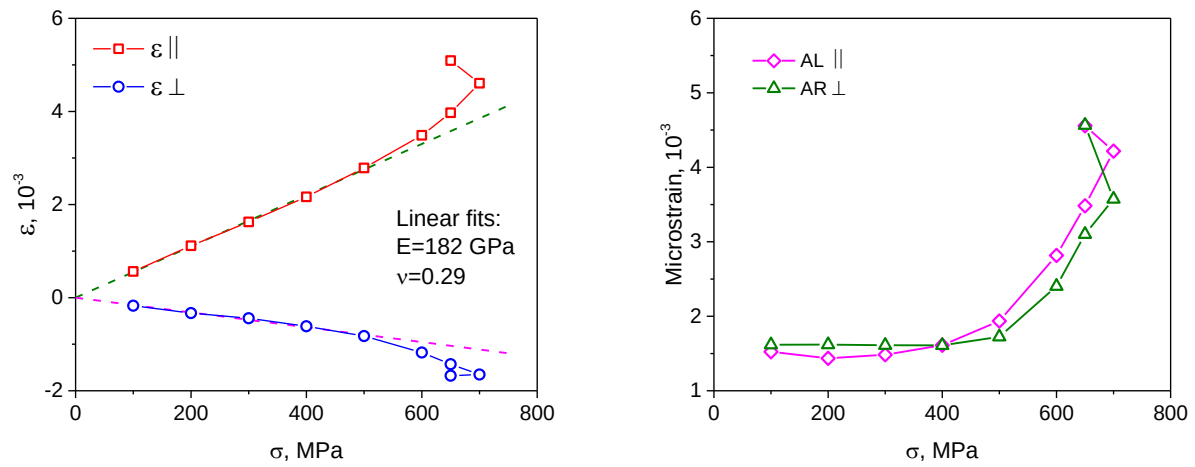

Fig. 1-16. *Evolution of diffraction spectra measured by 90°-detectors AL and AR, in the region of (111) austenite and (110) martensite peaks depending on the applied stress (a,b). Deformations of the crystal lattice for the austenite phase (c). From the linear approximation of the data in the elastic region (up to 400 MPa), estimates were made for the elastic modulus and Poisson's ratio for the austenite phase: E = 182 GPa, v = 0.29. Microdeformation averaged over all (hkl) as a function of the applied stress (d).*

Potentiometric measurements were performed using a desktop device *Spectroelph-FRR*, intended for spectral analysis of electrical signals. To study the deformation activity of the surface and surface strain waves formed during sample stretching, the time-frequency analysis technique was used. Spectrograms were obtained for all stresses, giving the value for the signal energy in the time-frequency neighborhood of the selected point. The preliminary analysis of the maps of surface potentiograms showed that at low stresses a slight increase in the signal intensity in the potentiograms begins at the center of the sample, and at stresses above 300 MPa the intensity grows significantly and becomes localized at the right part of the sample at the neck formation site at the end of mechanical tests. Further analysis of data aims at finding the relation between the crystal lattice deformation and deformation activity of the surface electrical potential, as well as detecting signs of formation and growth of fatigue embryonic cracks.

The metal-matrix composite Al/SiCp (17% SiC) subjected to thermal treatment was studied by neutron diffraction. On the basis of three isolated diffraction peaks from the SiC phase and four peaks from the Al-phase, lattice deformations were determined and compared with those calculated in the framework of the elastoplastic model, which made it possible to find the parameters determining the plastic deformation of the Al matrix (critical permissible shear stress and hardening parameter). Taking into account previous studies, it was shown that after elastic-plastic deformation, the mismatch in both phases decreases during plastic deformation. The approach combining diffraction experiments and self-consistent calculations was used to study the mechanical behavior of grain groups in stainless duplex steel and Al/SiC composites. Particular attention was paid to the role of second-order stresses in the stresses of phase fluidity, as well as the evolution of these stresses during the plastic process. The intercrystalline stresses were determined from lattice deformations measured *in situ* during the tensile tests. Diffraction experiments were performed at a

synchrotron (ID15B, ESRF, Grenoble, France) and neutron TOF-diffractometer (EPSILON, FLNP JINR, Dubna) [21].

The SKAT diffractometer was used to study the texture of quartz rocks from the Adula Nappe region in the Central Alps (Switzerland) which comprises pre-Mesozoic basement and minor Mesozoic sediments that underwent Paleogene eclogite-facies metamorphism. In the north, the Adula Nappe ends with a blade with a complex internal structure containing the Val-Scaradra shear zone with steeply dipping foliation. The texture analysis of the quartz rocks revealed the mechanisms of deformation processes occurring in the shear zone, **Fig. 1-17** [22].

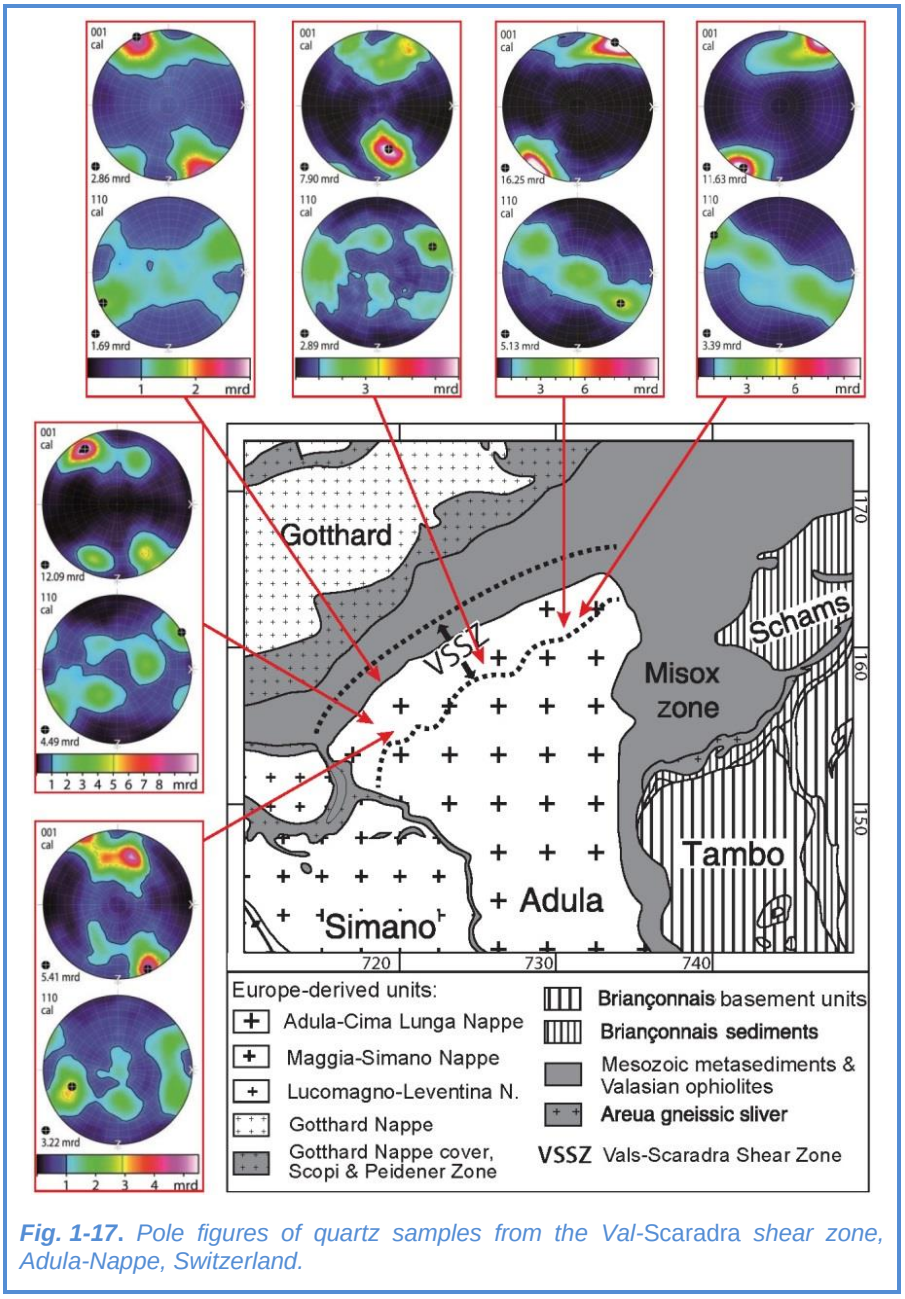

Fig. 1-17. *Pole figures of quartz samples from the Val-Scaradra shear zone, Adula-Nappe, Switzerland.*

Methods for estimating residual austenite and cementite in high-strength steels using neutron diffraction were developed [23]. Measurements of neutron diffraction spectra were performed on the SKAT texture diffractometer at FLNP JINR in order to exclude the influence of texture on the result. Measurements of calibration samples with the known content of austenite and cementite were made. On the basis of these measurements, calibration lines were constructed and used to determine the proportion of residual austenite and cementite in samples of medium-carbon steels (from 0.3 to 0.4%) with yield strength of 1500 MPa and 1700 MPa after treatment with different annealing temperatures (from 150 to 400°C) and quenching. The results agree well with dilatometry data. In addition, the methods for determining residual austenite and cementite were used for a number of other steels.

The texture in samples of concrete intended for radioactive waste utilization in storage facilities was studied. To obtain a better signal-to-background ratio, measurements were made for samples prepared with heavy water. For a sample with sand, 1368 diffraction spectra were obtained and corresponding pole figures (10-11) and (11-20) were plotted on a $5^\circ \times 5^\circ$ grid for the SiO_2 phase. The summed spectra measured with an interval of one year for two samples of different chemical composition were compared. The measurements were carried out under the same conditions. It was revealed that for one of the samples the background drastically increased, which is probably due to the high porosity and absorption of moisture from the surrounding atmosphere. For another sample, this effect was not observed, but in both samples the crystallization processes continue. It is planned to continue these studies for samples of other chemical composition and samples subjected to external stresses.

The crystallographic texture of shells of bivalve mollusks was studied. It was revealed that the texture of the calcite phase is very sharp for the mollusk species of Mytilus galloprovincialis, Mytilus trossulus, Mytilus edulis. The crystallographic texture of bivalve mollusk shells has a different character for different phases (calcite, aragonite). A hypothesis was proposed suggesting that the crystallographic texture for species of the same genus is very similar and different for species belonging to different classes. To confirm this hypothesis, new measurements are planned for shells of bivalve mollusks of other species.

At the spectrometer of neutron radiography and tomography, studies of objects of cultural heritage were continued. Thus, a Viking fibula was studied, for which a 3D model of the internal structure based on tomographic data was reconstructed (**Fig. 1-18**).

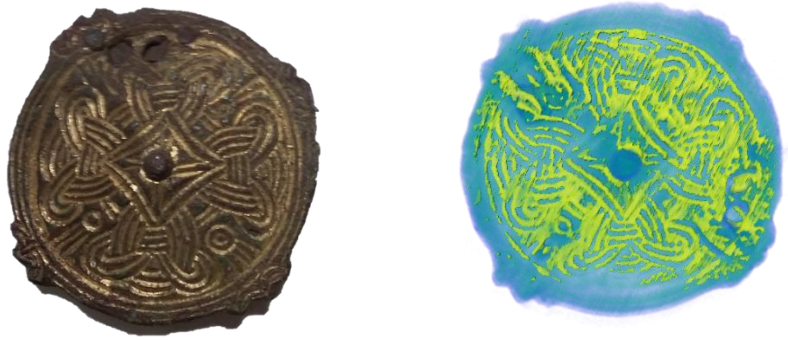

Fig. 1-18. *Photo (left) and tomographic 3D model of Viking fibula (right).*

The obtained results will allow us to analyze the features of ancient technologies for manufacturing similar objects in Scandinavia.

References

[1] D.P.Kozlenko, K.Drużbicki, S.E.Kichanov, E.V.Lukin, H.-P.Liermann, K.V.Glazyrin, and B.N. Savenko “Anomalous lattice compression and magnetic ordering in CuO at high pressures: a structural study and first principles calculations”, Phys. Rev. B, v. 95, p. 054115 (2017).
[2] N.O.Golosova, D.P.Kozlenko, S.E.Kichanov, E.V.Lukin, H.-P.Liermann, K.V. Glazyrin, and B. N. Savenko, “Structural and magnetic properties of Cr_2O_3 at high pressure”, Journal of Alloys and Compounds, v. 722, pp. 593 – 598 (2017).
[3] I.A. Bobrikov, N.Yu. Samoylova, O.Yu. Ivanshina, S.V. Sumnikov, R.N. Vasin, E.A. Korneeva and A.M. Balagurov “Abnormal phase-separated state of $Li_xNi_{0.8}Co_{0.15}Al_{0.05}O_2$ in the first charge: effect of electrode compaction”, submitted to Electrochimica Acta (2017).
[4] A.M. Balagurov, I.A. Bobrikov, J. Pons, J. Cifre, L.Y. Sun, I.S. Golovin “Structure of the Fe-Mn-Si alloys submitted to γ ↔ ε thermocycling”, submitted to Matt. Charact (2017).
[5] Snegir S.V., O.P. Artykulnyi, V.I. Petrenko, M. Krumova, V.Ye. Kutsenko, M.V. Avdeev, L.A. Bulavin, On the structure of assemblies of coated Au nanoparticles on silicon substrate. Applied Nanosciences (2017), submitted.
[6] Nagornyi A.V., Avdeev M.V., Elenich A.V., Solopan S.A., Belous A.G., Shulenina A.V., Turchenko V.A., Solviev D.V., Bulavin L.A., Aksenov V.L., Structural features of composite magnetic nanoparticles $Fe_3O_4/CoFe_2O_4$ by scattering of X-rays and neutrons, Cryst. Rep. (2017), accepted.
[7] Veligzhanin A.A., D.I. Frey, A.V. Shulenina, A.Yu. Gruzinov, Ya.V. Zubavichus, M.V. Avdeev, Characterization of aggregate state of polydisperse ferrofluids: some aspects of anisotropy analysis of 2D SAXS in magnetic field, J. Magn. Magn. Mater. (2017) in press.
[8] Lynchak O.V., Yu I. Prylutskyy, V. K. Rybalchenko, O. A. Kyzyma, D. Soloviov, V. V. Kostjukov, M. P. Evstigneev, U. Ritter and P. Scharff. Comparative Analysis of the Antineoplastic Activity of C60 Fullerene with 5-Fluorouracil and Pyrrole Derivative In Vivo. Nanoscale Research Letters, 2017, 12:8.
[9] Prylutskyy Yu.I., I.V. Vereshchaka, A.V. Maznychenko, N.V. Bulgakova, O.O. Gonchar, O.A. Kyzyma, U. Ritter, P. Scharff, D.M. Nozdrenko, I.V. Mischenko. C60 fullerene as promising therapeutic agent for correcting and preventing skeletal muscle fatigue. J. Nanobiotechnol., 2017, 15:8.
[10] Tropin T.V., Avdeev M.V., Aksenov V.L., Modelling of evolution of cluster size distribution functions in polar solutions of fullerene C60, Cryst. Rep. (2017), in press.
[11] Tropin T.V., Aksenov V.L., Theoretical studies of the effect of dilution of fullreren polar solutions by water, JETP Letters (2017), submitted.
[12] Avdeev M. V., Bobrikov I.A., Petrenko V.I., Characterization of Battery Materials: Neutron Methods, In Electrochemical Storage Materials – From Crystallography to Manufacturing Technology, Eds. D.C. Meyer, T. Leisegang, H. Stöcker, De Gruyter: 2017, in press.
[13] Petrenko V.I., I.V. Gapon, A.A. Rulev, E.E. Ushakova, E.Yu. Kataev, L.V. Yashina, D.M. Itkis, M.V. Avdeev, Studies of electrochemical interfaces by TOF neutron reflectometry at the IBR-2 reactor, Journal of Physics: Conf. Series. (2017) accepted.
[14] Tropin T.V., Schmelzer, V.L. Aksenov. On the possibility of modeling of kinetics of glass transition of polymers in a wide range of cooling and heating rates. Journal of Molecular Liquids, 2017, V. 235, pp. 172-177.
[15] Aksenov V.L., Tropin T.V., Schmelzer J.W.P., Kinetic equations for describing glass-liquid transitions in polymers, Theor. Math. Phys. (2017), accepted.
[16] Tomchuk O.V., Avdeev M.V., Bulavin L.A., Ryukhtin V.V., Ivankov O.I., Aksenov V.L., Nagornyi A.V. Study of tetraethoxysilane clusters in basic ethanol/water solutions by SANS contrast variation. Romanian Reports in Physics (2017), accepted.
[17] Artikulnyi A.P., Petrenko V.I., Bulavin L.A., Almasy L., Grigoryeva N.A., Avdeev M.V., Aksenov V.L., Effect of polyethylene glycol on the structure of micelle solutions of sodium oleate in water by small-angle neutron scattering, Cryst. Rep. (2017), accepted.
[18] Artikulnyi A.P., Petrenko V.I., Bulavin L.A., Ivankov O.I., Avdeev M.V., Impact of poly (ethylene glycol) on the structure and interaction parameters of aqueous micellar solutions of anionic surfactant. Romanian Reports in Physics (2017), accepted.
[19] Łuczynska, K.; Drużbicki, K.; Lyczko, K.; Dobrowolski, J.Cz. Structure-Spectra Correlations in Anilate Complexes with Picolines, Crystal Growth & Design, 16 (2016) 6069−6083.
[20] Juszyńska-Gałązka E., Zając W., Saito K, Yamamura Y., and Juruś N, Vibrational Dynamics of Glass Forming: 2-Phenylbutan-1-ol (BEP), 2-(Trifluoromethyl)phenethyl Alcohol (2TFMP) and 4-(Trifluoromethyl)phenethyl Alcohol (4TFMP) in their thermodynamic phases, Phase Trans., in press (2017), https://doi.org/10.1080/01411594.2017.1393813.
[21] Gadalinska, E., Baczmanski, A., Wronski, S., Wróbel, M., Wierzbanowski, K., Lodini, A., Klosek, V., Buslaps, T. & Scheffzuek, Ch.: Neutron and Synchrotron diffraction study of elastoplastic behaviour of Al/SiCp metal matrix composite. Materials Science Forum 905, 66-73 (2017).
[22] Kossak-Glowczewski, J., Froitzheim, N., Nagel, T.J., Pleuger, J., Keppler, R., Leiss, B. & Regent, V., Along-strike shear-sense reversal in the Vals-Scaradra Shear Zone at the front of the Adula Nappe (Central Alps, Switzerland). Swiss J. Geosci. 110 (2), 677-697 (2017).
[23] Lychagina, T., Zisman, A., Yashina, E. & Nikolayev, D. Directly verifiable neutron diffraction technique to determine retained austenite in steel. Adv. Eng. Mater. 1700559 (2017) (doi: 10.1002/adem.201700559).

2. MULTIMODAL PLATFORM FOR RAMAN AND NONLINEAR OPTICAL MICROSCOPY AND MICROSPECTROSCOPY FOR CONDENSED MATTER STUDIES

Activities in 2017 were implemented in accordance with the research programme and main tasks listed within the theme “A multimodal platform for Raman and nonlinear optical microscopy and microspectroscopy for condensed matter studies” included in the JINR Topical Plan 2017.

First of all, it should be noted that the work on the modernization of the optical platform conducted in 2016-2017 has made it possible to bring this instrument to the number of modern and unique Raman microspectrometers, which have no analogues in terms of their functional characteristics and capabilities in Russia and CIS countries today. The "CARS" microspectrometer is also quite competitive at the world level in the class of analytical instruments.

The studies in 2017 were focused on achieving the following major results:

1. First preliminary results on surface-enhanced micro-CARS from gold nanoparticle-immobilized organic molecules.
2. Assessment of the concentration detection limit of phospholipid molecules by SERS.
3. Investigation of SERS-signal intensity dependence on the shape of silver nanostructures grown in the porous SiO_2 template.
4. A complex study of structural and spectral properties, including upconversion luminescence, of oxyfluoride glasses and glass-ceramics doped with rare earth elements (REE).
5. Verification of tumor and stem cells by Raman microspectroscopy.

In addition, methodological studies aimed at further upgrading and modification of the CARS microscope were carried out during the period under review.

Surface-enhanced micro-CARS

Surface-enhanced Raman scattering (SERS) was investigated in 2017 for a new active substrate where gold nanoparticles were spread over a cerium dioxide (CeO_2) faceted dielectric film deposited on the aluminum layer. Molecules of thionitrobenzoic acid (TNB) were used as a reporter molecule since they are of interest for biochemical and immunological analysis.

The aim of the present work was the experimental study of SECARS generated by biochemically-relevant TNB and mercaptophenylboronic acid (MPBA) molecules attached to Au nanoparticles. The nanoparticles were immobilized in turn on the surface of the SERS-active metamaterial under study. The micro-imaging of the SECARS intensity at the characteristic Raman frequencies of TNB (1338 and 1558 cm^{-1}) and MPBA (1072 and 1571 cm^{-1}) was obtained by the picosecond excitation in the NIR spectral range. We investigated the resonant and non-resonant SECARS signals and determined the imaging contrast. Moreover, we thus obtained SECARS, SERS, and optical images of the investigated area of the metamaterial sample.

Epi-SECARS images were recorded using the laser scanning confocal CARS micro-spectrometer with high spatial resolution and high laser spot scanning rate (**Fig. 2-1**). The system is based on an Nd^{3+}:YVO_4 diode-pumped picosecond passively mode-locked laser (λ_s = 1064 nm, 7 ps,

85 MHz, 5 W) and a Lyot-filter- and temperature-tuned LBO crystal optical parametric oscillator which is synchronously pumped by 2 W at 532 nm (λ_p = 690-990 nm, 6 ps, 150-350 mW).

The line width of tunable pump radiation is ~5-7 cm^{-1}. Spatially- and temporally-overlapped collinear pump and Stokes beams of parallel polarizations are focused on the sample to a 1-2 μm diameter spot. Scanning of the laser spot across the surface areas up to 225x225 μm with a spatial resolution up to 1000x1000 pixels while detecting the CARS signal at a given Raman frequency is performed using a galvo-driven mirror system. Spectrally-filtered anti-Stokes radiation is detected using a photomultiplier (PMT) or a CCD. All measurements were performed at room temperature in ambient air.

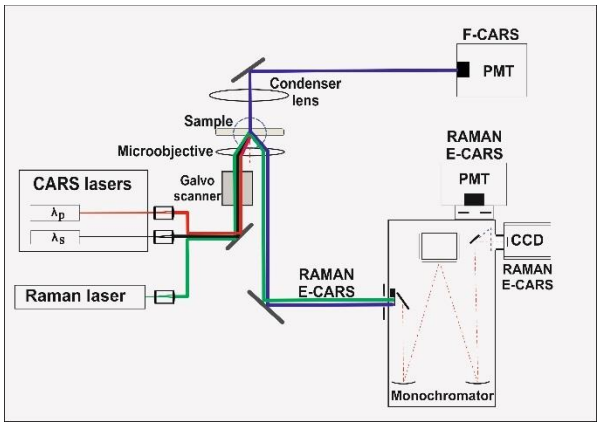

Fig. 2-1. *Schematic of the scanning confocal laser micro-CARS spectrometer.*

Au nanoparticles with the average diameter of 56 nm and covered with a monolayer of reporter molecules were spread over a faceted CeO_2 film after a monolayer of polycation (PDDA) had been deposited on the surface. The fraction of the CeO_2 surface occupied by islands of Au nanoparticles is evaluated to be ~ 5%. Epi-SECARS images at the Raman shifts of 1344 cm^{-1} (TNB) and 1571 cm^{-1} (MPBA) of CeO_2 film surface, with the dimensions of ~ 25x25 μm, supported by optical and scanning electron microscope images (**Fig. 2-2**), were obtained.

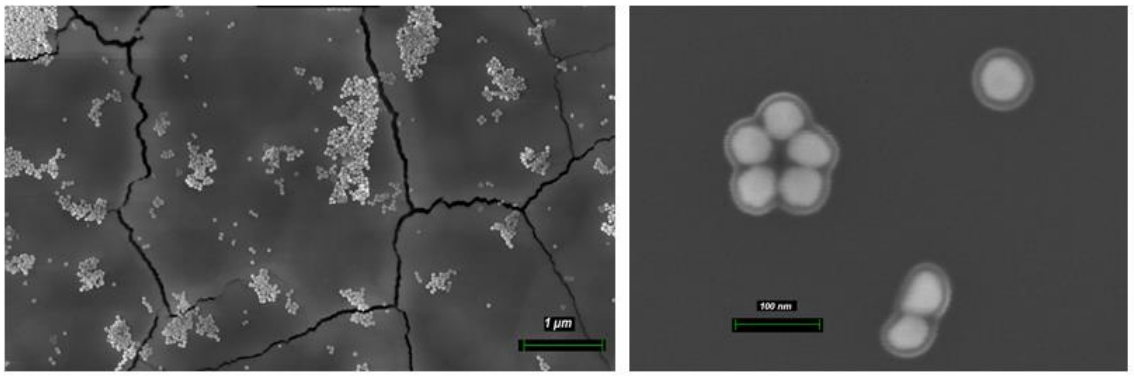

a) *b)*

Fig. 2-2. *SEM images of $CeO_2/Al/Al_2O_3$ sample surface with TNB-modified Au-NPs: a) ~ 7.5 μm×4.5 μm and b) ~ 0.6 μm×0.4 μm surface areas.*

The highest SECARS resonant signal levels in the bright spots reach ~ 1.5 $x10^4$ bits of a 16-bit ADC, while the nonresonant background level is almost equal to zero for our 30 s image

acquisition time (**Fig. 2-3**). Special attention was paid to a possible active area optical damage under focused laser beams.

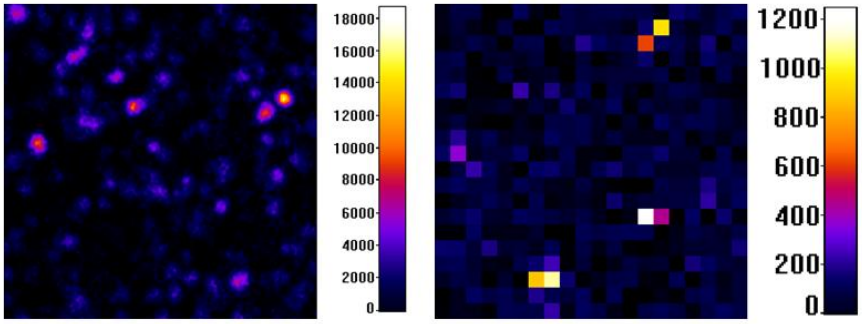

a) *b)*

Fig. 2-3. *SECARS Raman micro-images of a sample surface area with deposition of modified NPs: a) with TNB/Au-NP conjugates, b) with MPBA/Au-NP conjugates.*

The excellent chemical imaging contrast obtained is an indication of high detectability of reporter molecules by SECARS in the metamaterial under study. Further research will be focused on the study of the imaging contrast dependence on the CeO_2 film thickness, estimation of SECARS signal sensitivity to the probed reporter molecules, and the comparison of their detectability by using SECARS and SERS at the surface of the metamaterial under investigation.

Detection limit of DPPC phospholipid by SERS

The detection limit is the smallest amount of analyte concentration in the sample that can be reliably distinguished from zero. Following this rule the lowest concentration of analytes at which they are detectible was estimated when their least intensive Raman peak becomes unresolved at the background level.

Phospholipids are ubiquitous in nature forming a bilayer of cell membranes of all living tissues. They are responsible for elastic properties of membranes, stabilization of proteins within the membrane and transportation of lipids and fatty acids. Determination of their type, concentration and ratio in physiological liquids helps to recognize pulmonary, hepatic, sclerotic and many other diseases. Thus, sensitivity of the detection technique plays an important role in early diagnostics. However, their practical application is limited by a complicated sample preparation, necessity to use specific markers and difficulties in the interpretation of the results obtained.

Silver particles, predominantly with the size of 40–80 nm, were deposited onto porous silicon by immersion plating to form substrates appropriate for the detection of organic molecules by surface-enhanced Raman scattering technique. These substrates have demonstrated for the first time the possibility of detecting phospholipid molecules represented by dipalmitoylphosphatidylcholine at concentrations as low as 10^{-12} M.

Reference Raman and SERS spectra corresponding to DPPC molecules are presented in **Fig. 2-4**. The Raman spectrum was recorded for the solution containing 10^{-2} M of DPPC deposited onto SERS-inactive substrate. Three upper curves in **Fig. 2-4** represent SERS signals from dried solutions containing DPPC in concentrations between 10^{-6} and 10^{-12} M. The laser wavelength was 633 nm. Positions of the SERS peaks clearly correlate with the reference Raman peaks while some small deviations are observed. One more feature of the SERS spectra at low concentrations is their weak reproducibility in the 1527–1570 cm^{-1} wavenumber range associated with COO-C stretching. The lowest concentration at which DPPC was detected is estimated to be 10^{-12} M.

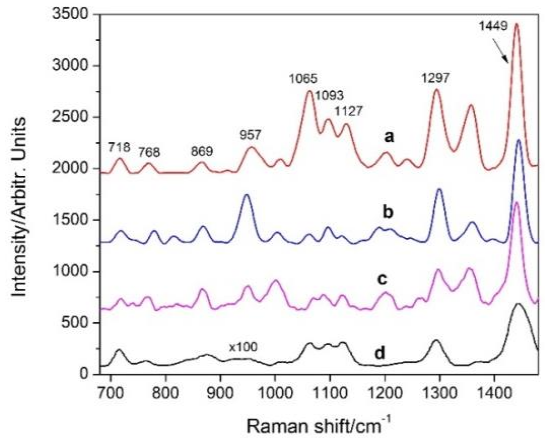

Fig. 2-4. *(a, b, c) SERS and (d) Raman spectra of (a) 10^{-6} M, (b) 10^{-9} M, (c) 10^{-12} M and (d) 10^{-2} M DPPC collected at the at the 633 nm wavelength.*

The detection of phospholipids at their concentration in a solution of about 10^{-12} M has been experimentally demonstrated for the first time using dipalmitoylphosphatidylcholine (DPPC) as an example. We believe that the detection limit demonstrated in this study for silvered porous silicon SERS substrates can be further improved by optimizing the technological process.

Dependence of SERS signal intensity on the shape of silver nanostructures

The aim of this study was to determine the relationship between the signal of SERS and the shape of silver nanoparticles under the influence of laser radiation with different power.

Plasmonic nanostructures were synthesized in silicon dioxide pores on a single-crystal silicon *n*-type substrate. The pores were formed using ion-track technology and selective chemical etching. Silver deposition was carried out by galvanic displacement method. Synthesis time was chosen as a parameter that allows controlling the shape of a silver deposit in the pores of silicon dioxide on the surface of single-crystal *n*-silicon during electrodeless deposition. Deposition time directly affects the shape of metal nanostructures.

The analysis of the dynamics of changes in the morphology of the metal deposit showed that as the deposition time increases, the metal evolves from individual metallic crystallites within the pores at a short deposition time into dendrite-like nanostructures at a long deposition time (**Fig. 2-5**).

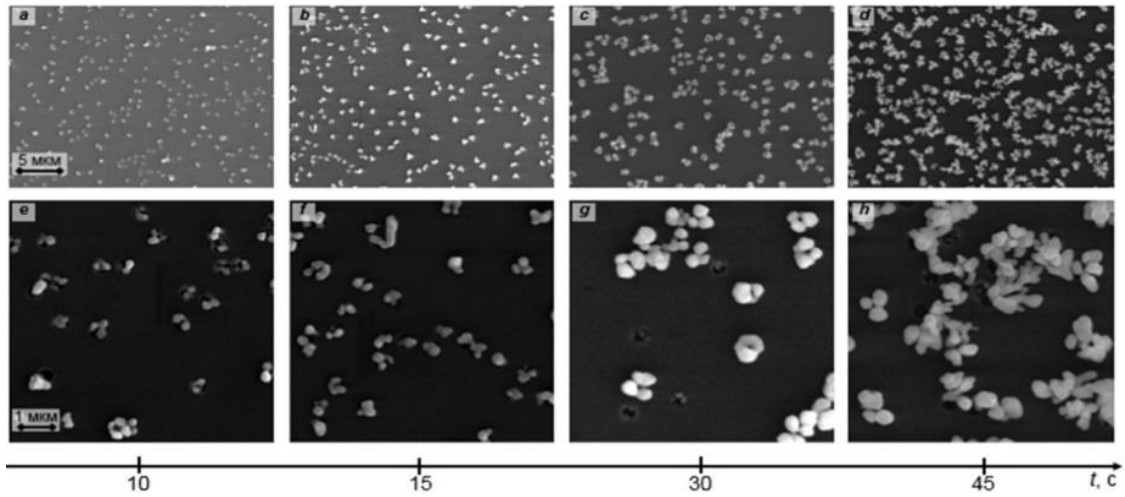

Fig. 2-5. *The growth dynamics of silver nanostructures in SiO_2 pores on n-type silicon substrate at deposition times: 5 s (a,e), 15 s (b,f), 30 s (c,g), and 60 s (d,h) (the same scale for each line).*

The dependence of the intensity of SERS spectra on the shape of the silver deposit was studied at a power of green laser (532 nm) from 2.5 μW to 150 μW using the model dye analyte Rhodamine 6G (**Fig. 2-6**). The optimum shape of the silver deposit and laser power was analyzed from the viewpoint of further design of active surfaces for SERS with nondestructive control of small concentrations of substances.

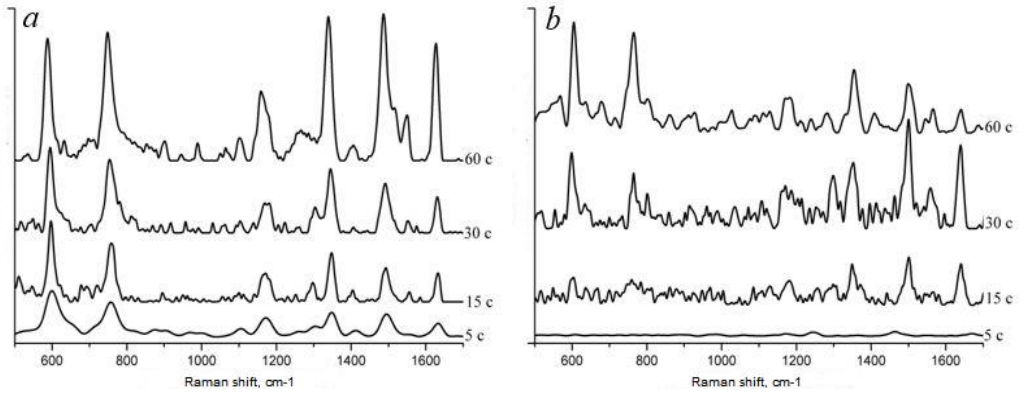

Fig. 2-6. *SERS spectra of Rhodamine 6G with a concentration of 10^{-6} M measured on silver NS grown in pores of SiO_2 on a silicon n-type substrate at a deposition time of 5 s, 15 s, 30 s and 60 s. a) spectra obtained at a laser power of 150 μW; b) at a power of 2.5 μW.*

Thus, a study was made of the efficiency of the use of SiO_2(Ag)/*n*-Si structures as SERS-active surfaces at different laser powers. It has been found that at an excitation power of 150 μW the analyte is gradually destroyed. Reduction of the laser power to 2.5 μW eliminates this problem.

A complex study of structural and upconversion luminescence (UCL) properties of oxyfluoride glasses and glass-ceramics (GC) doped with rare earth elements (REE)

In 2017 we completed our studies related to the structural properties and characteristics of UCL of oxyfluoride glasses and oxyfluoride glass-ceramics doped with REE. These optical matrices combine the advantages of low-phonon energy of fluorides, chemical durability and mechanical stability of oxides, as well as high optical quality of silicate glasses. We used the possibility of recording the response of the medium to the IR laser excitation in the anti-Stokes region of the spectrum for UCL studies.

In this study transparent oxyfluoride germanosilicate glass-ceramics containing Er:PbF_2 nanocrystals is synthesized on the basis of SiO_2–GeO_2–PbO–PbF_2 initial glass doped with Er_2O_3. For the preparation of glass-ceramics (GC), the as-cast glass was heat-treated at 350ºC (slightly below the T_g temperature) for 10-30 h. The glass-ceramics was transparent with a slight pink tinge. Its XRD pattern is shown in **Fig. 2-7a**, together with the peaks corresponding to a bulk β-PbF_2 crystal. In addition to a characteristic halo of the residual glassy phase, sharp diffraction peaks are observed corresponding to PbF_2 compound. The mean size of the nanocrystallites determined by the Scherrer equation is 8.5±0.5 nm.

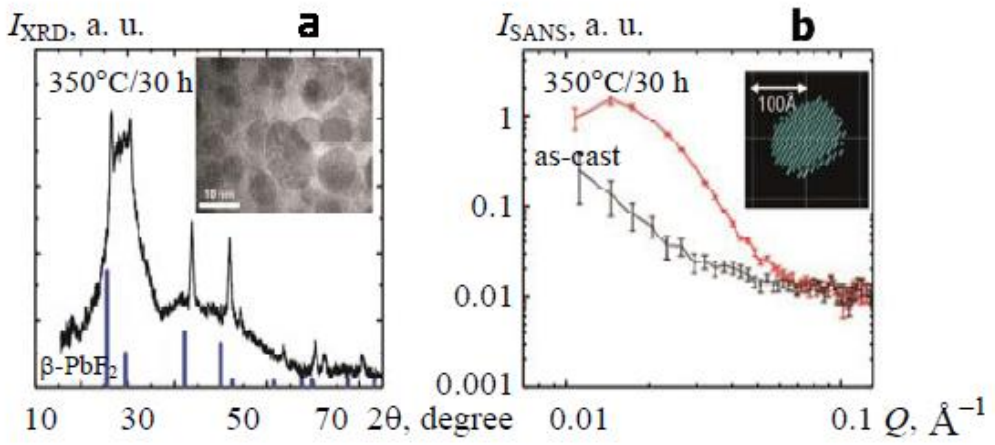

Fig. 2-7. (a) XRD pattern of GC heat treated at 350°C/30 h; vertical lines correspond to the peaks of the bulk β-PbF2 crystal; the inset represents an HR-TEM image;(b) SANS intensity vs modulus of scattering vector, Q, for precursor glass and GC; the inset represents ATSAS modelled shape of the nanocrystal.

For a structural characterization of GC, we also used small-angle neutron scattering (SANS) at the YuMO spectrometer of the IBR-2 pulsed reactor. The scattering intensity vs modulus of the scattering vector Q for both as-cast glass and GC treated for 30 h is plotted in **Fig. 2-7b**. The heat treatment induces a substantial change of the glass structure, which is clear from the scattering curves with a characteristic peak. To model the shape of nanocrystals (inset in **Fig. 2-7b**), we used the ATSAS software. The mean size of PbF_2 nanocrystals is around ~10 nm, which is consistent with XRD and HR-TEM data.

The morphology of GC was studied using SEM and is presented in **Fig. 2-8**.

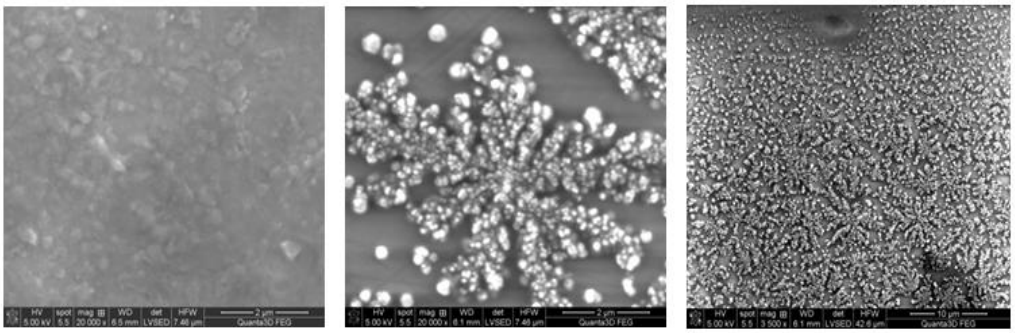

Fig. 2-8. SEM images of precursor (left) and glass-ceramics (middle and right).

The UCL process in glass and GC was excited at a wavelength of ~980 nm and is shown in **Fig. 2-9**. Both of them are normalized to unity for comparison. For the as-cast glass, the green emission dominates: two closely located bands centred at 522 and 544 nm are related to the transitions from $^2H_{11/2}$ and $^4S_{3/2}$ excited states to the $^4I_{15/2}$ ground state. The weak red band contains two components at 653/667 nm; it is related to the transition $^4F_{9/2} \rightarrow {}^4I_{15/2}$. The deep red bands at ~800 and 845 nm are related to the transitions $^4I_{9/2} \rightarrow {}^4I_{15/2}$ and $^4S_{3/2} \rightarrow {}^4I_{13/2}$, respectively.

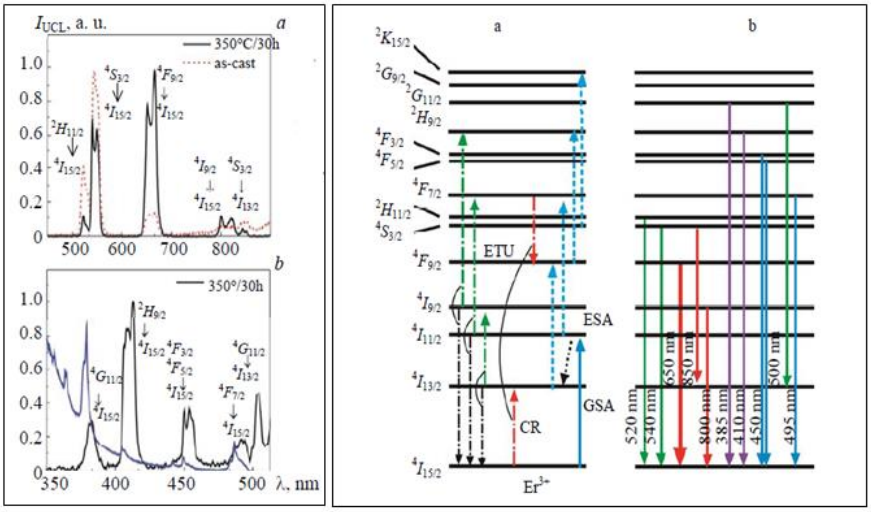

Fig. 2-9. Left: UCL spectra for GC treated at 350°C/30 h and as-cast glass (a,b); Right: scheme of energy levels of Er^{3+} ions.

No emission at the wavelengths shorter than 500 nm was detected (at least at an excitation power density of ~10^4 W/cm^2). This determines the green colour of the emission from the as-cast glass. The scheme of energy levels of Er^{3+} ions showing the potential channels of their excitation and observed UCL lines is shown in **Fig. 2-9** (right). Ground-state absorption (GSA) corresponds to $^4I_{15/2} \rightarrow {}^4I_{11/2}$ transition. Several excited-state absorption (ESA) channels exist for Er^{3+} ions.

The UCL intensity depends on the lifetime of the excited state, from which the radiative transition occurs (**Fig. 2-10**). For the green UCL, these are the states $^2H_{11/2}$ and $^4S_{3/2}$; for the red

UCL, this is $^4F_{9/2}$. Also, I_{UCL} depends on the lifetime of the intermediate state, from which the excitation steps (like ESA) occur. If this lifetime is long enough, the probability of further excitation increases. However, the shortening of the lifetime of the intermediate state can also work as a switch of different emission channels. This occurs for the $^4I_{11/2}$ state of Er^{3+} ions. If its lifetime is long, the $^4I_{11/2} \rightarrow {}^4F_{7/2}$ ESA process dominates, resulting in the strong green UCL. If it is short, fast non-radiative decay leads to the $^4I^{11/2} \rightarrow {}^4I_{13/2}$ relaxation and alternative $^4I_{13/2} \rightarrow {}^4F_{9/2}$ ESA channel, leading to the strong red UCL. The change of the environment of Er^{3+} ions from oxyfluoride (glassy) to pure fluoride (crystalline, PbF_2) can disturb all the above-mentioned lifetimes.

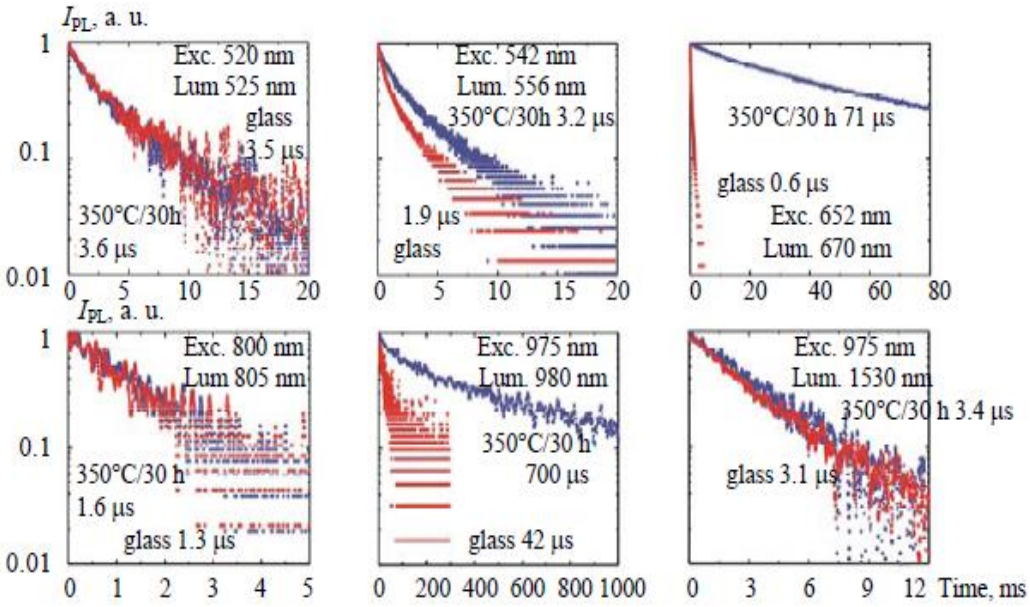

Fig. 2-10. *Decay curves for the visible and IR luminescence of Er^{3+}-doped glass and GC.*

After the heat treatment of the as-cast glass, the lifetime of $^4S_{3/2}$ state increases only to 3.2 μs, which means a slight enhancement of the green emission. For a less intense transition from $^2H_{11/2}$ state, the lifetime is nearly the same (3.6 μs). In contrast, the lifetime of $^4F_{9/2}$ state increases more than 100 times (to 71 μs). This is a key point to understanding the redistribution of intensity from green to red bands in the UCL spectrum of glass-ceramics. The lifetime for the intermediate state, $^4I_{11/2}$, is nearly 16 times longer (as compared to the as-cast glass). This prevents complete suppression of the green UCL for the glass-ceramics.

Novel transparent oxyfluoride germanosilicate glass-ceramics containing Er:PbF_2 nanocrystals have been synthesized on the basis of SiO_2-GeO_2-PbO-PbF_2 initial glass doped with Er_2O_3 using secondary heat treatment. GC is characterized by intense yellow-green emission. The redistribution of intensity between green and red emissions during the heat treatment is explained by the changes in the lifetime of the corresponding UCL bands. The UCL mechanisms for 11 lines in the UV, visible, and near-IR regions are described.

Verification of tumor and stem cells by Raman microspectroscopy

In the present study (2017) we compared Raman scattering spectra of undifferentiated glial tumor (C6 glioma cell) and mesenchymal stem cells (MSC). Raman spectroscopy is a sensitive analytical technique capable of providing highly detailed biochemical information on biological samples. In particular, it can be used to distinguish between normal and malignant tissues. Our goal was to find out whether the difference exists at the stage when cancerous and wholesome cells are undifferentiated.

Raman spectroscopy (**Fig. 2-11**, left) and CARS microscopy (**Fig. 2-11**, right) revealed a striking similarity of scattering spectra from rat's MSC and C6 glioma cells. This is in contrast to the study comparing spectra from the formed tumor versus normal differentiated tissue. In our opinion, there is one important detail in the obtained data: we compared undifferentiated MSC and C6 glioma cells. Therefore, namely the fact of insufficiency (or absence) of differentiation is the basis of the revealed identity of Raman scattering spectra of MSC and C6 glioma cells. Thus, the accumulated data from Raman spectra and CARS microscopy speak for being them a potential instrument for differential diagnostics and especially for intraoperative demarcation of tumor and healthy tissue.

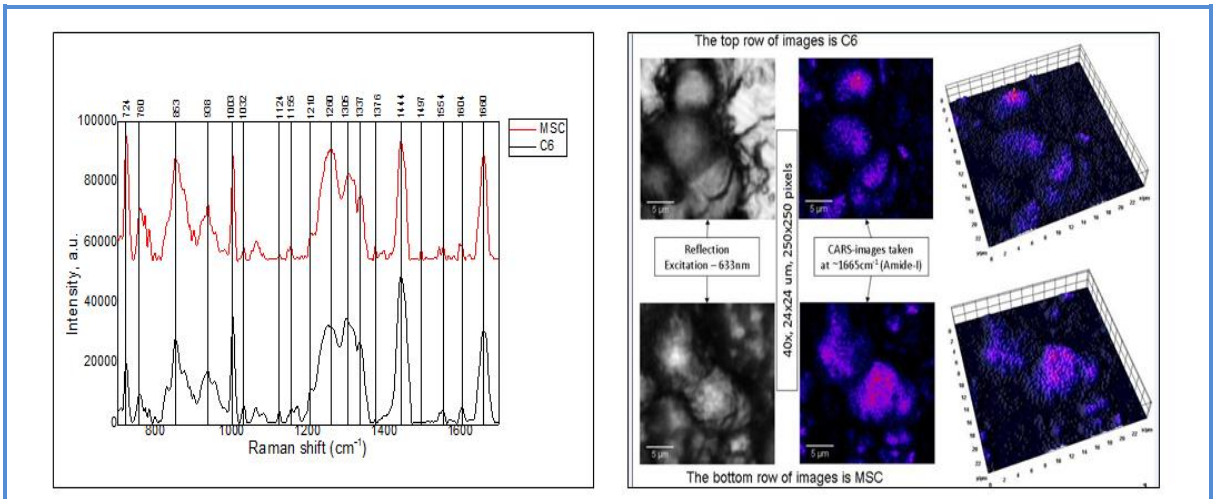

Fig. 2-11. The comparison of Raman spectra of rat's MSC and C6 glioma cells (left). Micrographs and CARS images of rat's MSC and C6 glioma cells (right).

Our results suggest possible relations between MSC and C6 glioma cells, which is in accordance with the studies reporting the expression of common antigens in stem cells and various types of tumor.

Thus, it has been demonstrated that at some stages of development and metabolic activity, malignant cells and normal stem cells can have nearly identical spectral "fingerprints. This phenomenon helps to understand the difficulty encountered by the immune defense system in a tumor-bearing organism, showing one of the ways for tumor cells to escape from the protective activity of immune cells. Our results also show potential pitfalls in cancer diagnostics.

3. NEUTRON NUCLEAR PHYSICS

In 2017, in FLNP the scientific activity in the field of neutron nuclear physics was carried out in the following traditional directions: investigations of time and space parity violation processes in neutron-nuclear interactions; studies of the fission process; experimental and theoretical investigations of fundamental properties of the neutron; gamma-spectroscopy of neutron-nuclear interactions; atomic nuclear structure, obtaining of new data for reactor applications and nuclear astrophysics; experiments with ultracold neutrons, applied research using NAA. The scientific program to study the inelastic scattering of fast neutrons ("TANGRA" project) is being successfully implemented. Despite some technical difficulties, the second stage of the LUE-200 accelerator was commissioned, and a series of applied studies were conducted on neutron beams of the IREN facility. A number of investigations in the field of fundamental physics and ultracold neutron physics were performed on the neutron beams of nuclear research centers in Germany, China, USA, France, Switzerland.

Measurement of ROT effect for gamma-rays in ^{235}U fission on a hot source of polarized neutrons

In the framework of the FLNP JINR – ITEP – FRM-II collaboration a series of experiments was continued to measure the ROT-effect in the emission of prompt γ-rays and neutrons in binary fission of ^{235}U and ^{233}U induced by polarized cold neutrons. The experiments were carried out on the POLI instrument at the FRM-2 reactor (Garching, Germany).

T-odd effects in the fission of heavy nuclei have been known for more than ten years. The first effect of this type (the so-called TRI-effect) was detected at the ILL reactor (Grenoble) by the collaboration of Russian and European institutes in the experiment aimed at finding a violation of the time reversal invariance (TRI) following the idea proposed by K. Schreckenbach. It was found that the probability of emission of an alpha particle in a ternary fission in the direction perpendicular to the plane formed by the neutron spin and the fragment momentum demonstrates a pronounced anisotropy. The magnitude of the effect turned out to be surprisingly high, and the current explanation does not imply the existence of such a violation, but is based on the interaction of the reaction products in the final state. In other words, the effect is not related to the violation of the invariance with respect to time reversal, but is connected with the mechanism of the fission process. Nevertheless, in the literature the effect is still called "TRI-effect".

In addition, it was noted that when the direction of the neutron beam polarization is changed, the angular distribution of α-particles is shifted by a small angle relative to the fragment emission axis, and the direction of the shift is determined by the direction of the neutron beam polarization. The authors called this effect ROT-effect. Both TRI- and ROT-effects are formally T-odd, but have no direct connection with the violation of time reversal invariance.

From the quasi-classical description of the ROT effect, which assumes the rotation of a polarized nucleus before its splitting into two (or three) fragments, it follows that an analogous phenomenon can be observed in the angular distribution of some other particles accompanying the fission of the nucleus into two fragments, if this distribution is anisotropic with respect to the axis of the deformation of the fissioning nucleus at the time of splitting, and the asymmetry relative to the initial direction of the deformation axis is completely or partially preserved after the fragments escape to infinity. Indeed, the analogous effect was observed in the emission of instant gamma-rays and

neutrons in the fission of ^{235}U and ^{233}U, though its magnitude was an order of magnitude smaller than for the emission of α-particles in triple fission.

At present, there are several theoretical models that can describe both effects. According to the model proposed in 2016, both effects depend on the quantum numbers J and K which characterize the fission channels. In fission induced by thermal (or cold) neutrons (for which all previous data were obtained), there is a mixture of several spin states whose contributions are unknown. The only way to obtain "clean" data is to perform measurements on isolated resonances. Such an experiment was carried out on the POLI facility at the FRM-II reactor in Garching, which provides a required polarized neutron beam of hot neutrons with an energy of 0.27 eV corresponding to the lowest resonance of ^{235}U.

A schematic of the experimental setup is shown in **Fig. 3-1**. A narrow neutron beam was monochromatized by a monochromator made of a mosaic of Cu crystals to the average energy of 270 meV (λ = 0.55 Å). The monochromator also makes it possible to simultaneously focus the neutron beam at a given position, providing maximum intensity of unpolarized neutrons of about $4 \cdot 10^6$ n/cm^2/s.

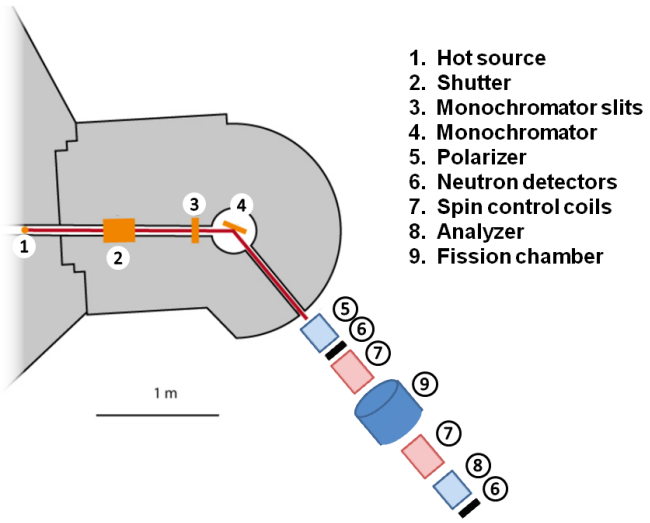

Fig. 3-1. *Schematic of the experimental setup at the POLI facility of the FRM-II reactor.*

Neutrons were polarized using specially constructed ^3He cells. The same cell type was used as an analyzer for measuring beam polarization. Since polarized ^3He nuclei have a very high spin-dependent neutron absorption efficiency over a wide energy range, a ^3He cell can be used as a broadband neutron polarizer or analyzer with the possibility of optimizing its efficiency for almost all neutron wavelengths. In our experiment, the cell size of Ø60 x 130 mm and a pressure of 2.5 bar ensured maximum neutron polarization of about 70%. The polarizer and analyzer cells were polarized in an external laboratory and placed in a special magnetic housing with a strong uniform constant magnetic field. Polarization of ^3He in the cell decreased exponentially with a time constant of about 40 h, so both cells were replaced every 24 h.

Both the polarizer and analyzer provided vertical neutron beam polarization, while the effect under study requires horizontal (longitudinal) polarization. To change the polarization direction from vertical to horizontal, a specially developed spin control system consisting of several magnetic coils with a μ-metal screen was used, which also made it possible to rotate the spin in a given position by 180^o every 1.3 s.

A schematic of the fission chamber surrounded by a set of gamma-ray detectors is shown in **Fig. 3-2**. The chamber is filled with CF_4 gas at a pressure of about 10 mbar. The uranium target containing about 82 mg of ^{235}U (99.99%) oxide deposited on both sides of a thick aluminum substrate with a thickness of 40 × 100 mm^2 was positioned on the chamber axis. Thin low-pressure multiwire proportional counters (MWPC) placed on both sides of the target were used as detectors for fission fragments. Eight cylindrical plastic scintillators and four NaI-based scintillators were inserted into the rotating holder at a distance of about 30 cm from the target center, which provided subsequent measurements of the coincidences of instant gamma-rays and neutrons with fission fragments at the angles of ± 22.5, ± 45, ± 67.5, ± 112.5, ± 135 and ± 157.5° relative to the average fragment detection axis. The detectors of gamma-rays and fission fragments were located in the plane orthogonal to the neutron beam direction, which also coincides with the polarization axis of ^{236}U nuclei.

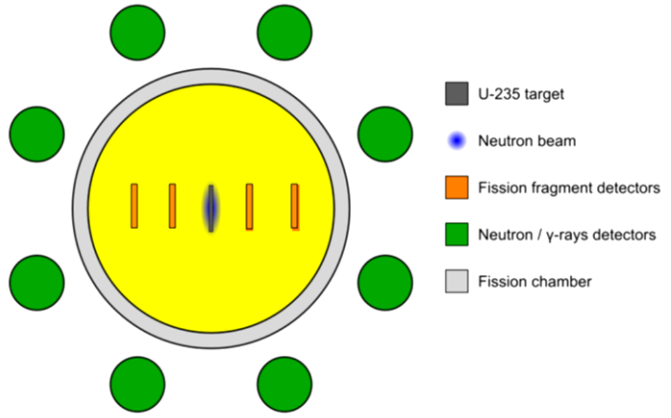

Fig. 3-2. Schematic of the fission chamber.

Separation of instant neutrons and γ rays could be done using the time-of-flight technique (**Fig. 3-3**). Each event matching coincidence of signals from neutron and fragment detectors is digitized by multichannel TDC CAEN V775N and stored together with the information about the direction of polarization of the neutron beam. Reverse of polarization occurs at a frequency of 1 Hz; the input signal of TDC is delayed by the spin flip time of the neutron. At the same time, for the on-line control of the setup, the coincidence count rates of neutrons/γ-rays and fission fragments were registered by counters which were read out every 5 min for each detector. The values of asymmetries, calculated by the formula $R=(N^+ - N^-)/(N^+ + N^-)$ were constantly monitored. Here N^+ and N^- are the coincidence count rates for opposite directions of neutron polarization. The asymmetry of count rates of the fragments was simultaneously measured and controlled.

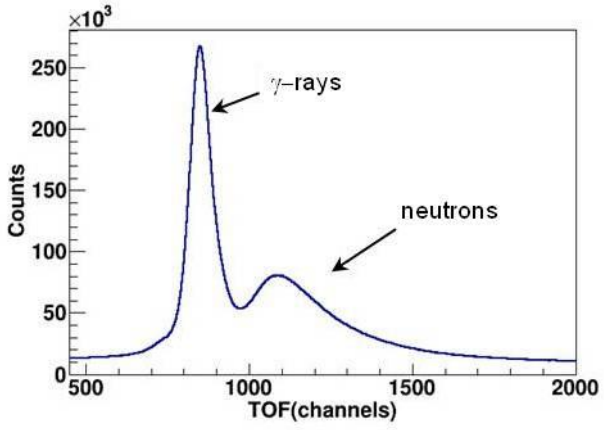

Fig. 3-3. Time-of-flight spectrum from a plastic detector allowing separation of gamma-rays and neutrons.

The total time for the experiment at the POLY facility was 27 days. The installation, detector calibration, adjusting of the spin control system, and so on took five days. Statistics was accumulated during 22 days.

Also, the measurment of neutron fluxes in the experiment gave $2 \cdot 10^7$ cm^{-2} s^{-1} at the exit from the neutron channel (i.e. at the entrance of the polarizer) and $3.3 \cdot 10^7$ cm^{-2} s^{-1} at the front part of the fission chamber.

A full analysis of the experimental data will take quite a long time. The only conclusion that can be drawn at this stage of analysis is that the statistical uncertainty of the experimental data is about half of that obtained in 2016. At the same time, the sensitivity of the new experimental setup is approximately 5 times higher, mainly due to the use of position-sensitive detectors of fission fragments. Such statistical accuracy and sensitivity would certainly be sufficient to observe the effect, if its magnitude were the same as the measured effect in the region of cold neutrons. However, a new model of the ROT-effect (proposed recently) predicts a decrease of the effect in the 0.3 eV resonance of ^{235}U. The preliminary analysis of the data shows that the effect actually diminishes, but a more detailed analysis is required to obtain its exact value or determine its upper limit.

Investigation of prompt neutron emission in neutron induced nuclear fission

In 2016-2017 a complex spectrometer consisting of a double ionization chamber with Frisch grids (DIC) and a scintillation (BC501) fast neutron detector was developed and designed in the Department of Nuclear Physics. The spectrometer is intended for experimental studies of fission processes in the late stages of the evolution of the fissioning system (after passing through the "saddle point") using the IBR- and IREN neutron sources. To date, fission in the reactions ^{252}Cf(sf), ^{235}U(n_{res},f), ^{235}U(n_{th},f), have been studied; for which masses of correlated fission fragments (FF), their kinetic energies and the cosines of the angles ($\Theta_{1,2}$) between the direction of FF emission and the fixed axis of a cylindrical coordinate system, were measured. Since the detector was located at a fixed distance from the coordinate system, the measured cosines of the angles ($\Theta_{1,2}$) were equal to the cosines of the angles between the direction of FF emission and prompt fission neutrons (PFN) emitted in the fission process. The fast neutron detector made it possible to measure the speed of PFN and suppress the background of prompt gamma-radiation by analyzing the pulse shape.

The implementation of the procedure for determining these characteristics for each fission event became possible due to the use of synchronous ADCs that simultaneously sampled detector pulses at a frequency of 250 MHz and amplitude resolution of 12 bits. The launching of these digitizers was done with the help of specially developed electronic equipment in the NIM standard, hereinafter referred to as the "trigger". The unit could generate pulses to trigger the sampling of detector pulses and store them in the local ADC memory. The ADCs had a local segmented high-capacity memory that made it possible to organize data acqusition in the local ADC memory practically without dead time (since the data from the local ADC memory were transferred to the PC memory in the intervals between the source pulses). The pulse digitizer was installed in the PCIe bus expansion module of the PC motherboard. The communication of the specified module with PC was carried out through the optical interface "SONET". Specially developed PC software could specify synchronization modes, acqusition algorithms, storage in the local memory and transformation of obtained data to PC for on-line or off-line processing modes, as well as data

storage. At present, two sets of spectrometer electronics have been manufactured, one of which is used at IBR-2 and the other at IREN. The experimental study of the PFN emission process in the $^{235}U(n_{th},f)$ reaction was necessary, since the available data were obtained more than 50 years ago and are somewhat ambiguous. New measurements were made on IBR-2 beamline 11B equipped with a curved mirror neutron guide effectively suppressing gamma radiation from the neutron source. The obtained results [1] made it possible to correct the available data and for the first time obtain FF mass distribution, which is in good agreement with the data obtained at a spectrometer with a resolution of about 0.5 amu. The dependence of the number of PFN on FF mass carries very important information on the impact of quantum effects (nuclear shells of forming FF) on the FF formation processes. For example, in **Fig. 3-4**, the experimental data acquired under identical conditions with identical detectors obtained in the reactions $^{252}Cf(sf)$ and $^{235}U(n_{th},f)$ are given for comparison.

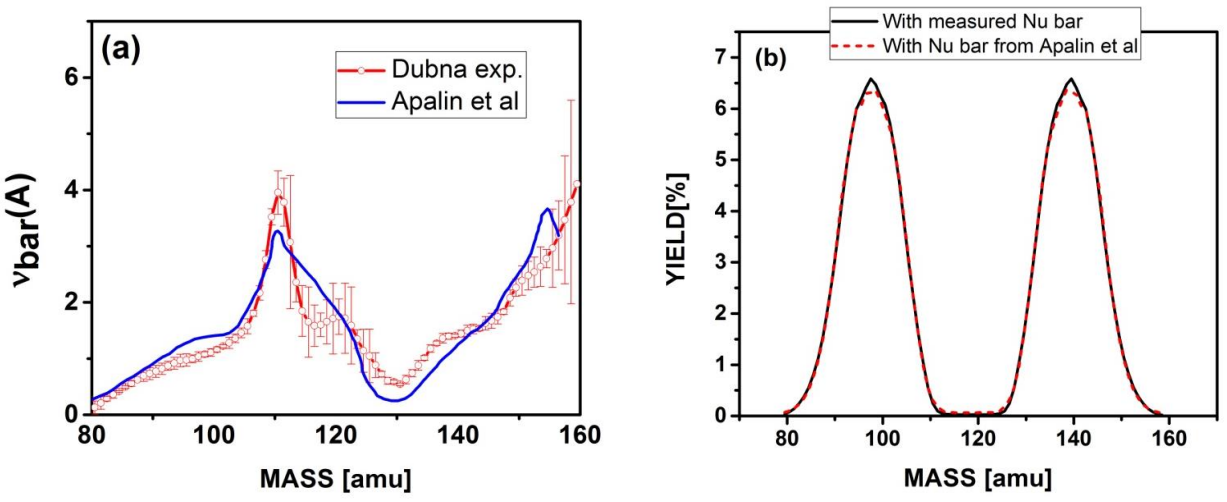

a) *b)*

Fig. 3-4. *a) Comparison of dependence of PFN average number in $^{235}U(n_{th},f)$ reaction obtained in Dubna with the results published in [2]. b) Comparison of mass distributions obtained using our data and data from [3].*

The PFN yield for fragments with mass numbers in the region of A ~ 118 for the $^{235}U(n_{th},f)$ reaction is siginificantly lower than for the $^{252}Cf(sf)$ reaction (**Fig. 3-5**). This is a consequence of the fact that the shell of the correlated fragment for ^{252}Cf is almost filled whereas for ^{235}U in the region of A ~ 120 the shells of both fragments are half-filled. Nuclei with filled shells have a shape close to a spherical one and, hence, a more tightly bound structure that resists deformation more strongly. Another argument in favor of greater incompactness of nuclei with unfilled shells is the fact that in the $^{252}Cf(sf)$ reaction the average PFN number is larger than in the $^{235}U(n_{th},f)$ reaction due to a higher PFN yield in the region of A ~ 120 for $^{252}Cf(sf)$. The anomalously small PFN yield in the region of A ~ 132 is explained by high stability of the spherical configuration in this region and high resistance of the correlated fragment to deformation (high rigidity of configuration [4]). As the excitation energy increases, the shell effects are suppressed and configurations of fissioning nuclei become more elongated with a lower total kinetic energy (TKE) and an increase in the total deformation energy

(TDE) of the fragments. In this case, mainly the excitation energy of heavy fragments increases. This phenomenon was usually explained by the fact that during the formation of fragments, an intensive energy exchange occurs between the fragments with a uniform energy distribution between the degrees of freedom. Since a heavy fragment has a greater number of degrees of freedom, it takes a larger portion of the excitation energy.

From this it was also concluded that the excitation energy is spent to increase the temperature of the fragments at equal temperatures of the fragments. However, the experiments studying the nuclear level density in the energy range of up to 6-7 MeV show that the last statement is incorrect. The temperature of nuclei does not change with increasing excitation energy due to the fact that pair correlations lead to an effective increase in the number of degrees of freedom in the nuclei in proportion to the increase in their excitation energy [5]. Cooper pairs of neutrons and protons decay so that the average excitation energy per nucleon, and, hence, the temperature, remains constant. However, due to the differences in the level densities, the temperature of the light FF appears to be higher than the temperature of the heavy FF. The fissioning nucleus up until the point of rupture can be considered as two independent nuclei connected by a neck and being in thermal contact [6]. The superfluidity mode leads to the fact that the energy transfer between FFs occurs during the transition of Cooper pairs from the light to heavy FF, in which pairs have a lower binding energy and decay with higher probability. Since the number of degrees of freedom increases after pair decay, the temperature of the heavy FF does not change, but its excitation energy increases. This effect, as proposed by the authors of [6], explains the reason for the increase in the number of PFN (mainly through the increase in the excitation energy). However, if a heavy FF has a shape close to a spherical one (closed outer shell) then the energy transfer process can go in reverse. Thus, the study of the PFN emission process in fission is of special interest, especially regarding the dependence of the average number of PFN on the fragment mass, since the variations in the number of PFN are directly related to the process of excitation energy redistribution between the fragments.

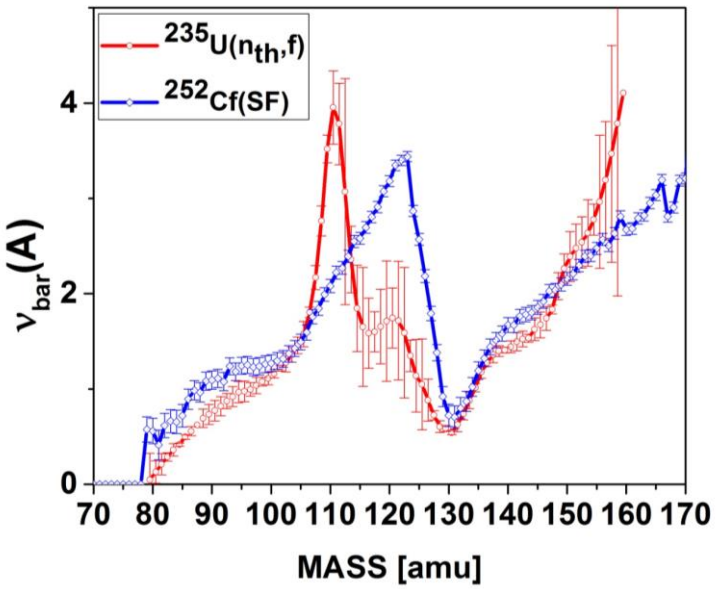

Fig. 3-6. *Comparison of the average number of PFN in the $^{235}U(n_{th},f)$ reaction with the results for $^{252}Cf(sf)$.*

Position-sensitive ionization chamber for the investigation of PFN in resonance neutron induced fission

The progress in understanding the fission process is largely due to the development of more advanced experimental methods. The rapid development of electronics and information technology has recently been one of the most powerful incentives for increasing the informativeness of experimental research. A huge role in this was played by the development of digital technologies, which by now have almost completely superseded the traditional analog paradigm not only in nuclear physics, but also in the modern industry. A significant improvement in the systems of detector signal normalization became possible due to the miniaturization of electronics, which allowed the creation of compact equipment for position-sensitive detectors. Owing to these technical achievements, we succeeded in designing a compact position-sensitive double ionization chamber (DIC) for FF spectrometry. The developed design of DIC [7-9] allowed simultaneous measurement of kinetic energies, masses and orientation of FFs in a 3D cylindrical coordinate system. As noted above, the most valuable information on the fission process can be obtained in PFN emission studies. The application of the DIC developed in the work makes it possible to increase the efficiency of these experiments by more than an order of magnitude due to the use of a larger number of fast neutron detectors. The development of the detector was carried out in two stages. At first, specialized software was created to calculate 2D electrostatic fields, necessary for studying charge induction on the chamber electrodes during the drift of electrons in ionization chambers. As a result, the ambiguities in the procedures for determining the amplitudes and directions of the FF motion were eliminated. Then, the programs were improved in order to be used for studying charge induction on the electrodes of the position-sensitive DIC with strip anodes. Numerical simulation was carried out for two variants of signal processing organization, and both variants were realized and tested. At present, data have been processed only for one of the variants. As a result of numerical simulation, it was found that the magnitude of the induced charges in the chain of anode strips in the cross-section Y = const is proportional to the ratio of the lengths of the strip segments along the Y axis. It was assumed that the projection of the particle trajectory along the Y axis is directed along the Y axis. The scheme of arrangement of electrodes in the chamber is presented in **Fig. 3-7**.

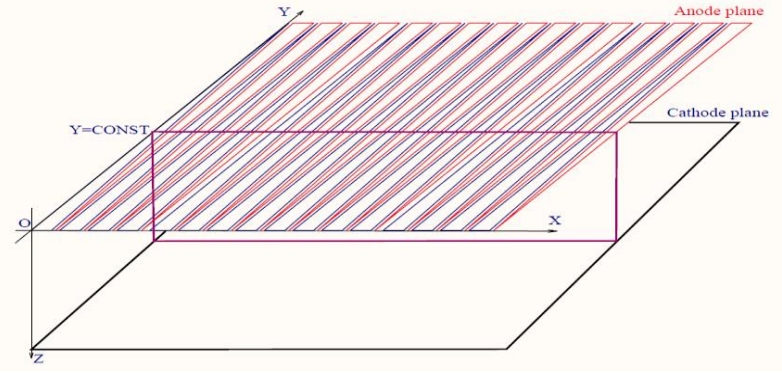

Fig. 3-7. *Design of ionization chamber with strip anodes. Pair of strips (red and blue) is formed by cutting a rectangular metal plate along diagonal.*

Figure 3-8 shows the dependence of the calculated weighting potential in the plane Y = const for one strip under unit potential and zero potential on all other electrodes in the chamber. According to the Shockley-Ramo theorem, the charge induced in the chains of adjacent strips when electrons moving in the plane Y = const from point *a* to point *b* can be calculated by formula (1), where Q is

the induced charge, *e* is the electron charge, $\Phi(a)$ and $\Phi(b)$ are weighting potentials at points *a* and *b*, respectively.

$$Q = e \cdot (\Phi(a) - \Phi(b)) \quad (1)$$

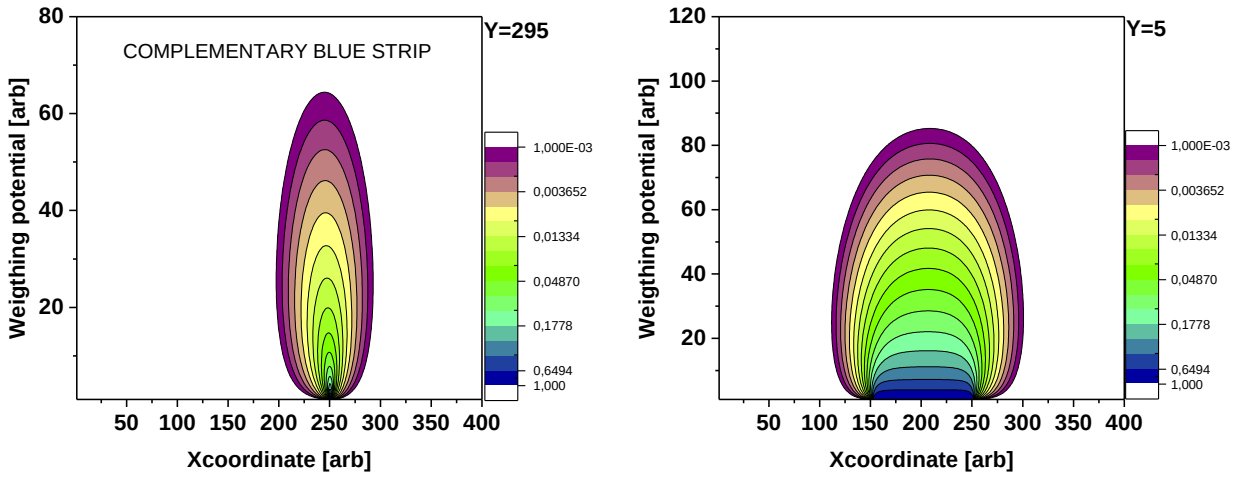

Fig. 3-8. Coordinate dependence of charge induced in chain filter.

From the analysis of the graphs in **Fig. 3-8** it follows that under the conditions indicated above the ratio of the charge induced on the strip is proportional to the Y coordinate with a uniform ionization density in the plane Y = const. To verify the results of the calculations, measurements were made with the chamber shown schematically in **Fig. 3-7**. To encode coordinates, an electronic strip connection circuit was proposed (**Fig. 3-9**).

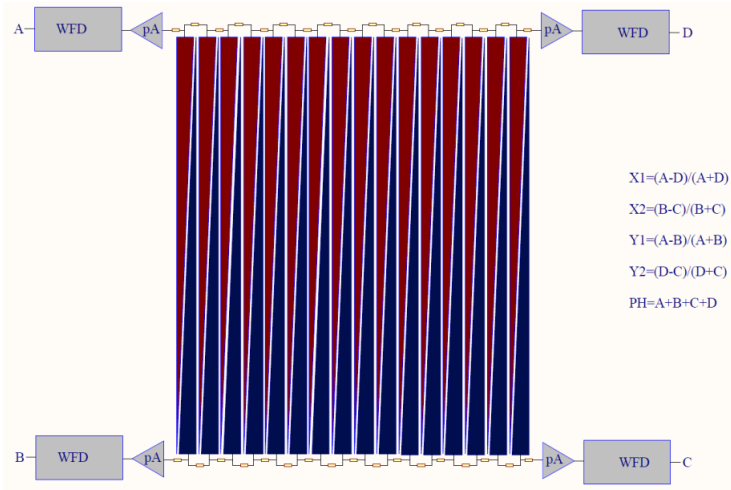

Fig. 3-9. Scheme of strip connection to resistive chain filter. Blue and red strips are electrically isolated from each other.

With this type of connection, the electrical capacitance of the strips together with the resistors connecting the adjacent strips formed two chain filters. The charge induction on the strip was transformed into current pulses in both chains of the chain filters. The pulse propagation in the chain filters was investigated using the operational calculus. The links of the chain filters were considered as passive four-poles with a wave impedance load at the ends. In this case, the current pulse is transmitted without distortion, and it was shown that the induced charge is

divided equally between the strips and propagates towards the corresponding ends of the chain filters. The fact that the pulse propagation causes a decrease in the pulse amplitude proportional to the number of the filter links was used to determine the point of the charge injection into the chain filter. As was shown above, the charges induced in adjacent strips are divided proportionally to the distance between the injection point and the middle of the strips:

$$y = L_y \cdot (\frac{1}{2} + \frac{Q_A - Q_B}{Q_A + Q_B}) \quad (2),$$

$$x = L_x \cdot (\frac{1}{2} + \frac{Q_A - Q_D}{Q_A + Q_D}) \quad (3).$$

Thus, formula (2) gives the y-coordinate of the "center of gravity" of the charge distribution of ionization electrons which arise as a result of deceleration of charged particles in the working volume of the chamber. Similarly, the x-coordinate of the "center of gravity" can be determined using formula (3), where Q_A, Q_B, Q_C Q_D are the amplitudes of pulses at the terminal points of the chain filters.

To determine the degree of decrease of the pulse amplitude during the pulse propagation in the chain filter, calculations were made for the signal attenuation function after passing K links (in K-range from 0 to 16) of the chain filter. The results are shown in **Fig. 3-10**.

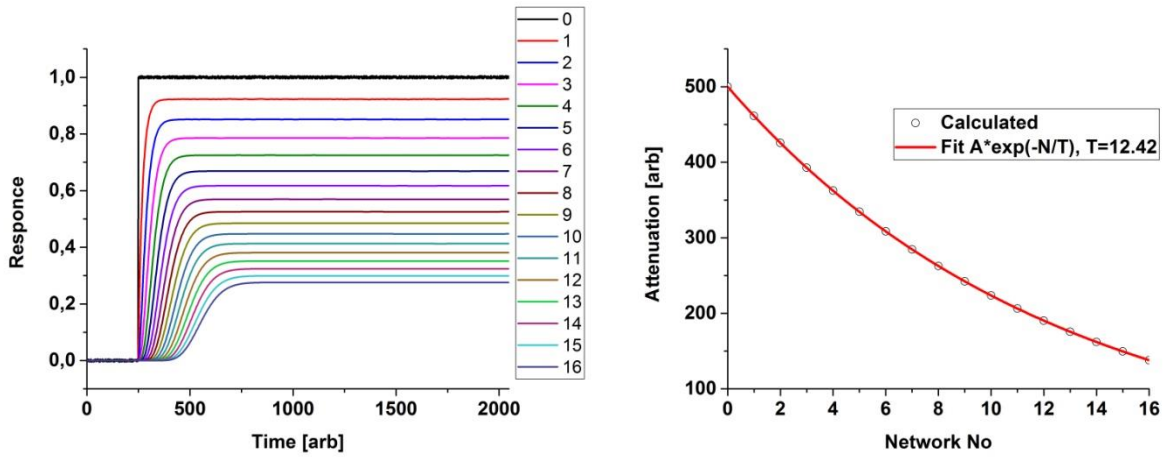

Fig. 3-10. Calculations of signal attenuation after passing K links of chain filter.

These results were used to correct the information on coordinates determined by formulas (2) and (3).

Empirical model of cascade gamma-decay and studies of parameters that determine superfluid properties of the nucleus

In 2017, the analysis of the nuclear data obtained with the help of the developed in Dubna empirical model of the cascade gamma decay of the neutron resonance was improved. This model makes it possible (from the approximation of experimental intensities of two-quantum cascades) to determine simultaneously (with percentage accuracy) the parameters of the density of nuclear levels, ρ, and parameters of partial widths, Γ, of the emission of nuclear reaction products. To date, the cascades of two successively emitted gamma-rays have been measured in the capture of thermal neutrons by 44 nuclei in the mass range of 28 < A < 200.

The most probable ρ- and Γ-values can be obtained only from the approximation of intensities of cascades between fixed initial levels and any intermediate and final levels of the excited nucleus. The two-quantum cascade (TQC) is determined by the energies of initial, intermediate and final levels, as well as the probabilities of electromagnetic transitions between them.

After the sequence order of quanta in cascades is determined (using the maximum likelihood method, from the condition that the primary transitions in cascades to different finite levels have the same energy, and also using the available spectroscopic data), the $I_{\gamma\gamma}(E_1)$ dependence only on the energy of the primary transition, E_1, can be extracted with an acceptable accuracy from the experimental spectrum $I_{\gamma\gamma}(E_\gamma)$. Without this operation, the experimental distribution $I_{\gamma\gamma}(E_\gamma)$ can be accurately described by the infinite number of significantly different functions ρ and Γ because of their correlation. In a small interval, ΔE, of energies E_1 of primary transitions, the sum of the intensities of TQC from the initial levels λ to the group of low-energy finite levels f through the intermediate levels i can be represented by the equation:

$$I_{\gamma\gamma}(E_1 \pm \Delta E/2)=\sum_{\lambda,f}\sum_{i}\frac{\Gamma_{\lambda i}}{\Gamma_{\lambda}}\frac{\Gamma_{if}}{\Gamma_{i}}=\sum_{\lambda,f}\sum_{j}\frac{\Gamma_{\lambda j}}{<\Gamma_{\lambda j}>M_{\lambda j}}n_j\frac{\Gamma_{jf}}{<\Gamma_{jf}>m_{jf}}. \qquad (4).$$

In the interval ΔE, $n_j=<\rho_j>\cdot\Delta E$ is the number of excited cascade levels, $<\rho_j>$ is the average density of levels of all types, $<\Gamma_{\lambda j}>M_{\lambda j}$ is the sum of partial widths $\Sigma_j\Gamma_{\lambda j}$ of primary transitions to $M_{\lambda j}$ of intermediate levels, $<\Gamma_{jf}>m_{jf}$ is the sum of partial widths $\Sigma_j\Gamma_{jf}$ for secondary transitions to m_{jf} finite levels (since $<\Gamma_{\lambda j}> = \Sigma_j\Gamma_{\lambda j}/M_{\lambda j}$ and $<\Gamma_{jf}> = \Sigma_j\Gamma_{jf}/m_{jf}$).

Since it is impossible to determine parameters of all cascades in experiments, to solve the system of equations (4) in the entire energy range of primary transitions and simultaneously determine ρ and Γ, the experimental intensities $I_{\gamma\gamma}(E_1)$ are approximated using model representations of functions $\rho(E_{ex})=\varphi(p_1,p_2\ldots)$ and $\Gamma(E_1)= \psi(q_1,q_2\ldots)$ for all observed primary gamma-transitions. In all experiments *FWHM*s of the resolved peaks do not exceed 2 – 4 keV.

The inadmissibility of using experimentally unverified representations for $\rho(E_{ex}) = \varphi(p_1,p_2\ldots)$ and $\Gamma(E_1) = \psi(q_1,q_2\ldots)$ was discussed in detail in the previous versions of the data analysis showing that the uncertainty of the parameters ρ and Γ is mostly determined by a systematic error due to inaccuracy of model representations of experimental data. One can estimate the error and the way to correct the model representations about $\rho = f(p_1, p_2, ..)$ and $\Gamma = \varphi\ (q_1, q_2, \ldots)$ only by comparing various versions of their description.

For model representation of the level density, we used the model of n-quasiparticle nuclear excitations (usually applied in the study of pre-equilibrium reactions in nuclei [10]) and a phenomenological coefficient of an increase in the density of collective levels (balance in the changes of entropy and energy of quasiparticle levels) from the model [11] modified by taking into account a breakup in the Cooper pairs of nucleons. The strength functions of electrical and magnetic transitions were presented, as in the model [12], with the addition of one or two local peaks to accurately describe the experimental distributions $I_{\gamma\gamma}(E_1)$. Studies performed in 2017 confirmed the need to add local peaks to the smooth parts of strength functions and showed that the influence of their different descriptions on the obtained parameters is insignificant.

Even at the initial 'model-free' stage of our method, when the TQC intensities were approximated without any theoretical representations for $\rho(E_{ex})$ and $\Gamma(E_1)$, a step structure was revealed in the $\rho(E_{ex})$ function. Further analysis of the experimental data showed that the level densities are not reproduced with the accuracy of the experiment by the models ignoring the existence of the boson state of nuclear matter. For all investigated nuclei, the presence of steps, probably caused by the breakup of the Cooper pairs in the nucleus, is confirmed by the changes in the representations of $\rho(E_{ex})$ and $\Gamma(E_1)$ introduced by the development of the empirical model. The number of investigated nuclei increases, while the fraction of phenomenological representations of the extracted parameters ρ and Γ is minimized for the verification of the data obtained.

The analysis of new results confirmed the obtained earlier dependence of dynamics of interaction between Fermi and Bose nuclear states on the nucleus shape. In the mass dependence of Cooper pair breaking thresholds (parameters of $\rho(E_{ex})$ function) obtained from the fit, breaking pair thresholds in spherical nuclei ($A < 150$) are higher than in deformed nuclei ($A > 150$). It also follows from the ratios of densities of vibrational and quasi-particle levels that this interaction manifests itself in the neutron binding energy range and probably differs for nuclei with various nucleon parities.

The verification of ρ and Γ obtained in early fits and the estimation of the achieved accuracy of the model were made by comparing experimental gamma-spectra with their calculation from the practical gamma-decay model. The analysis of the sources of systematic errors in ρ and Γ made it possible to conclude about a possible description of spectra of products from any nuclear reaction by the practical model with an accuracy of several percent.

Investigations of neutron-charged particle reactions

Experimental and theoretical investigations of neutron-charged particle reactions induced by fast neutrons were carried out. The experiments were conducted at the Van de Graaff accelerators EG-5 in FLNP JINR and EG-4.5 of the Institute of Heavy Ion Physics of Peking University. Data on the neutron reactions with the emission of charged particles induced by fast neutrons are of much interest for studying the mechanisms of nuclear reactions and atomic nuclear structure as well as in choosing engineering materials and in performing calculations in the development of new facilities for nuclear power engineering.

A paper devoted to the study of the $^{144}Sm(n,\alpha)^{141}Nd$ and $^{66}Zn(n,\alpha)^{63}Ni$ reactions at E_n= 4.0, 5.0 and 6.0 MeV has been published. The data have been obtained for the first time. The experimental

values of cross sections are compared with the available libraries and calculations using the TALYS-1.6 code. Our results support the EAF-2010 data and are in good agreement with TENDL-2015.

The cross sections for the $^{10}B(n,t2\alpha)$ three-body reaction and $^{10}B(n,\alpha)^{7}Li$ reaction at E_n=4.0, 4.5 and 5.0 MeV were measured. The measurements were performed on the 4.5-MV Van de Graaff accelerator at Peking University. An ionization chamber manufactured at FLNP JINR was used as a detector. A new system for acquisition and accumulation of experimental data developed on the basis of a high-speed digitizer, was employed. Due to the fact that there are several channels of the reaction with emission of a triton and two α-particles, detailed calculations were made for analyzing the experimental data. As an example, **Figure 3-11** shows an amplitude spectrum of events from the region of effective events and time window of multidimensional experimental spectrum at E_n = 4.0 MeV.

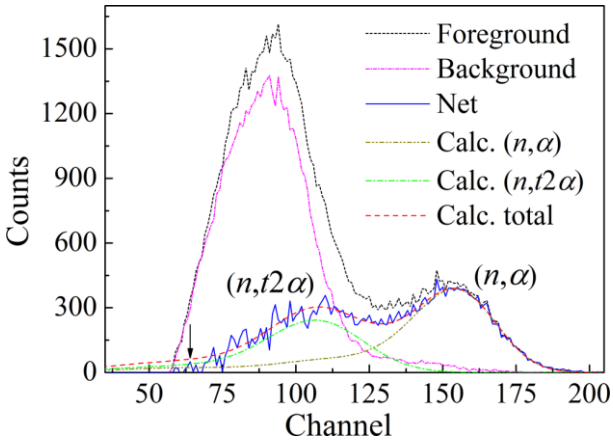

Fig. 3-11. Amplitude spectrum of events from the region of effective events and time window of multidimensional experimental spectrum at E_n = 4.0 MeV.

The results on the cross sections and errors of the measurements of the $^{10}B(n,t2\alpha)$ and $^{10}B(n,\alpha)^{7}Li$ reactions are given in **Fig. 3-12** and **Table I**.

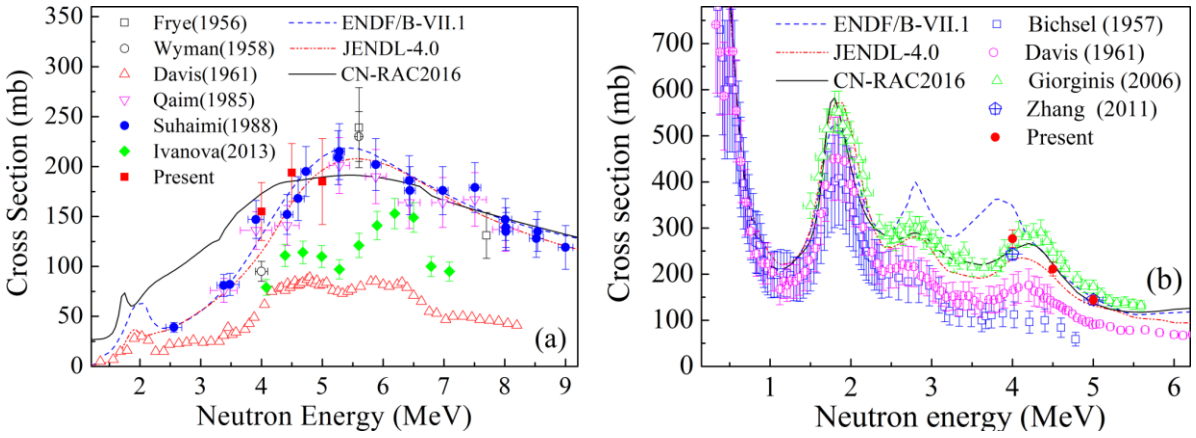

Fig. 3-12. Our results on cross-sections in comparison with previous measurements and data libraries: a) for $^{10}B(n,t2\alpha)$ reaction and b) for $^{10}B(n,\alpha)^{7}Li$ reaction.

Table I. Measured cross sections for $^{10}B(n,t\,2\alpha)$ and $^{10}B(n,\alpha)^{7}Li$ reactions.

E_n (MeV)	$\sigma(n,t\,2\alpha)$ (mb)	$\sigma(n,\alpha)$ (mb)			
		Total	Leaking	Forward α	Backward α
4.0	155 (19%)	277 (7%)	35 (9%)	143 (11%)	99 (9%)
4.5	194 (15%)	211 (7%)	30 (10%)	107 (11%)	74 (9%)
5.0	185 (23%)	144 (7%)	22 (10%)	72 (12%)	50 (9%)

Investigations of nuclear reactions induced by gamma-rays and fast protons

Work was carried out to estimate cross sections, isomeric ratios, and other effects in nuclear reactions with neutron yield induced by photons and fast protons. The calculations were made using the Talys software and own computer codes. The Talys software system is intended to determine nuclear reaction cross sections and the structure of the atomic nucleus and operates mainly under Linux with a simple and efficient interface.

Cross sections, isomer relations, forward-backward asymmetries and other parameters of (γ, n), (γ, p), (α, γ), (α, n), (p, n) reactions on isotopes of Sn, Sm, In and other nuclei were obtained. The theoretical estimates were compared with the literature experimental data, and a good agreement was found. Addtional nuclear data such as parameters of the nuclear potential, nuclear state and level densities were detetermined.

The obtained theoretical estimates may find application in both fundamental and applied areas of nuclear physics. From the fundamental point of view, the results can be useful in studies of mechanisms of nuclear reactions, structure of nucleus, and astrophysical problems. Regarding applied problems, the nuclear data may be helpful for obtaining new isotopes for medicine, electronics and industry, as well as for improving gamma-ray activation methods and creating new neutron sources.

These estimates and calculations were done to develop and continue programs on nuclear data at the basic facilities of FLNP JINR including the IBR-2 research reactor, new neutron source IREN and electrostatic generator EG-5.

Activities within the n_TOF collaboration, CERN

In 2017, within the framework of the TOF-collaboration at CERN with the participation of FLNP specialists, the precision measurements of the neutron capture cross section of fissioning nuclei $^{235,236,238}U$ [13-15], ^{240}Pu [16] and ^{241}Am [17] were performed for a wide range of neutron energies. This work is necessary for the design and licensing of a new generation of nuclear reactors. The experiments were carried out with isotope targets ^{7}Be [18] and ^{33}S [19], which are important for clarifying the nucleosynthesis scenario.

Activities within the framework of TANGRA project

Determination of physical characteristics of gamma-detectors and optimal geometry of BGO-based detector system

In 2017, the detector system of the TANGRA facility was upgraded, which involved the replacement of gamma-ray detectors based on NaI crystals with more efficient BGO crystal detectors. Each detector is a scintillation assembly consisting of a BGO crystal (76 mm in diameter and 65 mm thick) and Hamamatsu R1307 photomultiplier. In total, there are 24 detectors which can be arranged in different geometric configurations relative to the target depending on the problem being solved.

The physical characteristics of the system, such as resolution, efficiency, optimum operating voltage for the new detectors were tested.

To determine the operating voltage and test each detector of the new system, a specialized test setup was constructed (**Fig. 3-13**). Calibration sources ^{137}Cs (E_γ – 662 keV), ^{60}Co (E_γ – 1127 keV and 1332 keV) were placed in the center. The voltage was varied from 800 to 1500 V; the upper limit was selected according to the photomultiplier specifications.

Fig. 3-13. First test geometry for BGO-based detectors.

The optimum operating voltages at the photomultipliers of all detectors were selected on the basis of the experimentally obtained dependences of the amplitude of detector signals on the applied high voltage. The energy and time resolution of the detectors were also determined for the energies of gamma-rays emitted by the calibration sources and for the lines of ^{12}C (4.43 MeV), ^{14}N (5.1 MeV) and ^{16}O (6.13 MeV).

To determine the optimal geometric configuration of detector arrangement, various configuration variants were tested. **Figures 3-14 and 3-15** show different configuration variants with 10 detectors with and without a collimator.

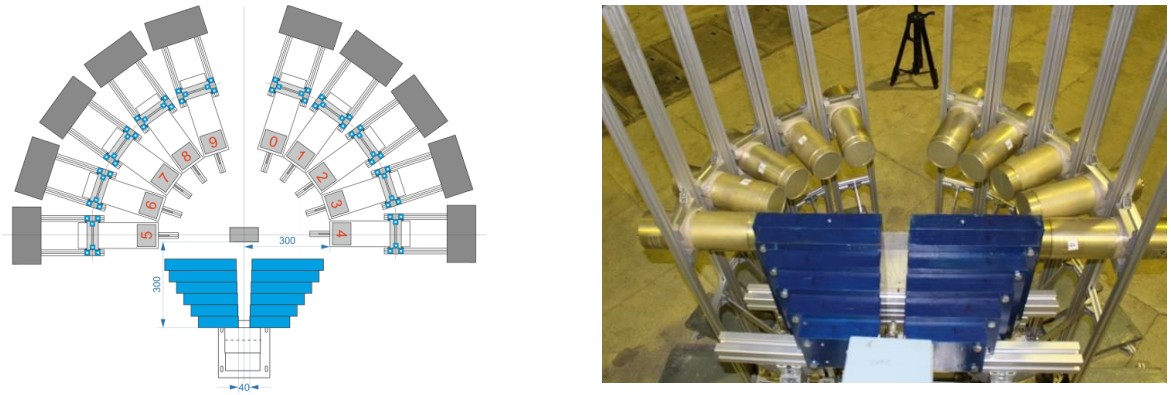

Fig. 3-14. System with 10 detectors, configuration variant "A" – compact geometry with a collimator.

a) *b)*

Fig. 3-15. a) *System with 10 detectors, configuration variant "B" – compact geometry with a collimator, detectors are located at a distance of 100 cm from the sample position; b) System with 10 detectors, configuration variant "C" – compact geometry without a collimator, detectors are located at a distance of 100 cm from the sample position.*

The result of the test measurements with a carbon target for three presented variants is shown in **Fig. 3-16**.

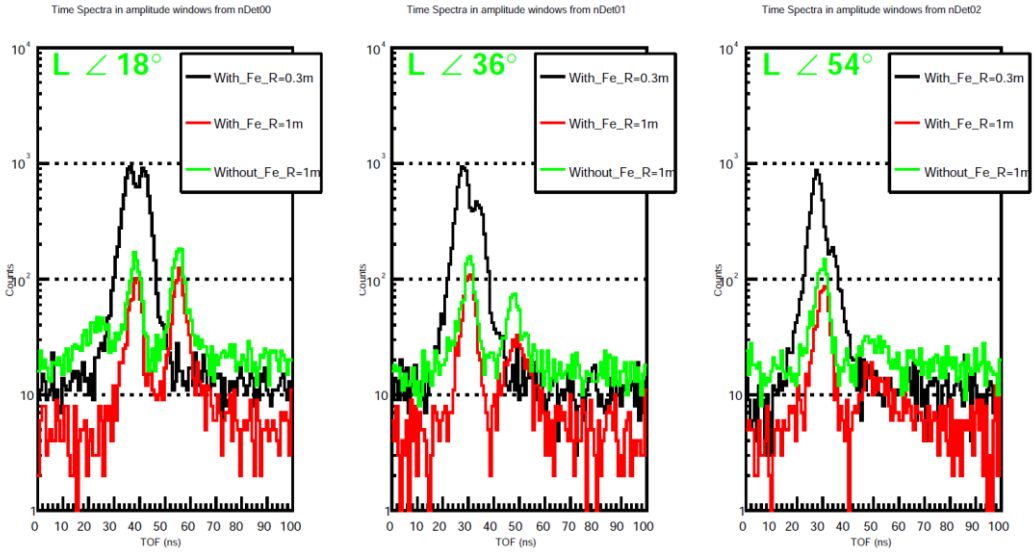

Fig. 3-16. *Time spectra of signals coming from gamma-detectors.*

It can be seen from the figure that at a target-to-detector distance of 100 cm (green and red curves), the time-of-flight separation of neutrons and gamma-rays is much better than for the compact arrangement of the detectors (black curve). But the number of events registered during the same time period decreases by almost an order of magnitude. At the same time, the comparison of measurements for a distance of 100 cm with and without a collimator (red and green curves) shows that at such large distances the collimator is no longer needed. This allows one to position the target under study as close as possible to the neutron generator, thus achieving a gain in statistics due to a higher neutron flux on the target. Further test measurements together with simulations showed that the detector-sample distance of 65 cm is sufficient for effective separation of neutrons and gamma-rays by time of flight, while the statistics acquisition rate increases by almost an order of

magnitude as compared to the old configuration with NaI-based detectors. The final geometry of the facility involves the use of 36 tagged neutron beams and 18 BGO-detectors (**Fig. 3-17**).

Fig. 3-17. *Schematic of TANGRA experimental facility: 1 – generator ING-27, 2 – target, 3 – target holder, 4 – aluminum frame, 5 – support for gamma-ray detector, 6 – gamma-ray detector.*

Determination of the position of a tritium target and direction of tagged neutron beams using a 2D silicon strip detector

One of the criteria of correct measurement of neutron beam profiles can be the experimental determination of the position of a tritium target in the ING-27 neutron generator, as well as the comparison of the obtained results with the specification data stated in the generator certificate. A 2D strip silicon profilometer consisting of 16 crossed strips (8 vertical and 8 horizontal strips) producing 64 square zones (pixels) with sides of 15 mm was used as a neutron detector. The detector and preamplifiers were placed in an aluminum housing equipped with a support, which makes it possible to easily move the profilometer in vertical and longitudinal directions. The neutron detection by the profilometer is done by detecting protons and alpha particles produced in the reactions ^{28}Si(n,α)^{25}Mg (reaction energy threshold B_α = 9.985 MeV) and ^{28}Si(n,p)^{28}Al (B_p = 11.586 MeV), which, in its turn, imposes restrictions on the minimum energy of detected neutrons.

To accomplish this task, a number of measurements were made, in which the distances from the end face of the ING-27 neutron generator to the profilometer varied in the direction of the neutron beam, Z. **Figure 3-18a** shows the distribution of tagged beams obtained at a distance of 10 cm from the generator. When the distance from the generator to the profilometer is changed, this distribution also changes, which makes it possible to plot the position of the centroid of the tagged beam (**Fig. 3-18b**) as a function of the distance and thus determine the trajectories of neutrons composing the tagged beam. The result of this procedure for one Y-coordinate is presented in **Fig. 3-18c**.

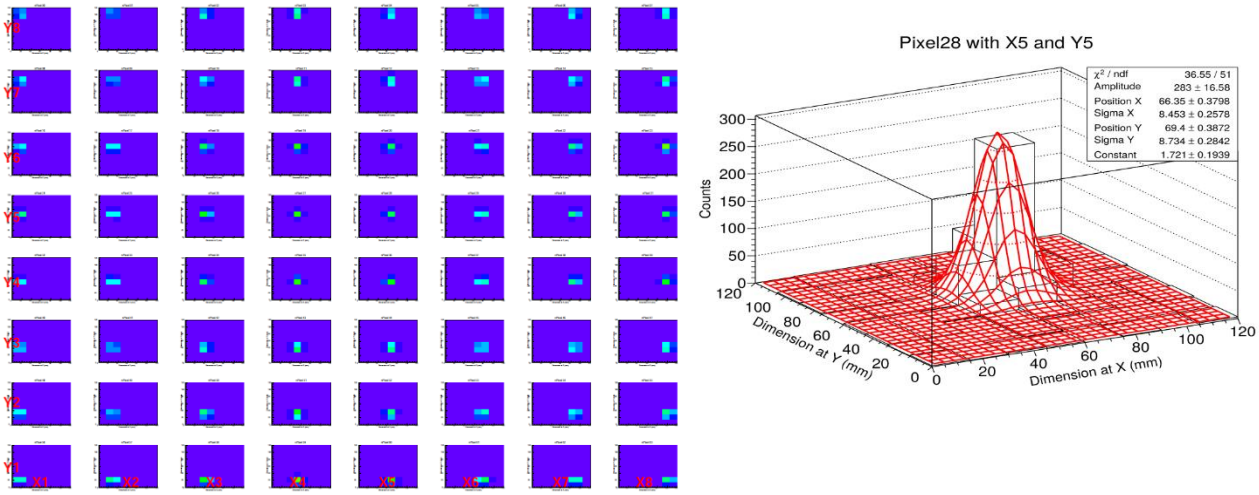

a) *b)*

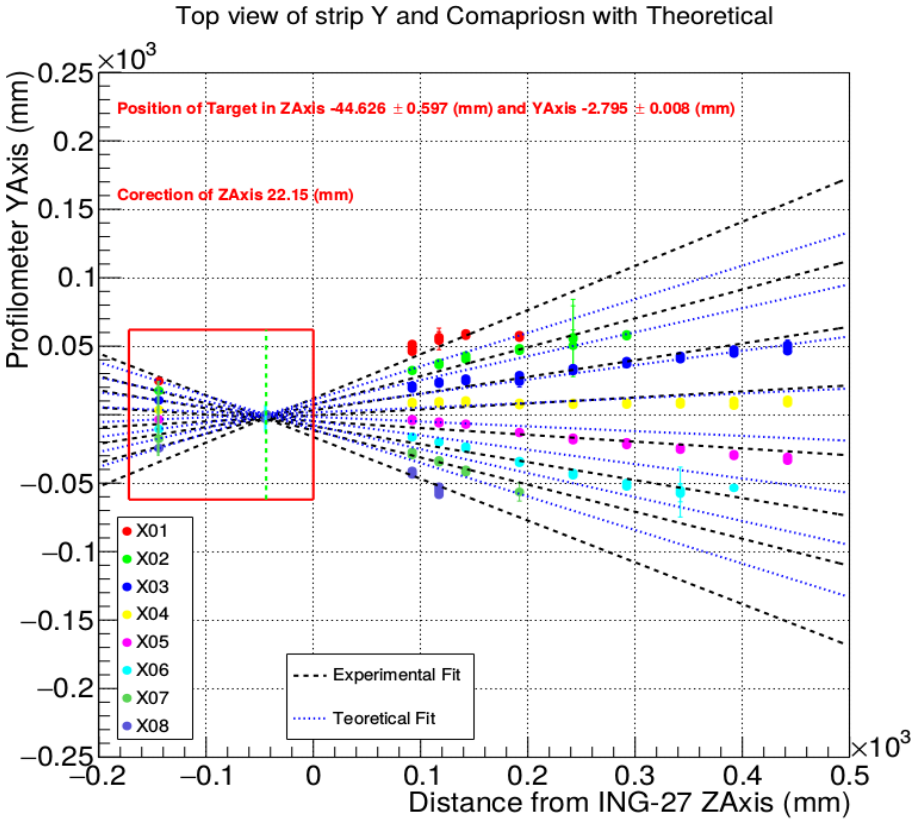

c)

Fig. 3-18. a) Distribution of tagged beam profiles obtained in the described experiment. b) 2D approximation of position of tagged beam. c) Neutron trajectories estimated by centroids of tagged beams in XZ plane (X-strips are summed).

Calculation of angular distribution of gamma-radiation emitted in the process of inelastic neutron scattering by atomic nuclei

The search for a correct theoretical description of angular distributions of gamma-rays emitted by nuclei as a result of inelastic neutron scattering is an important problem to be solved in the course of studying inelastic neutron scattering. The available experimental data differ from each other quite a lot, and theoretical predictions could significantly improve the situation in this area. In addition, information on the relationship between the easy-to-measure angular distribution of gamma-rays and properties of the nucleus is of importance for obtaining information about the nuclear structure.

The process of inelastic neutron scattering by nuclei can be described in two fundamentally different approaches, namely using the direct reaction approximation or the compound nucleus approximation.

As a "first step", it was decided to perform calculations within the framework of the compound nucleus model, because, first, this approach is much better described in the literature than the alternative model, and, second, there is evidence of "impurity" in the complex mechanism of the scattering of fast neutrons by light nuclei [20].

To calculate the angular distribution of gamma-rays emitted in inelastic scattering, the following model was proposed: a neutron hits the target nucleus, which captures the neutron and as a result, makes a transition to an excited state; then it emits a neutron, and the residual excitation is removed by emitting a gamma-ray. The scheme of this process is shown in **Fig. 3-19**.

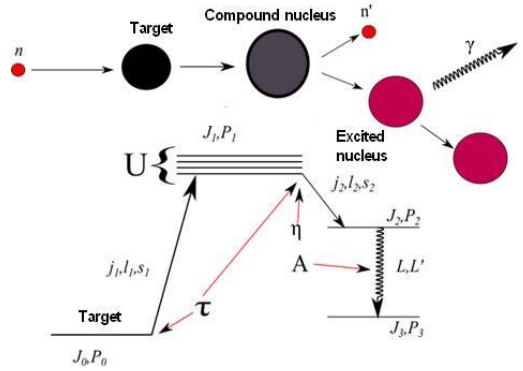

Fig. 3-19. *Scheme of inelastic scattering process.*

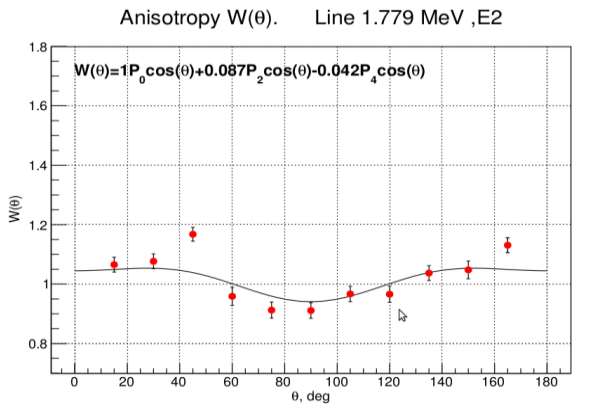

Fig. 3-20. *Comparison of the results of calculations with experimental data for ^{28}Si, E_γ = 1.779 MeV, transition E2.*

The results obtained for light nuclei are in poor agreement with the experimental data (**Fig. 3-20**), which, in principle, is expected, since the fraction of processes which occur with the formation of compound nuclei is small for light nuclei.

Measurements of the probability of small heating and total losses of UCN on the surface of Fomblin oil

New processing of the results from the measurements (made by us in 2011-2015) aimed at studying the UCN interaction with the surface of Fomblin oil was performed. The new processing gave a higher accuracy in determining the probability of small heating on Fomblin.

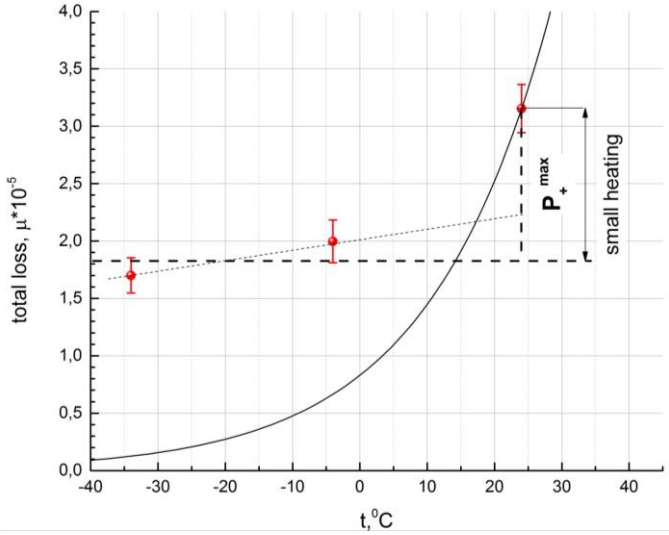

Fig. 3-21. *Upper limit of probability of UCN small heating on Fomblin. Red points follow the temperature dependence of total UCN losses; solid line shows the temperature dependence of probability of UCN small heating.*

The main result is the following: if earlier, when measuring the probability of small heating, we could speak only about its lower limit, now, on the basis of the comparison of the results from these measurements with the probability of total UCN losses, one can also speak about the upper limit of the probability of small heating (**Fig. 3-21**).

The probability of small heating of UCN on Fomblin at 240°C is in the range of $(1.05 \pm 0.02_{stat}) \times 10^{-5} - (1.31 \pm 0.24_{stat}) \times 10^{-5}$. In addition, it can be stated that since the spectra of heated UCN are the same for all the substances measured, the upper limit of the probability of small heating for all these substances is about 1.3 times higher than the lower limit.

Development and manufacturing of a ^{10}B monitor of thermal neutrons

The putting into operation of a new type of UCN source being developed by a group of FLNP specialists will make it possible to increase the UCN flux density by three orders of magnitude in comparison with the existing sources. In particular, this will provide higher accuracy for measurements in the traditional for UCN experiments. For example, it will be possible to measure the neutron lifetime with accuracy better than 0.1 s. An increase in the statistical accuracy requires more attention to systematic errors of measurements. One of the sources of systematic errors in the measurements with UCN is the detection systems used.

For UCN detection, proportional ^{3}He-gas counters with a thin entrance window of Al or Ti (often with a seal made of polymeric materials) are usually used. Our studies have shown that ^{3}He can diffuse through the polymeric seals of the windows and get into the UCN storage volume. This can lead to systematic errors in the measurements, which are difficult to be taken into account. A UCN detector with Teflon seal can lose up to 15% of ^{3}He per year, with Viton seal - up to 3% of ^{3}He per year. Metal window seals are also not reliable enough, because can lead to microdamages of window foils.

A radical solution of the problem of ^{3}He penetration into the UCN storage volume is the replacement of ^{3}He with another sensitive element.

The existing UCN detectors usually have a thickness of ~ 5 cm, small number of wires and use charge-sensitive preamplifiers. They provide a maximum count rate of ~10^3-10^4 s^{-1}. For the new UCN source, it should be increased by two-three orders of magnitude.

To test the manufacturing technology and verify the specified characteristics of such a detector, we designed and manufactured a thermal neutron monitor with ^{10}B sputtered on the rear wall. The monitor is a multiwire proportional gas counter coated with B_4C (^{10}B enrichment 85%) with a thickness of 0.2 μm. The thickness of the working area of the monitor is 12 mm. The reaction used to detect neutrons is:

$$^{10}B+n \rightarrow^{(93.7\%)} \alpha(1.47MeV) + {}^{7}Li(0.84Mev) + \gamma(0.48MeV)$$
$$\rightarrow^{(6.3\%)} \alpha(1.78MeV) + {}^{7}Li(1.01MeV) \qquad \sigma = 3835\ b$$

The detection efficiency for neutrons with a wavelength of $\lambda = 2$ Å is 1×10^{-2}, which provides the probability of UCN detection close to 100%. It was shown that a monitor equipped with a fast current preamplifier can provide a count rate of up to 10^6 s^{-1}.

Neutron diffraction by a moving grating

In the FLNP Annual Report for 2016, we reported about the experiment carried out at the Institute of Laue-Langevin that year. Its purpose was to verify the theoretical prediction that at a certain height of the profile of a moving grating a substantial suppression of the zero-order diffraction is possible with a corresponding increase in the intensity of the peaks of other orders. If this prediction is true, then one can increase the efficiency of energy transfer to the neutron during diffraction on a moving grating by choosing the grating profile.

A new grating, prepared as before, on the periphery of a silicon disk had 84000 radial grooves with a profile depth of 0.22 μm, in contrast to the previously used grating with a profile depth of 0.14 μm.

Basing on the results of the study of the grating profile by atomic force microscopy (ACM) reported in 2016, we indicated that the teeth and grooves of this grating have not a rectangular but a substantially trapezoidal profile. The comparison with the spectrum obtained for a grating with a smaller profile depth supported the prediction that the zero-order intensity can be significantly suppressed (**Fig. 3-22**). This was the main result of this experiment.

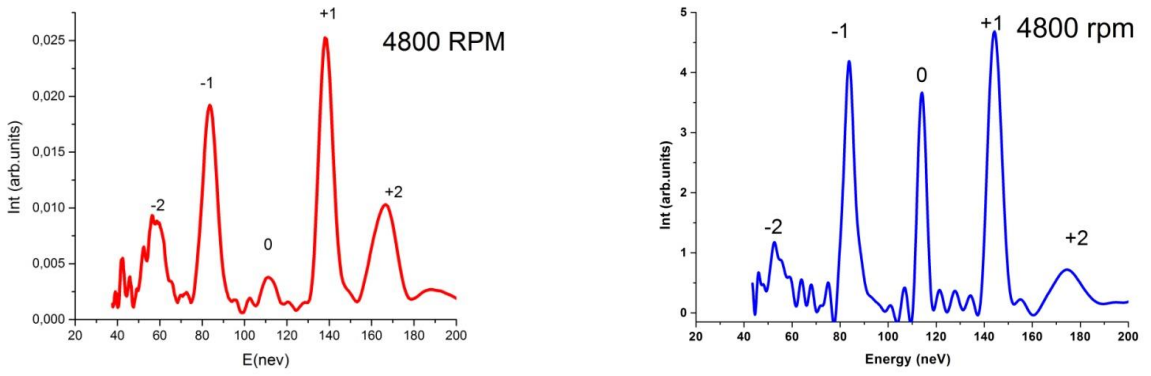

Fig. 3-22. Neutron diffraction spectra from a moving deep-profile grating (at the left) in comparison with the previously measured spectrum for a grating with a smaller profile depth (at the right). It can be seen that the zero-order intensities differ significanlty.

At the same time, the experimental spectra were not in satisfactory agreement with the results of the calculation based on the AFM data. The reason for this discrepancy was not entirely clear, and, as noted in the report, a more detailed analysis was required to clarify it. In 2017, the corresponding work was carried out, which enabled us to answer previously raised questions.

First, the analysis of the AFM data and consultations with specialists brought us to the conclusion that the data most likely were erroneous. Repeated measurements with the same AFM in ESRF (Grenoble) yielded different results, and the source of the previous methodological error was found. The new results showed that the grating profile is much closer to a rectangular one than was previously thought.

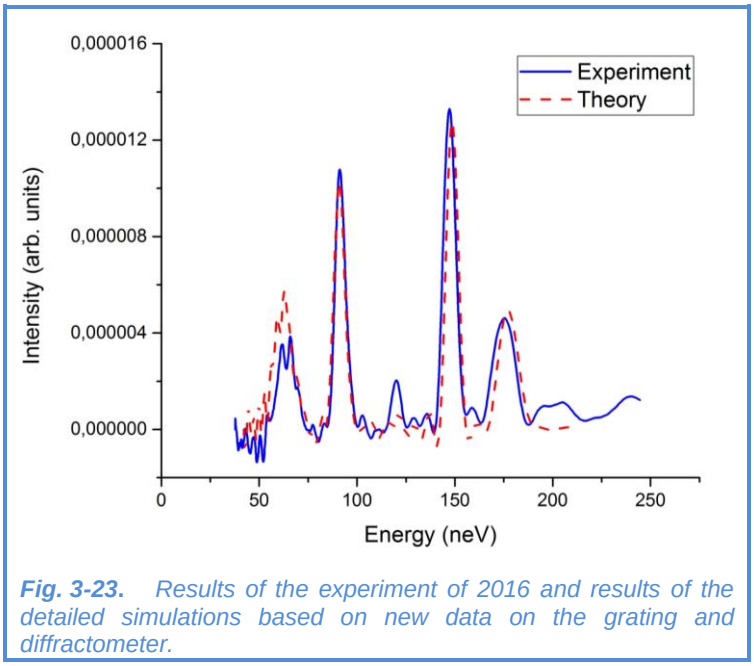

Fig. 3-23. *Results of the experiment of 2016 and results of the detailed simulations based on new data on the grating and diffractometer.*

Second, we performed detailed Monte-Carlo simulations, which made it possible to reveal a number of systematic effects of the time-of-flight Fourier diffractometer used in the experiment. The detailed simulation of the experiment based on the dynamic theory of diffraction from a moving grating, new AFM data and realistic diffractometer parameters led us to the result that was in satisfactory agreement with the experiment (**Fig. 3-23**). Thus, all the uncertainties in the interpretation of the experiment of 2016 were removed.

Preparation of the experiment on the observation of the interaction of UCN with an oscillating barrier under giant accelerations

The purpose of the upcoming experiment is to check up the validity of the model of the effective potential under giant accelerations of the sample. An important step in the preparation of the experiment is quantum calculations of the interaction of the neutron wave packet with a potential structure oscillating in space at different magnitudes of the maximum acceleration of the object $w_{max} = A(2\pi f)^2$, where A and f are the oscillation amplitude and frequency, respectively.

Design of sample-resonator

The realization of the experiment requires samples with the surface oscillating at a frequency of the order of 2 MHz without significant deformation. To solve this problem, an approach employing a bulk half-wave quartz resonator was used. The resonator is a quartz plate about 3 cm in diameter and 270 μm thick, which corresponds to half the wavelength of ultrasound in quartz. Thin aluminum films serving as electrodes are deposited on flat surfaces of the resonator. When the alternating voltage is applied to the electrodes, the sample is deformed, and the deformation value reaches its maximum in resonance. The amplitude-frequency characteristic of the sample has a rather complex

structure, which is indicative of the presence of multiple oscillation modes.

In 2017, for experimental investigations of the resonator, a special stand—vibrometer—for mapping the surface of an oscillating sample was constructed (**Fig. 3-24**). It consists of a laser interferometer and two-coordinate table. For successful operation of the device and the analysis of the results, special computer software was developed. The device allows us to measure the shape of the surface in simultaneous synchronization with the phase of the sample movement. The measurement of the surface profile of the resonator oscillating at a resonant frequency of the order of 2.1 MHz showed that the sample surface does not remain flat and various fragments of the sample oscillate in antiphase forming a complex spatial structure (**Fig. 3-24**).

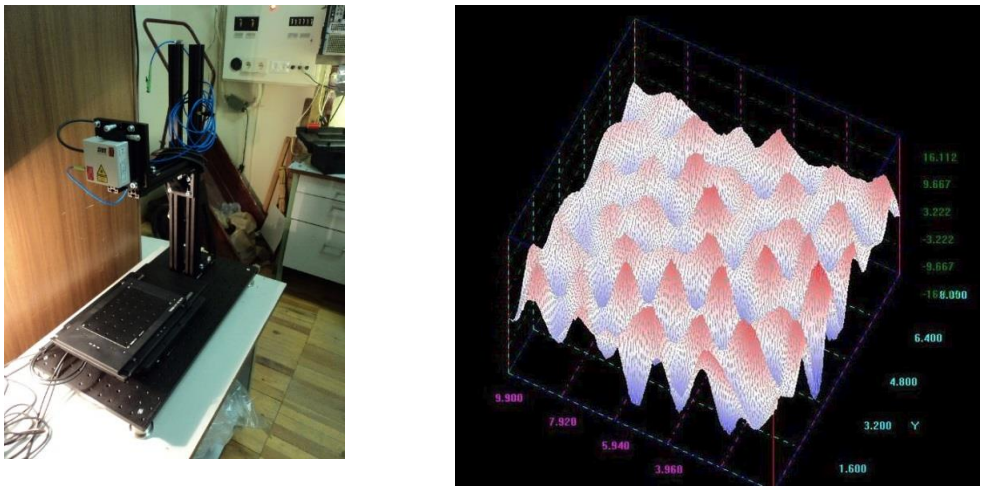

Fig. 3-24. *2D laser vibrometer (at the left) and instantaneous state of the resonator surface oscillating at 2.1 MHz.*

At present, the possibility for computer calculations of the deformation of piezoelectric resonators is considered, which is quite a challenge. These calculations will make it possible to find the best sample configuration.

Quantum calculations of nonstationary neutron-optical effects

In parallel with the work on the creation of the sample, we carried out investigation of UCN interaction with a potential structure oscillating in space with a high frequency. In the absence of the theory of dispersion of neutron waves in an accelerating substance, a quantum nonstationary problem of neutron interaction with an oscillating potential structure, based on the ordinary dispersion law is under study. Since it was previously shown that in the simple case of an oscillating potential barrier oscillating with the necessary frequency and amplitude, the non-stationary effects for the transmitted state are very

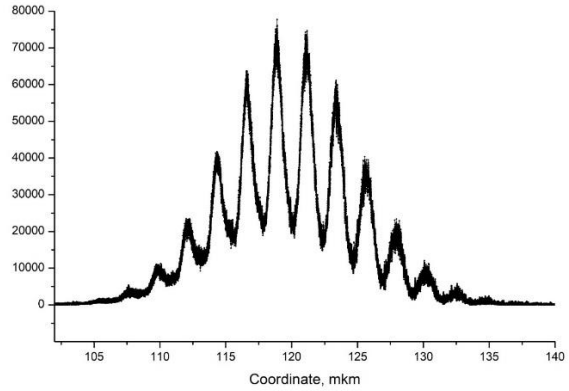

Fig. 3-25. *Structure of a wave packet after passing through a resonance structure oscillating in space. Results of quantum calculations.*

small, we considered an approach in which neutrons pass through an oscillating resonance structure consisting of two barriers with a well between them. Calculations based on the method of splitting the evolution operator demonstrated again significant oscillation of the neutron flux passing through such a structure (**Fig. 3-25**). This geometry was selected as a priority for further research.

At the same time, the analysis of the obtained results has raised a number of questions. At present, it is not entirely clear whether they are connected with the calculation errors or are a manifestation of not yet fully understood details of the phenomenon. The work will be continued using the resources of the LIT JINR cluster (Hybrilit).

Neutron diffraction from surface ultrasonic waves

Previously in 2017, in collaboration with IPTM RAS (Chernogolovka) and the Max Planck Institute (Munich, Germany), an experiment was performed to observe neutron diffraction from surface ultrasonic waves. This work extended a relatively short list of non-stationary quantum experiments with neutrons.

In 2017, considerable theoretical work was done to study the diffraction of neutron waves from stationary and moving gratings with a sinusoidal profile, as well as also from a standing surface wave.

Applied research

Application of resonance neutrons for the search for palladium in the engine components of the Proton rocket

The IREN facility makes it possible to perform time-of-flight experiments to determine the elemental and isotopic composition of samples by characteristic neutron resonances. The cross section for the interaction of neutrons with matter in the neutron energy region from fractions of eV to hundreds of keV has a pronounced resonance structure, and the position of neutron resonances, as well as their intensity (the area under the resonance) are unique for each element, which allows us to identify various elements and their isotopes with high accuracy. The sensitivity of the method is different for different elements and depends on a number of factors (the presence of resonances in the required energy region, neutron cross-section value in resonances, presence of background resonances from other elements in the same region, etc.). Neutrons have great penetrating power; therefore, the method makes it possible to analyze rather massive samples and requires no preliminary preparation, cutting, etc.

Palladium is one of the elements for which the resonance method works particularly well, because for this element very strong resonances are observed in the energy range up to 100 eV (where the sensitivity of the method is high), which makes it possible to determine the presence of palladium even in very small amounts.

In the experiment, we investigated gas generator components of the engine of the second and third stages of a Proton heavy-lift rocket, comprising soldering with a significant content of palladium. The presence of palladium in these components is an indicator of faults in the technological process of manufacturing of the engine, which can lead to an accident. To detect palladium in the samples provided by Roscosmos, they were placed in a neutron beam inside the "ROMASHKA" scintillation spectrometer consisting of 24 NaI(Tl) crystals.

First we made measurements with a sample consisting of pure metallic palladium. **Figure 3-26** shows a time-of-flight spectrum of a 5-g palladium sample, which was obtained at our facility at a measurement time of 1 hour. The observed resonances correspond to the known tabulated values for various palladium isotopes.

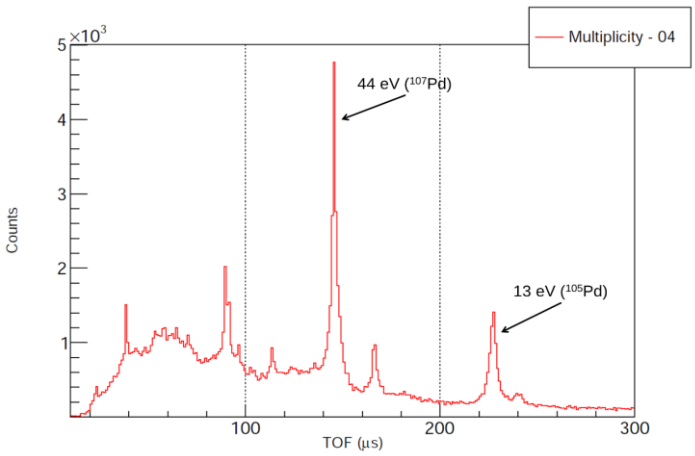

Fig. 3-26. *TOF spectrum of a palladium sample with a mass of 5 g.*

The measurements were carried out at a flight path of 11.2 m. The operating mode of the IREN facility: pulse repetition rate – 25 Hz, electron pulse duration ~ 100 ns, peak beam current – 1-1.5 A, electron energy ~ 50 MeV. The integral neutron yield is ~ $3 \cdot 10^{11}$ s^{-1}. To control the neutron flux intensity, we used a neutron counter placed directly at the beam entrance to the experimental hall.

To test the possibility of determining the presence of a palladium-containing solder by this method, we used two parts of the sample (about 60 g each) provided by Roscosmos. The palladium-containing solder was found only in sample 1. The presence of palladium in sample 1 and its absence in sample 2 were tested by X-ray fluorescence analysis at the Institute of Physical and Technical Problems.

To detect gamma rays emitted by the irradiated target, we used a system of 24 NaI(Tl) gamma-spectrometers (“ROMASHKA"). To reduce the number of neutrons arriving at gamma-detectors, a cylinder of boron carbide was installed inside the "ROMASHKA" setup. In addition, for the same purpose a collimator made of borated polyethylene was placed immediately in front of the entry point of the neutron beam. The irradiated samples were suspended in the center of the detector system.

Figure 3-27 presents time-of-flight spectra for various multiplicities of gamma-rays recorded by the "ROMASHKA" detector system for different samples.

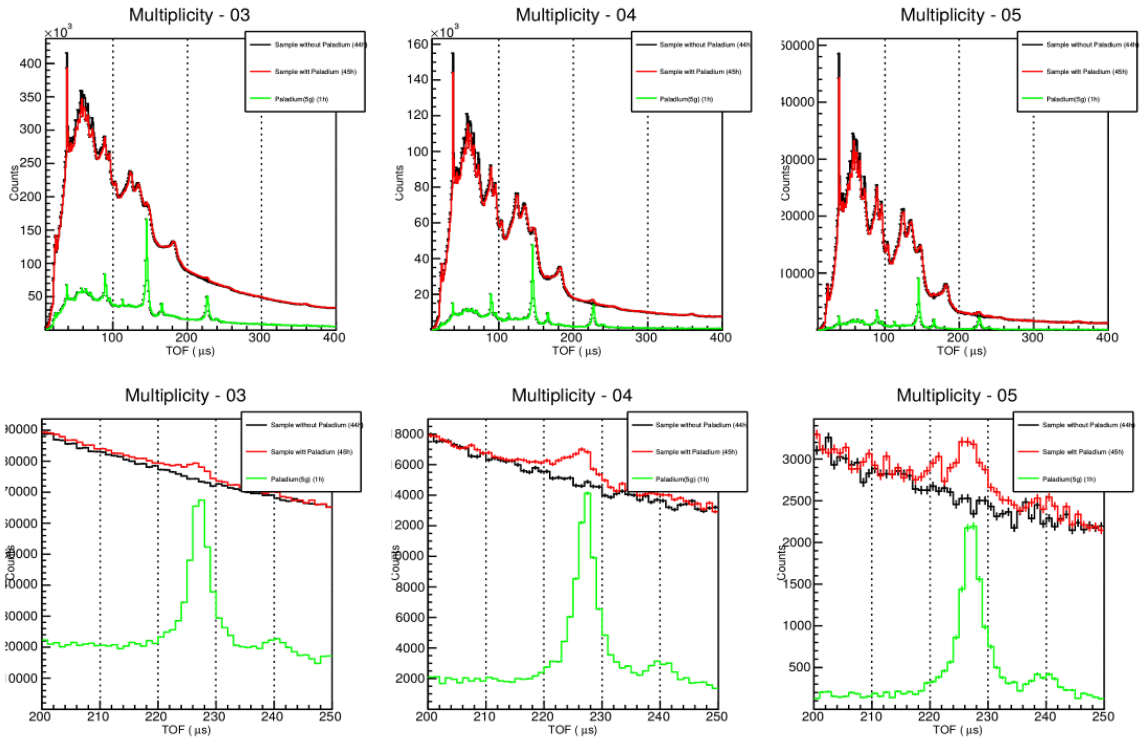

Fig. 3-27. *Top: time-of-flight spectra for various gamma-ray multiplicities corresponding to the analyzed samples: with palladium No. 1 (red), without palladium No. 2 (black) and pure palladium (green). Bottom: parts of spectra in the palladium resonance region of 13 eV.*

These spectra demonstrate that the technique can reliably diagnose the amount of palladium of the order of 100 mg in samples of about 60 g.

Application of the neutron resonance analysis method to investigate the elemental composition of archaeological finds

In 2017, at the IREN facility, experiments were carried out to determine the elemental composition of a number of archaeological atrefacts provided by the Institute of Archeology, RAS (**Figs. 3-28a**, **3-29a**, **3-30**). The studies were done using the neutron resonance capture analysis (NRCA), the main principles of which are described in [21] and in the previous section. A large liquid scintillation detector was used as a γ-ray detector [21].The measurements were made at a 60-m flight path of IREN beamline 3. Some time-of-flight spectra obtained in the measurements are shown in **Fig. 3-28b** and **3-29b**.

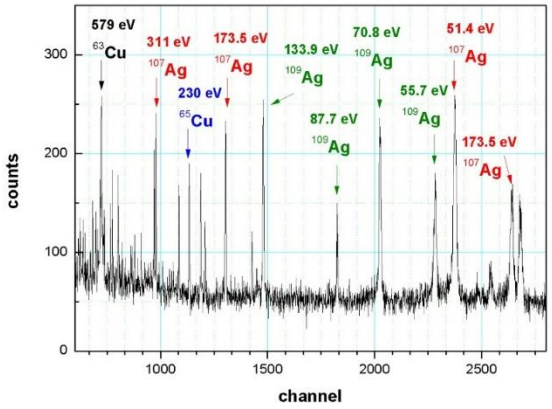

a) ***b)***

Fig. 3-28. *a) Coins (Bosporus staters) from the Phanagoria's treasure (3rd century AD).b) Part of the time-of-flight spectrum from the radiative capture of neutrons obtained in measurements with coins from the Phanagoria's treasure.*

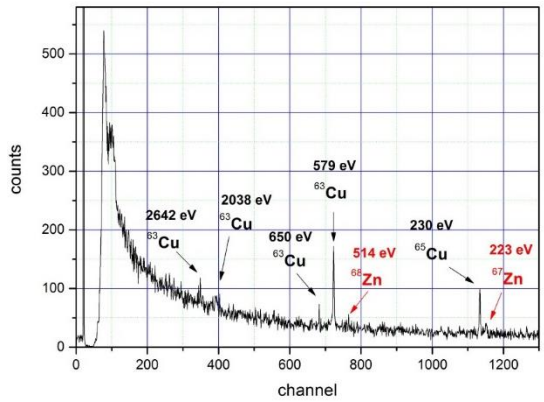

a) ***b)***

Fig. 3-29. *a) Fibula from the Podbolotievsky burial ground, Vladimir region (10th century AD). b) Part of the time-of-flight spectrum from the radiative capture of neutrons obtained in measurements with a fibula.*

Fig. 3-30. *A silver medallion and zoomorphic figurine (information on the location and age of the finds have not yet been provided).*

For the quantitative determination of elements in the objects under study we used a relative method — additional measurements were made with samples with the known parameters, containing the identified elements. The preliminary results on the study of staters and fibula are presented in **Table II**.

Table II. The content of elements from time-of-flight spectra of the objects under study.

	Weight, g	Cu, g	Zn, g	Ag, g	Au, g
Coins	73.033	62.0 ± 3.1	-	6.762 ± 0.086	-
Fibula	19.98	13.5 ± 1.5	1.06 ± 0.39	-	0.0171 ± 0.0027

The errors listed in Table II take account of only statistics of registered events. At present, studies are underway to identify possible sources of systematic errors in the analysis and estimate their values.

The applied analytical research method is quite new for FLNP. However, as can be seen from the preliminary results, it could find application in the study of unique objects of archeology and cultural heritage, since it is absolutely non-destructive, requires no special sample preparation procedures (for example, cleaning from patina), and leaves practically no induced radioactivity in objects under study.

Analysis of human remains from the necropolises of the Moscow Kremlin

A neutron activation analysis (NAA) of three samples of human remains of the 16th and 17th centuries from the necropolises of the Moscow Kremlin has been carried out at FLNP JINR. The samples were irradiated at two facilities: the IREN source of resonance neutrons and the IBR-2 reactor. Spectra of the induced activity of the irradiated samples were measured using the automatic measurement system developed in FLNP JINR. This system consists of a high-purity germanium detector with spectrometric electronics, a sample changer, and control software. Mass fraction of arsenic, mercury, and some other elements were calculated using two NAA methods—relative and absolute (**Table III**).

Table III. Mass fractions of arsenic and mercury in the samples.

№ sample	Arsenic (As)		Mercury (Hg)	
	Mass fraction, mg/kg	Relative error, %	Mass fraction, mg/kg	Relative error, %
1	0,19	30	0,36	19,1
2	0,23	30	0,2	29,5
3	1,18	18,3	46,6	2,5

The obtained values confirm the fact of acute mercury poisoning of Anastasia Romanovna, the first wife of Tsar Ivan the Terrible (sample 3, fragment of hair). High levels of mercury were detected in the bone remains of Tsarevich Ivan Ivanovich (sample 1, **Fig.3-31**), the son of Tsar Ivan the Terrible, and Prince Mikhail Vasil'evich Skopin-Shuiskii (sample 2).

Fig. 3-31. Sample №1 after cleaning.

The results provide an opportunity to introduce into scientific circulation the exact values of mass fraction of mercury, arsenic, and other elements in the samples taken from the burials of the Russian historical figures of the second half of 16th–early 17th century.

Analytical investigations on charged particle beams of the EG-5 accelerator

In 2017, the EG-5 electrostatic accelerator operated for 515 hours. The elemental depth profiles of near-surface layers in various samples were studied using a variety of nuclear-physical analytical techniques including Rutherford backscattering (RBS), elastic recoil detection (ERD) and particle induced X-ray emission (PIXE).

In cooperation with the Lebedev Physical Institute of the Russian Academy of Sciences the process of accumulation and redistribution of deuterium and hydrogen atoms in the assemblies of two high-purity zirconium and titanium foils under high-temperature pulsed action of deuterium plasma at the PF-4 plasma focus setup was studied. Using analytical methods, namely Rutherford Backscattering Spectrometry (***RBS***) and Elastic Recoil Detection (***ERD***), it was found that the redistribution of implanted deuterium and hydrogen gas impurities in the assemblies of irradiated foils occurs to great depths that far exceed the ranges of deuterium ions. The observed phenomenon can be explained by the redistribution of the implanted deuterium and hydrogen under the influence of powerful shock waves formed in the metal foil under the action of high-temperature pulsed plasma.

In cooperation with Maria Curie-Skłodowska University (Lublin, Poland), a large amount of research has been conducted on the effect of heavy ion implantation on the optical properties and chemical composition of near-surface layers of GaAs crystals. The investigation of the complex dielectric function in the near-surface layers was carried out using the ellipsometry technique. The chemical composition of the surface layers was studied using the X-Ray Photoelectron Spectroscopy (XPS) technique. The investigation of the real and imaginary parts of the dielectric function and of the atomic and chemical composition was performed near the surface of GaAs crystals implanted with indium ions at an energy of 250 keV and a dose of $3 \cdot 10^{16}$ cm^{-2}. The influence of heat treatment in the temperature range 400°C-900°C on the structure and optical properties of GaAs crystals implanted with indium ions was also investigated. A series of studies was made of the effect of implantation of Ne, Ar, Kr, Xe ions at an energy of 100 keV and doses from $1 \cdot 10^{12}$ cm^{-2} to $3 \cdot 10^{15}$ cm^{-2} on the change in the dielectric function and atomic composition in the surface layer of GaAs crystals.

The effect of fluence and the mass of implanted ions on the optical properties and chemical composition of the near-surface layers of implanted GaAs(100) crystals was studied as well. Depth profiles of heavy elements in these studies were measured using the RBS technique. To study the oxygen content in the surface layers subjected to heavy ion implantation, the resonant scattering of helium ions with an energy of 3,045 MeV by oxygen atoms (NRA technique) was used, which ensured a high accuracy in measuring depth profiles of oxygen in the samples under study.

In cooperation with the Institute of Electrical Engineering of the Slovak Academy of Sciences we investigated the structural, magnetic and electrical properties of $La_{0.67}Sr_{0.33}MnO_3$ epitaxial films grown on (001) $SrTiO_3$ crystalline substrates. Depth profiles of various elements in silicon carbide samples prepared by Plasma Enhanced Chemical Vapour Deposition (PECVD) were studied using RBS and ERD techniques. The characteristics of these samples ensured their use for various applications, such as the absorption of electromagnetic energy in the spectral region of 0.1 - 2.0 THz, the creation of transparent photocathodes by depositing a film on a quartz glass substrate, as well as providing the possibility of using layered structures in the aggressive environment.

Analytical investigations at the IBR-2 reactor

In 2017, the REGATA facility was used for multi-element instrumental neutron activation analysis of about 1900 environmental samples (vegetation, soil, air filters), a number of technological, biological and archaeological samples, as well as of samples of extraterrestrial origin in the framework of programs and grants of the JINR Member States and Protocols on scientific and technical cooperation with the JINR Non-Member States. Investigations of test samples were conducted for an interlaboratory comparison of the results under the IAEA program. The elemental analysis of ~ 500 samples were performed using a *Thermo Scientific iCE 3500 Atomic Absorption Spectrometer*.

Development of the NAA&AR experimental base at IBR-2

In order to replace aluminum transport containers with containers with less induced radioactivity, new materials were tested by irradiating them in pneumatic transport systems and vertical channels of the reactor. In addition, materials with a sufficiently high radiation resistance and low gamma background of induced radioactivity were chosen to replace the aluminum foil currently used as a packaging material for long radiation exposure. Trial batches of transport containers made of PTFE 40 and various modifications of polyetheretherketone (PEEK) were manufactured. Containers made of PTFE 40 were irradiated for 5 hours, and of PEEK – for 30 hours without significant changes in mechanical properties and, obviously, this is not the limit.

A deionizer and specialized laboratory glassware washer were installed and put into operation for preparation of samples for the atomic absorption spectrometer.

On a low-background detector, long-term measurements of background were conducted to determine possible ways to reduce it. The work is carried out in cooperation with the specialists from Comenius University (Bratislava, Slovakia). To verify the correctness of the calculation of the detector efficiency for different sample geometries, a contract was concluded with VNIIM (St. Petersburg) to manufacture volumetric radioactivity standards.

Work has started on the preparation of documents for gaining accreditation of research activities using NAA. The upgrade of the software for automation of NAA on the basis of the accumulated operational experience is in progress and includes the following steps:

- Several new functions that simplify working with experimental data were added to the "NAA Database" program;
- ClosedXML library was imported to the concentration calculation program to link Microsoft Excel directly with the results of the program;
- FTP-server was reinstalled with the CentOS7 Unix system, which allowed more delicate adjustment of experimental data backup;
- The measurement program is being transferred to the VCS technology, which uses the git version control system and allows flexible versioning of the code to fully control all changes.

The plans for the software development in the Sector include the following activities:

- Modification of the database architecture to optimize data interactions;
- The client part is planned to be transferred under the Web platform to increase the flexibility and usability of the system.

Biomonitoring of air pollution

In 2017, the summing-up of the activities conducted in 2010-2015 in the framework of the international program "Heavy metal atmospheric deposition in Europe – estimations based on moss analysis" was done (Nickel et al., 2017). In cooperation with the Laboratory of Information Technologies of JINR a cloud system was developed to collect, store and process information on biomonitoring of atmospheric deposition of heavy metals and other toxic elements in the framework of the UN Programme on air of Europe (Uzhinskiy et al., 2017; Kutovskiy et al., 2017; Ужинский, Ососков, Фронтасьева, 2017). In 2017, a review on moss biomonitoring of heavy metal air pollution in Romania was published (Stihi et al., 2017). During the reporting period, a number of papers have been published on the analysis of data of atmospheric deposition of heavy metals and other elements in Albania (Lazo, Steinnes et al., 2017), Serbia (Milićević et al., 2017; Vuković et al., 2017). In cooperation with Adam Mickiewicz University in Poznań we started a NAA study of peat columns from Poland to investigate the retrospective deposition of inorganic atmospheric pollutants. The first results have shown the advantages of using NAA in such studies. On the basis of the analysis of moss-biomonitors an important study of the impact of mining, metallurgical and chemical industries as well as agriculture on the environment of the Tula region was performed. The estimates of atmospheric deposition of toxic elements that accompany these types of environmental contaminants have shown that many of the elements indicate the rising levels of pollution as compared with the previous studies (Gorelova, Frontasyeva, 2017). The results of moss and lichen biomonitoring of air pollution in the Western Cape were reported at the conference in Montenegro (Ntombizikhona Beaulah Ndlovu, M. V. Frontasyeva et al., 2017). In cooperation with the Polish specialists, studies were performed to determine the atmospheric deposition of trace elements on the territory of King George Island in Antarctica (Mroz et al., 2017). In cooperation with the Department of Ecological Chemistry of Baku State University, we conducted an assessment study of air pollution on the Absheron Peninsula in Baku, the capital of Azerbaijan (Gajieva, M.V. Frontasyeva, A.I. Madadzada et.al., 2017).

Biotechnologies

In 2017, in cooperation with the microbiologists from the Institute of Microbiology and Biotechnology of the Academy of Sciences of Moldova, work was started on the synthesis of selenium, gold and silver nanoparticles by protein and carbohydrate fractions isolated from cyanobacterial biomass.). In 2017, the studies of processes of extraction of toxic metals from model solutions and wastewater using microalgae *Spirulina platensis* were continued (Zinicovscaia, Cepoi et al. 2017). In collaboration with the A.N.Frumkin Institute of Physical Chemistry and Electrochemistry of RAS we investigated the processes of accumulation and biosorption of metals (vanadium, chromium, uranium, lanthanum) from mono- and multicomponent systems by bacteria *Pseudomonas putida*. The results obtained showed that the concentrations of metals accumulated by the microbial biomass in the process of bioaccumulation were 15-40 times higher than in the biosorption process (Zinicovscaia, Safoniov et al. 2017). In collaboration with the Institute of Experimental Physics, SAS in Košice a study was conducted on the extraction of heavy metals from model solutions using poplar sawdust (Demcak et al., 2017). In cooperation with the Department of Chemistry of University of the Western Cape, South Africa, we studied the problems of green synthesis of silver-doped titanium dioxide used as an antimicrobial agent. The results were reported at the Symposium on Bacterial Genetics and Ecology in Aberdeen, Scotland (N. Kobese et al., 2017). In cooperation with the M.F.Vladimirskiy Moscow Regional Research and Clinical Institute and National Research Center "Kurchatov Institute", studies were started to evaluate the effect of silver nanoparticles on cognitive functions in mice. The neutron activation analysis was used to determine the silver content in liver, blood and brain samples of mice (Ivlieva, ... Zinicovscaia, Pavlov, Frontasyeva., 2017).

Environmental assessment

To continue the work on the assessment of the environmental situation in the basin of the Nile River and its delta, an additional statistical data analysis of the whole amount of the results on soils and sediments was performed (Badawy, E.H.Ghanim et al., 2017) and concentrations of natural and man-made radionuclides in the Nile Valley and its delta were determined (Badawy et al., 2017). In cooperation with the National Research Center in Dokki, Cairo, work was done on modeling the coordination bonds of a number of elements (Na, Mg, Ca, Fe, Ni, and Zn) with organic acids (Okasha et al., 2017). In 2017, NAA studies of coral samples from the Red Sea to assess its pollution by heavy metals and other toxic elements (Abdo et al., 2017) as well as of algae from the coastal aquatic areas of the Mediterranean sea along Alexandria city (Nassar et al., 2017) were carried out in the framework of the Protocol on Cooperation with Cairo University. Within the framework of the pilot project, we performed the analysis of therapeutic muds (peloids) from Cuban SPAs ("Sanus per Aquam", or "Sanitas pro Aqua", which in Latin means "health by means of water" or "health through water").

In collaboration with the A.O.***Kovalevsky Institute of Marine Biological Research*** (Sevastopol) the analysis of the samples of macroalgae-biomonitors (red, green and brown) collected in the coastal zone of the Black Sea for the assessment of the state of the Crimea coastal ecosystem was completed. The study of the seasonal variation of concentrations of 46 elements in phytoplankton of coastal areas of the Black Sea was completed. The obtained results have shown that phytoplankton can be successfully used as a biomonitor of aquatic ecosystems.

SCIENTIFIC HIGHLIGHTS

In 2017, in cooperation with the Faculty of Biology of Moscow State University the long-term (2014-2016) investigation on the determination of the elemental composition of soil, bottom sediments, terrestrial and aquatic vegetation to assess the transport of pollutants in the strategically important areas of the Black Sea (coastal area of Anapa, Novorossiysk and Tuapse) was completed (P.Nekhoroshkov et al, 2017).

Analysis of food products

In cooperation with the specialists of the Moldovan wine industry, geographical origin identification of various wines was performed using a multielement NAA technique (Zinicovscaia, Duliu, Culicov et al., 2017).

Geology

In cooperation with the Western Cape University (South Africa) we conducted a NAA study of new samples of coal fly ash from the Matla coal power station in the Mpumalanga province in South Africa, as well as of soil and vegetation. Soil samples obtained from the Institute of Geology and Geophysics of the National Academy of Sciences of Azerbaijan and the National Center for Nuclear Research of Azerbaijan were analyzed as well. For the first time, the analysis of these samples was performed by the neutron activation method. The obtained data are of great practical interest for the Geological Survey of Azerbaijan.

Analysis of materials of extraterrestrial origin

In 2017, a multielement NAA of ferrous and carbonaceous meteorites received from the United States and Serbia was performed. For the first time, iridium content was determined in exotic clay samples from the famous Fish Clay collected by Serbian scientists at the coastal cliff Stevns Klint in Denmark. Most researchers believe that the Ir enrichment of this clay resulted from the impact of a chondritic asteroid striking the Earth about 65 millions years ago (P.I. Premović, M.G. Đorđević et al., 2017),

Medicinal plants

In 2017, we continued investigations in a new promising line of research – determination of the elemental composition of plants used in medicine. These studies are conducted in cooperation with the specialists from Mongolia and Poland (University of Wrocław and Pedagogical University of Cracow).

Materials science

In 2017, in cooperation with the Scientific and Practical Materials Research Center of the National Academy of Sciences of Belarus, a number of investigations of great practical interest were carried out in the framework of the BRFBR-JINR joint grant including studies on crystallization processes and characterization of artificial diamonds, as well as determination of the impurity composition of copper disulphide obtained at high pressures.

References

[1] Zeinalov Sh.S., Sedyshev P.V., Shvetsov V.N., Sidorova O.V. Prompt fission neutron investigation in $^{235}U(n_{th},f)$ reaction, EPJ Web of Conferences 146,04022 (2017), ND2016.
[2] V.F. Apalin, Yu. N. Gtitsuk, I.E. Kutikov, V.I. Lebedev, and L.A. Mikaelyan, Nucl. Phys., **55**, 249 (1964).
[3] Geltenbort P., Gonnenwein F., and Oed A., Radiat. Effects, 57, 1986.
[4] Gonnenwein F. ISINN25 Dubna 20-25 May 2017.
[5] T. von Egidy and D. Bucurescu, Phys. Rev. C 72, 044311 (2005).
[6] K.-H. Schmidt., and B. Jurado., Entropy Driven Excitation Energy Sorting in Superfluid Fission Dynamics. Phys. Rev. Lett. 104 212501 (2010)
[7] A. Göök, W. Geerts, F.-J. Hambsch, S. Oberstedt, M. Vidali, Sh. Zeynalov. A position-sensitive twin ionization chamber for fission fragment and prompt neutron correlation experiments, Nucl. Instr. and Meth, *A* 830, 366-374 (2016).
[8] Zeinalov Sh.S., Sedyshev P.V. Sidorova O.V., Shvetsov V.N Numerical simulation and experimental investigation of position sensitive ionization chamber, ISINN25 Dubna 20-25 May 2017.
[9] Zeinalov Sh.S., Sedyshev P.V. Sidorova O.V., Shvetsov V.N. Position sensitive ionization chamber for nuclear fission investigation. Accepted in Journal of Modern Physics: Conference Series; available online at www.creteconf.org/presentations/ShZeinalov_Crete2017.pdf
[10] Strutinsky V.M., *in* Proc. International Congress on Nuclear Physics, Paris, France, 1958, p. 617.
[11] Ignatyuk A.V., Report INDC-233(L), IAEA (Vienna, 1985).
[12] Kadmenskij S.G., Markushev V.P. and Furman W.I, Sov. J. Nucl. Phys. **37,** 165 (1983).
[13] Mingrone F., Altstadt S., Andrzejewski J.,et al., High precision measurement of the radiative capture cross section of 238U at the n_TOF CERN facility, EPJ Web of Conferences 146, 11028, Phys. Rev., C 95, 034604
[14] Balibrea-Correa J., E Mendoza E., D Cano-Ott D., et al., Measurement of the neutron capture cross section of the fissile isotope 235U with the CERN n_TOF total absorption calorimeter and a fission tagging based on micromegas detectors, EPJ Web of Conferences
[15] Mastromarco M., Barbagallo M., Vermeulen M.J.,et al., The 236U neutron capture cross-section measured at the n_TOF CERN facility, EPJ Web of Conferences 146, 11054
[16] Stamatopoulos A., Tsinganis A., Colonna N., et al., Measurement of the 240Pu (n, f) cross-section at the CERN n_TOF facility: First results from experimental area II (EAR-2), EPJ Web of Conferences 146, 04030
[17] Mendoza E., Cano-Ott D., Altstad S. et al., Measurement of the 241Am neutron capture cross section at the n_TOF facility at CERN, EPJ Web of Conferences 146, 11022
[18] Barbagallo M., Colonna N., Aberle O., et al., ^{7}Be (n, α) and ^{7}Be (n, p) cross-section measurement for the cosmological lithium problem at the n_TOF facility at CERN, EPJ Web of Conferences 146, 01012
[19] Wright T., Guerrerro C., Billowes J., et al. (The n_TOF Collaboration), The $^{33}S(n,\alpha)^{30}Si$ cross section measurement at n_TOF-EAR2 (CERN): From 0.01 eV to the resonance region, Phys. Rev. C **96**, 064601
[20] B. A. Benetskii, I. M. Frank. Angular correlation between gamma rays and 14-mev neutrons scattered inelastically by Carbon // JETP. —1963. — Vol. 17. — P. 309.)
[21] Bazhazhina N.V., Mareev Y.D., Pikelner L.B., Sedyshev P.V., Shvetsov V.N., Analysis of Element and Isotope Composition of Samples by Neutron Spectroscopy at the IREN Facility.Physics of Particles and Nuclei Letters, Volume 12, No. 4, 2015, pp. 578–583

4. INSTRUMENTATION AT THE IBR-2

DN-6 diffractometer

The straight end section of a 7-m mirror neutron guide was replaced with a focusing device with vertical parabolic geometry for studies of microsamples under extreme conditions (**Fig. 4-1**).

Fig. 4-1. Neutron focusing device with vertical parabolic focusing at the DN-6 diffractometer.

The gain factor in the intensity of the incident neutron beam was estimated to be about four.

FSD diffractometer

On the FSD diffractometer, heating control during experiments with metal samples by electric current up to 800°C (with temperature control) on a mechanical uniaxial testing machine LM-29 became possible. It allows one to study the behavior of structural materials under external uniaxial stresses of both tensile and compressive types, up to a maximum value of 29 kN directly in a neutron beam. This opens up new opportunities for studying thermomechanical characteristics of materials *in situ* when combining external stresses and high temperatures. Special software ReMeSys makes it possible to specify any necessary combination of values of external stress and temperature on the sample under study.

In the framework of tests of the testing machine at FSD, several neutron diffraction experiments were successfully performed with stretching/compressing of samples from constructional materials (steel, alloys) at various temperatures. Thus, for a widespread aluminum alloy D16, the degradation of elastic characteristics of the material subjected to uniaxial tension was studied for different values of the sample temperature (**Fig. 4-2**, a). The accuracy of determination of crystal lattice deformations at the FSD diffractometer proved to be rather high, which made it possible to reliably observe the difference in ε(σ) curves for different temperatures and estimate the changes in the elastic properties of the material as a function of temperature. Using the results of the experiments, it was found that the modulus of elasticity of the material monotonically decreases from 76 to 62 GPa in the temperature range of 13-150°C (**Fig. 4-2**, b). The analogous temperature dependence was also observed for the ultimate strength of the material.

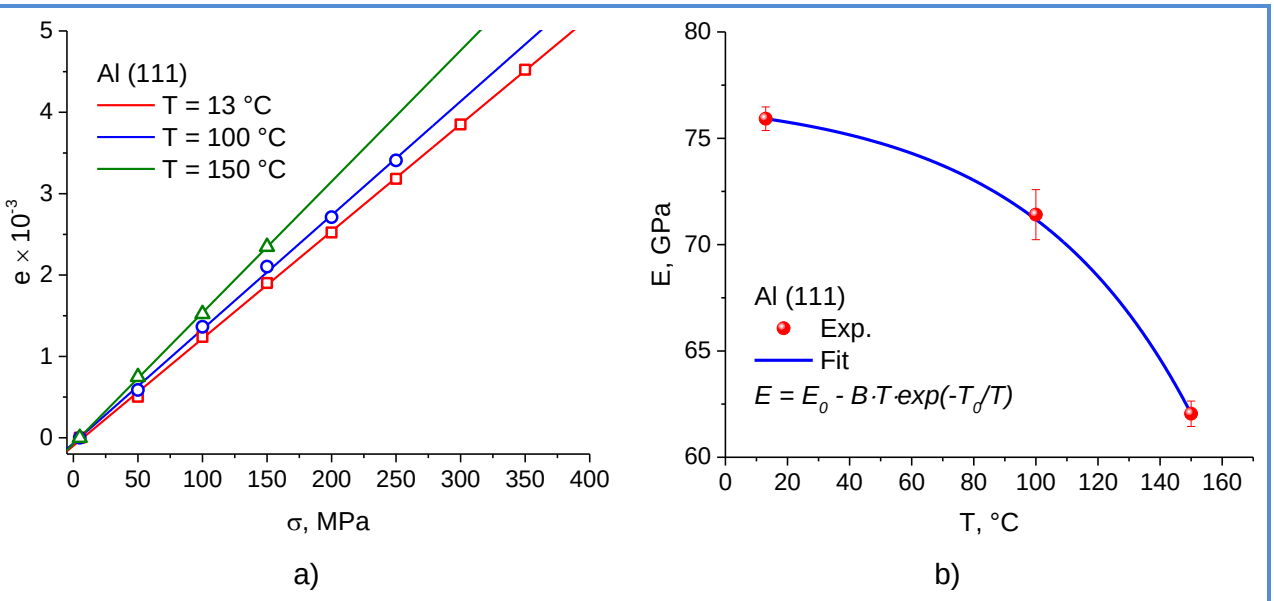

Fig. 4-2. *a) Crystal lattice deformation for peak (111) in aluminum alloy D16 versus the applied stress measured at different temperatures. b) Temperature change in the elastic modulus of alloy D16.*

In addition, on FSD, the work was continued on improving the algorithms for reconstructing diffraction spectra from "raw" data registered in the list-mode. In particular, the version of the algorithm for multi-detector systems was implemented, which allows one to simultaneously reconstruct high-resolution spectra from all connected detectors or detector elements with individual parameters of the time-of-flight scale. This made it possible to realize separate spectrum accumulation and precise electronic focusing for individual elements of the back-scattering detector BS, which resulted in a better line shape and higher detector resolution.

FSS diffractometer

On beamline 13 of the IBR-2 reactor, in cooperation with the SC department, the work on the construction of the FSS Fourier diffractometer is in progress. In 2017, a Fourier-chopper was installed in the mirror neutron guide and put into opertation (**Fig. 4-3, a**). The diffractometer control software on the basis of SONIX+ was installed. The optimum positions of individual photomultipliers of the second 90°-detector West for the new geometry were calculated, followed by the detector assembling and connection. In front of both 90° Ost and West detectors, radial collimators were installed (**Fig. 4-3, b**).

First test experiments were performed in a high-resolution mode (RTOF-mode) with the Ost and West detectors to estimate the quality of geometric alignment of individual photomultipliers, as well as to estimate the resolution function of the diffractometer (**Fig. 4-4**). Data from both 90°-detectors are accumulated by a new MPD-32 analyzer in the list-mode, which allows one to flexibly set parameters of the time-of-flight scale, introduce necessary corrections and ensure high accuracy of electronic focusing for individual detector elements.

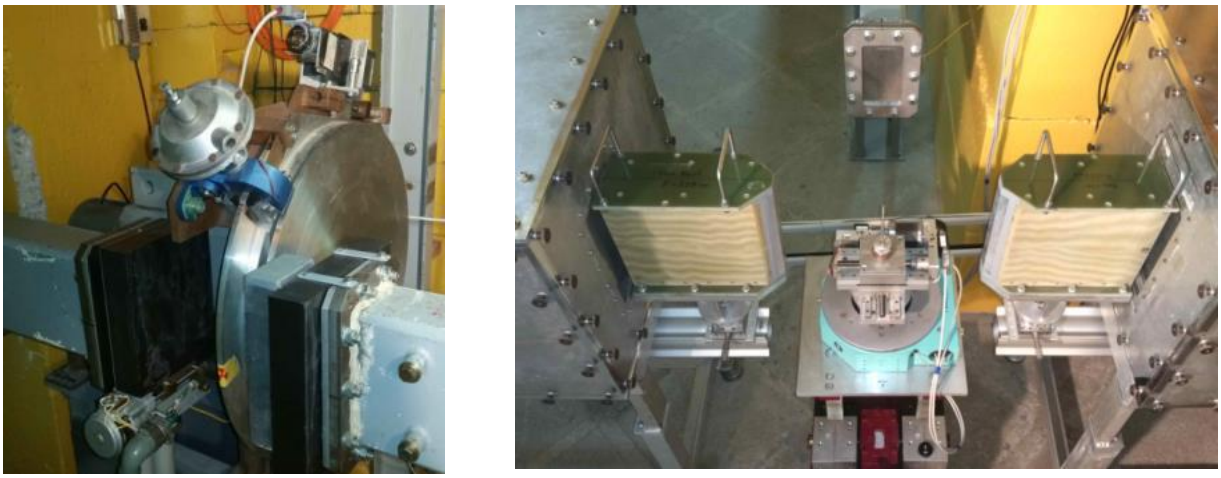

a) b)

Fig. 4-3. a) Fourier-chopper of FSS installed in-between the sections of the mirror neutron guide. b) Sample position at FSS. The photo shows the end of the mirror neutron guide, goniometer with a sample, Ost and West detectors with radial collimators installed in front of them.

To improve the diffractometer characteristics, it is planned to replace the mirror neutron guide together with the vacuum housing. For this purpose, calculations were performed and basic parameters of a new neutron guide were determined, which will allow a several-fold increase in the flux density in the short wavelength range. The neutron guide is designed as parallel-sided in the horizontal plane (window width 10 mm) and linearly converging in the vertical plane (heights of entrance and exit windows are 126 and 50 mm, respectively).

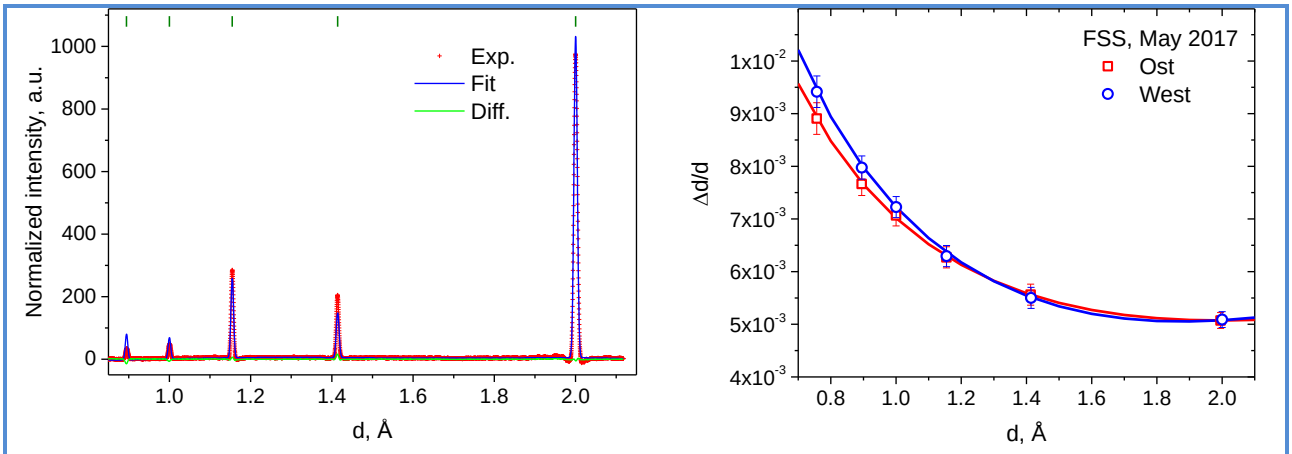

a) b)

Fig. 4-4. a) First high-resolution spectrum from ARMCO iron sample measured by the Ost detector of FSS with the refinement using the Rietveld method. b) FSS resolution function measured at the maximum chopper speed V_{max} = 2000 rpm.

A super-mirror Ni/Ti-based glass coating with the critical index m = 2 is projected. At present, the manufacturing and installation of mirror sections and vacuum housing of the neutron guide are in progress. In addition, it is planned to install a new automated aperture at the exit of the mirror neutron guide, which will make it possible to regulate dimensions of the incident neutron beam at the sample under study. A contract was concluded with the company JJ X-RAY (Denmark); the manufacturing of the device is in progress.

EPSILON diffractometer

The EPSILON diffractometer was equipped with a three-axis high-pressure cell to produce deformations in porous rock samples (length 60 mm, diameter 30 mm) in a neutron beam by applying axial stress, confining pressure and pore pressure. The axial pressure can vary in the range of up to 150 MPa, confining pressure – up to 70 MPa and pore pressure – up to 70 MPa. All three load types change independently, so the deformation rate can be controlled individually.

GRAINS reflectometer

On the GRAINS multifunctional reflectometer, controllable beam collimating apertures to improve the background conditions at the sample position were designed, manufactured and successfully tested (**Fig. 4-5**).

The control function over the slit-type apertures was added to the SONIX software of the control computer, which makes it possible to remotely specify the required neutron beam dimensions directly at the sample position.

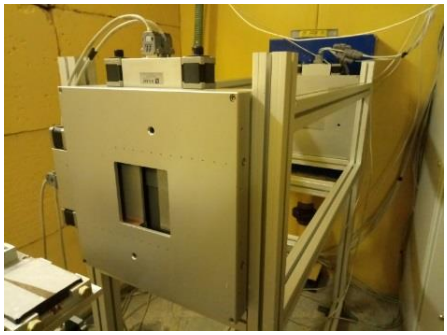

Fig. 4-5. Controllable slit-type apertures for collimating beam directly at the sample position on the GRAINS reflectometer.

REMUR reflectometer

On the REMUR reflectometer, a polarization analyzer with a cross section of 20×20 cm^2, consisting of 150 supermirrors (**Fig. 4-6**), was put into operation.

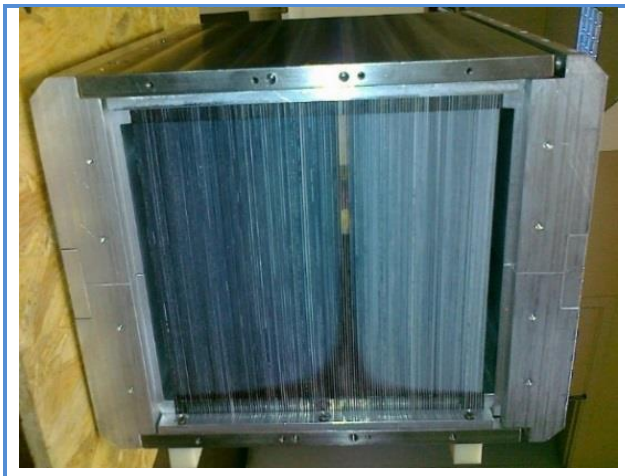

a)

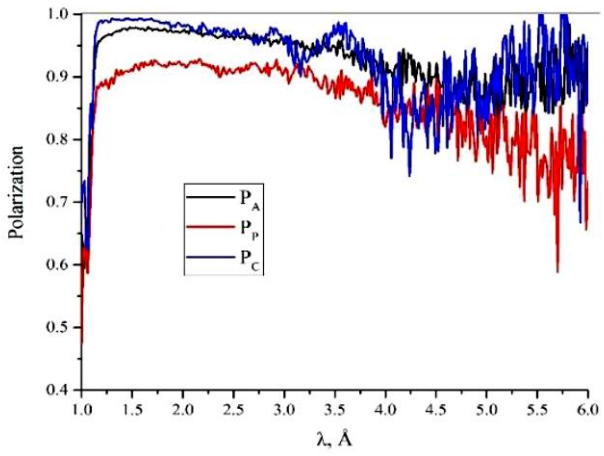

b)

Fig. 4-6. (a) Polarization analyzer with a cross section of 20□20 cm2 at the REMUR reflectometer. (b) Long-wavelength dependences of the neutron polarization efficiency of polarizer Pp (beam cross section 40 □ 2.5 mm) and neutron polarization analyzer Pa (grazing angle 3.5 mrad).

Investigations of neutron channeling in planar waveguides were continued [1]. Planar neutron waveguides convert a conventional neutron beam with a width of 0.1 to 10 mm into a very narrow divergent beam with an initial width of about 0.1 μm, which is then used to scan local microstructures in the volume with a high spatial resolution. An important characteristic of planar waveguides is the channeling length (distance at which the neutron wave attenuates within the waveguide by a factor of *e*). To determine expermentally the neutron channeling length as a function of the waveguide parameters, a neutron absorber was placed on the surface of the film, and the microbeam intensity from the end of the waveguide was measured by varying the absorber length. It was found that the neutron channeling length grows exponentially with increasing thickness of the upper layer, decreases for higher resonance orders (n = 0, 1, 2) following the function ~1/(n + 1) and shows a linear increase with increasing depth of the potential well of the waveguide (**Fig. 4-7**). The experimental results confirm the qualitative theoretical predictions.

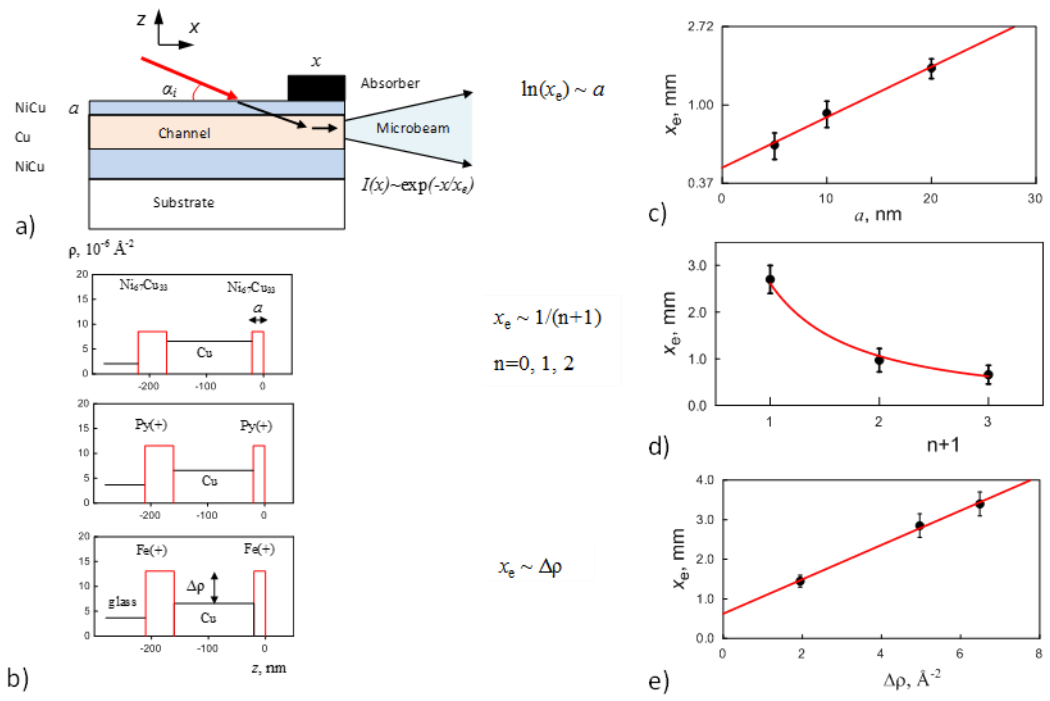

Fig. 4-7. *Design of the experiment (a). Potential of interaction of neutrons with the structure (b). Dependences of channeling length on thickness of the first layer (c), order of resonance mode (d) and depth of the potential well (e).*

REFLEX reflectometer

The reconstruction of the REFLEX reflectometer on beamline 9 of the IBR-2 reactor into a spin-echo small-angle neutron scattering (SESANS) spectrometer was continued. The main task was to test the performance of spin rotators produced by the Research Center of Jülich (Germany). Spin rotators *A, B, C, D* were installed at the sample position of the REFLEX reflectometer in a permalloy shielded chamber in accordance with the design of the SESANS spectrometer, as shown in **Fig. 4-8**. Each of the spin rotators was individually supplied with a constant current of 10 A, which induced periodic oscillations of the polarization vector of the beam passing through the spin rotators. The magnetic field in the spin rotators is directed along their axis in parallel to the larger side; the beam

polarization is perpendicular to the magnetic field of the spin rotators and is directed along the Z-axis. Test measurements of the so-called spin-echo focusing without a sample—an important characteristic of any spin-echo spectrometer—were carried out. When the lengths of two arms are equal and the modulus of magnetic fields are the same at the same time, the z-component of polarization, P_z, should not change as neutrons pass consecutively the two arms. In case when pulsed magnetic fields are used, this statement is valid not for the entire wavelength range, but only for certain intervals [2]. When generating time-linear field pulses with a frequency of 400 Hz and an amplitude of about 100 Gs, a quasi-plateau was obtained in the $P_z(\lambda)$ dependence. The spin-echo focusing curves were measured in the spectral ranges corresponding to the quasi-plateau. One of the arms was varied within the spatial limits available inside the chamber. The obtained curves are shown in **Fig. 4-8**. Insufficient damping of oscillations is explained by a small amplitude of the linear field pulse, as well as by a low pulse repetition rate. Nevertheless, the curves are satisfactorily described by the model function, which confirms the observation of spin-echo focusing. On the basis of the results of experimental tests, the electronic power scheme was redesigned and the spin rotators themselves were upgraded, which would significantly reduce the power of electronics and simplify the control of the spin rotator current.

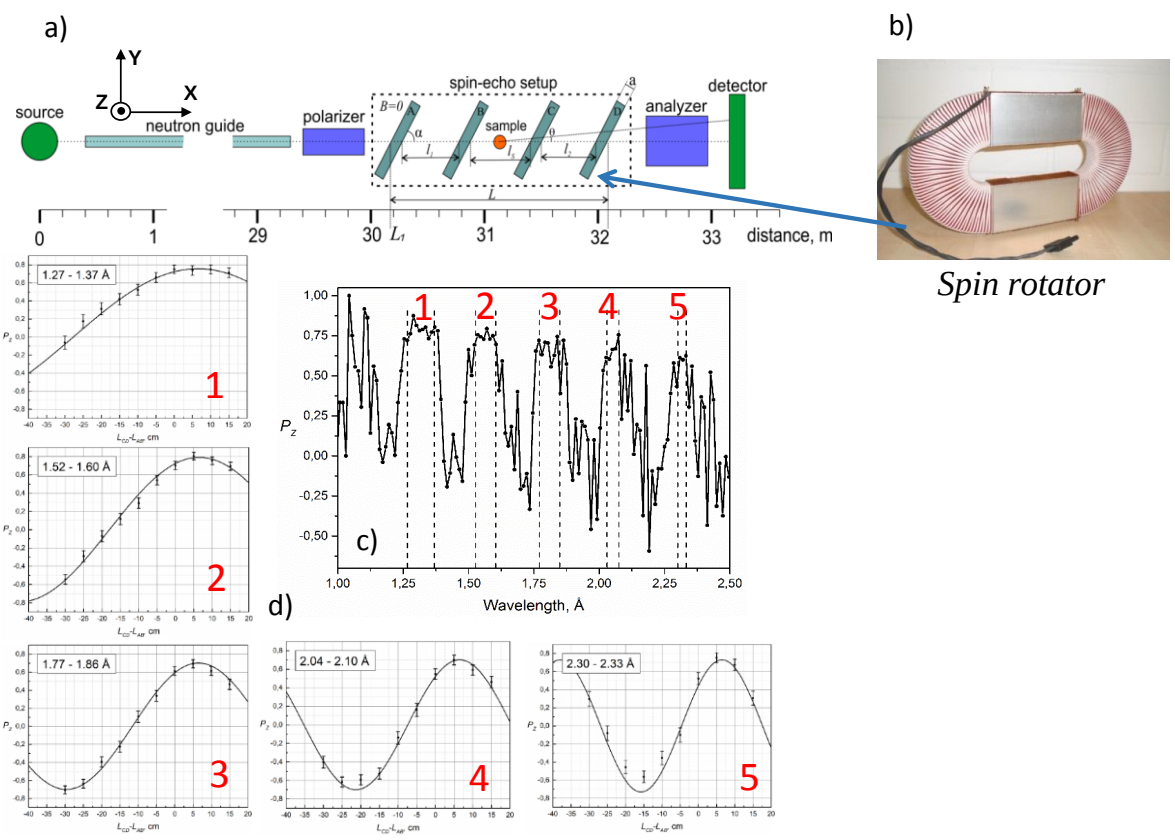

Fig. 4-8. *Scheme of the spin-echo small-angle neutron scattering spectrometer (a). Spin rotator used in the experiment consists of four separate electromagnetic coils forming a closed magnetic circuit (b). Wavelength dependence of polarization of the neutron beam that passed two spin-echo arms (c). Spin-echo signals for different wavelength ranges (1,2,3,4,5). The solid line denotes theoretical calculations (d).*

YuMO spectrometer

The upgrade of the YuMO spectrometer was continued. The main areas of activities included the design of a new replaceable collimator, development of sample environment and studies related to the application of the chopper. In addition, work is underway with a position-sensitive detector of a new type, which is to be put into operation. The spectrometer software was upgraded and extended. In particular, in cooperation with the SC department algorithms were developed and tested in the measurements using a new spectrometer positioning program. In cooperation with LIT, algorithms for the SAS program were developed and tested. It was shown that the overlapping method realized in these algorithms not only provides a qualitatively new level of small-angle neutron scattering curves, but also allows one to improve statistics in the range of the overlapping curves from different detectors [3]. The experiments with the delay of the chopper made it possible to optimize this parameter. In addition, possibilities for improving the obtained spectra from weakly scattered samples by doubling the rotation frequency of the chopper were considered. A technical design for the collimator in general and its units in particular was proposed. The necessary calculations were made to simulate the scattering at the spectrometer with a model collimator.

Experiments were carried out to estimate the necessary time per measurement at the YuMO spectrometer. Two variants with one and two detectors were considered. It was shown that the two-detector experimental scheme reduces the required exposition time by more than half. In solving structural problems using modern software, the two-detector system provides a new qualitative level of data for further analysis. The results of the work can be used in planning experiments at the YuMO spectrometer and during the modernization of the instrument, as well as at other time-of-flight spectrometers.

NRT spectrometer

For the neutron radiography and tomography spectrometer, a modernized two-mirror CCD-based detector system was manufactured. Its application will improve the spatial resolution of experimental data.

References

[1] Kozhevnikov S.V., V.D. Zhaketov, Yu.N. Khaydukov, F. Ott, F. Radu, Channeling of Neutrons in a Planar Waveguide, JETP 125 (2017) 1015-1025.

[2] Bodnarchuk V., V. Sadilov, S. Manoshin, R.V. Erhan, A. Ioffe, Journal of Physics: Conf. Series 862 (2017) 012003.

[3] Soloviev A.G., T M Solovjeva, O I Ivankov, D V Soloviov, AV Rogachev and A I Kuklin. SAS program for two-detector system: seamless curve from both detectors. IOP Conf. Series: Journal of Physics: Conf. Series 848, 1, (2017) 012020.

5. NOVEL DEVELOPMENT AND CONSTRUCTION OF EQUIPMENT FOR THE SPECTROMETER COMPLEX OF THE IBR-2 FACILITY

Complex of cryogenic neutron moderators

In 2017, the pelletized cold moderator CM-202 successfully operated for physical experiments in the 2nd, 4th and 8th cycles of the IBR-2 reactor operation at a power of 2 MW. In the 8th cycle, the cold moderator CM-202 operated with a new cryogenic system, which made it possible to reduce the temperature in the moderator chamber by 8 K (down to 23 K) at a reactor power of 2 MW as compared to the previous cryogenic system. This allowed a significant increase in the yield of cold neutrons from the surface of the cold moderator. In addition, the new cryogenic system was tested under simultaneous cooling of the CM-202 cold moderator chamber and CM-201 test stand at a zero reactor power. The results showed that the use of the new cryogenic system allowed a three-fold reduction in temperature (down to 20 K) in both chambers as compared to the previous cryogenic system.

To investigate the possibility of extending the cold moderator operation time for physical experiments, work is under way to study the amount of hydrogen produced in the moderator material (mixture of mesitylene and m-xylene) after irradiation during one reactor cycle (~ 11 days). For this purpose, a setup with a closed cycle cryorefrigerator was designed and assembled, in which a chamber with a sorbent was cooled to absorb hydrogen present in helium after mesitylene decomposition in a neutron beam. As a result of the experiment it was preliminarily found that the content of the by-product gas fraction of hydrogen in helium at the end of the reactor cycle with cold neutrons may amount to 5% or more in molar terms. These results require further validation by alternative methods.

On the basis of the developed technical specifications, the following elements of the control system of the CM-201 cold moderator were installed and successfully tested: thermometric sensors, control system of cryogenic valves for the new cryogenic system, new software (**Fig. 5-1**).

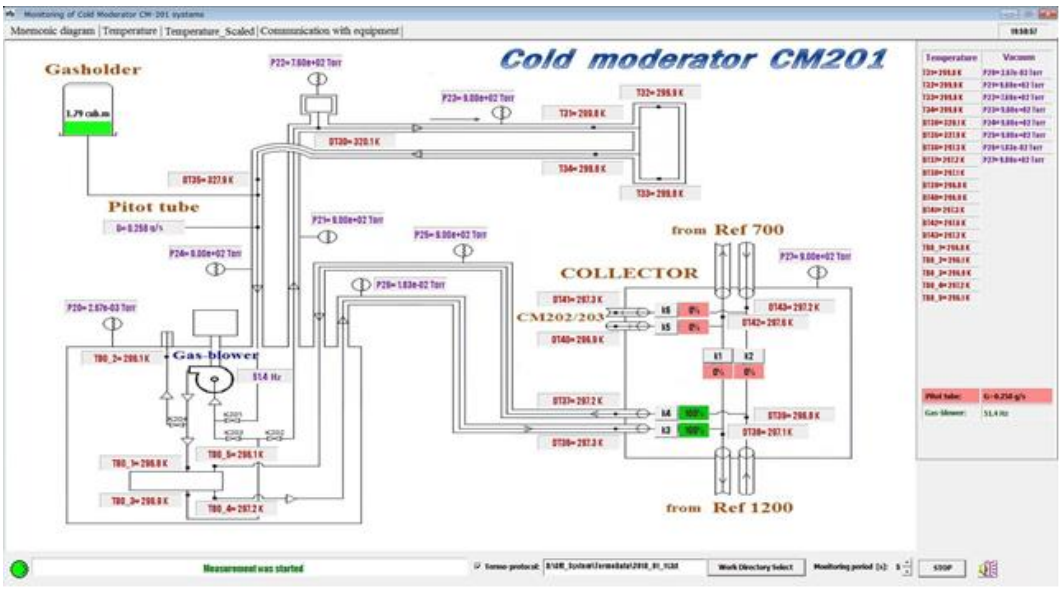

Fig. 5-1. *Control program for the CM-201 pelletized cold moderator with a new cryogenic system.*

Technical specifications for a screw-type discharging device for the CM-201 moderator were developed. This device is designed for continuous replacement of the moderating substance in the moderator chamber.

Radiation research facility

In 2017, the following activities were performed on the radiation research facility at IBR-2:

- new control panel for facility transfer was successfully tested and put into trial operation;
- biological shielding was installed, thus significantly improving radiation conditions on IBR-2 beamline 3;
- technical specifications were developed for installation of a robotic arm for handling highly active samples;
- in cooperation with the Laboratory of Magnetic Sensors of the Lviv Polytechnic National University, the investigation of radiation resistance of magnetic sensors (3D Hall sensors) was
- continued within the framework of international projects for the development of ITER and DEMO fusion reactors;
- in cooperation with DLNP, VBLHEP JINR and BSTU (Republic of Belarus) experiments on the irradiation of samples of silicon scintillators were conducted to study changes in their electrical and physical properties under irradiation;
- In cooperation with VBLHEP JINR, Academy of Sciences of the Republic of Uzbekistan and Ural Federal University (Yekaterinburg) we continued the investigation of the nature of radiation-induced defects in topaz samples (radiation staining) (**Fig. 5-2**), as well as exploration of possibilities of producing medical isotopes at IBR-2 beamline 3.

Fig. 5-2. *Topazes after irradiation at IBR-2 beamline 3.*

Future pulsed neutron source at JINR

In 2015-2017, with an active participation of specialists from the FLNP Spectrometers' Complex Department, possible variants of the future pulsed neutron source at JINR were considered and analyzed, since the service life of the IBR-2 reactor is expected to expire by about 2032. In 2017, we convincingly demonstrated that a fissionable isotope of neptunium (^{237}Np) is more preferable to be used as a nuclear fuel for a high-intensity pulsed neutron source (both in a variant of a pulsed periodic reactor and in a variant of a multiplying neutron-producing target of a proton accelerator) than plutonium-239. The advantage lies not only in the abandonment of the use of a weapons-grade nuclear material, but also in the possibility of obtaining much shorter bursts of thermal neutrons (20 μs instead of 200 μs) with a record peak flux density up to 10^{17} n cm^{-2} s^{-1}, which is an order of magnitude higher than the same value for the most intense European source ESS with a proton beam power of 5 MW (to be put into operation in 2019). In addition, the background noise power in a neptunium-based source will be 2-2.5 times less than in the reactor based on other fissile materials, and the duration of reactor operation without refueling will be significantly increased (15-20 years). The work done can serve as a basis for the development of a detailed design of the future source (**Fig. 5-3**).

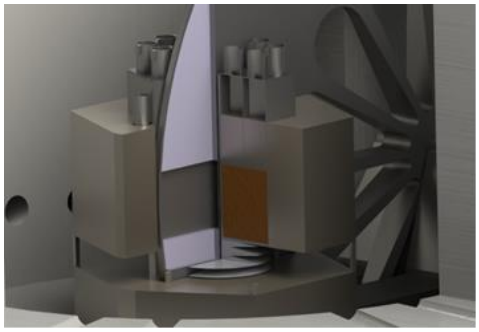

Fig. 5-3. *Model of 237Np-based reactor.*

Calculations and simulation of spectrometers

In 2017, we continued the development and support of the modules of the program for simulating neutron spectrometers and experiments for VITESS (Virtual Instrument Tool for European Spallation Source). Almost half of all VITESS modules have been developed in FLNP; in particular, the tasks of simulating neutron instruments for polarized neutrons have been almost completely carried out. The simulation of spin-echo spectrometers with time-dependent magnetic fields and model systems has been successfully performed. The magnetic fields can be both model (built into modules) and calculated by an external program (MagNet, Ansys, etc.). Virtually all existing neutron-optical elements (neutron guides, benders, mirrors, lenses, prisms and their combinations) have been built into VITESS (and successfully used) as well as the possibility of simulating neutron detectors (including position-sensitive ones) with time focusing has been provided. More detailed information about VITESS can be found in the review article of the jubilee issue of the journal "Physics of Elementary Particles and Atomic Nuclei" (Volume 47, Issue 4, pp. 1228-1248) devoted to the 60th anniversary of JINR.

In 2017, the development of special mathematical models and corresponding programs for simulating full reflectometric and GISANS experiments with samples, including multilayer rough samples and magnetic scattering, was completed. Various modifications of the kinematic approximation were developed and analyzed taking into account the penetration depth, refraction, final resolution of the instrument, and renormalization of collected data.

It has been shown that the modified kinematic approximation used in the simulation of specular reflection, which takes account of the effect of neutron wave refraction at an interface, gives fairly good agreement with the available experimental data and the Parratt method, which is considered to be the most accurate method of the dynamic theory.

Two systems with a silicon matrix were considered. In the near-surface layer of the systems, cubic nickel nanoparticles (edge length 150 Å) were distributed to form a 3D tetragonal lattice. For the primitive tetragonal Bravais lattice the parameters were $a = b = 400$ Å, $c = 500$ Å, while for the body-centered lattice − $a = b = 400$ Å, $c = 1000$ Å. A layer of silicon 50 Å thick was placed above the first layer of nanoparticles, and only four layers of nanoparticles were distributed in the depth of the sample. Ten periods in each direction were chosen in the lateral plane. For this problem, the penetration depth of the neutron wave was not introduced and the resolution of the spectrometer was not taken into account.

The results of simulations of full diffraction patterns for the two systems described above using the modified kinematic approximation are presented in **Fig. 5-4**. At the left, systematic extinctions characteristic for the body-centered tetragonal lattice are clearly visible. At the same time, at the right, there are no systematic extinctions in the diffractionpattern, as it should be in the case of a primitive lattice. In both cases, the lateral lattice parameters ($a = b = 2\pi\ 0.0157 = 400$ Å) can be found from the obtained diffraction spectra.

It should be noted that the diffraction pattern in the specular channel of neutron reflection is identical in both cases of the tetragonal distribution of nanoparticles in the matrix. Consequently, from specular reflection data one can evaluate only the distance between the nearest nanoparticle layers and the total number of layers in the sample, while the type of spatial ordering of nanoparticles in the matrix cannot be determined.

The problem of simulating specular reflection from a system of cubic nickel nanoparticles (edge length 400 Å) forming a square lattice (lattice parameter 1200 Å) on the surface of a nickel substrate was solved as well. It was assumed that the cubes were placed in an organic solvent with a scattering length density corresponding to that of ribonucleic acid (RNA) which is approximately half the value characteristic for natural nickel.

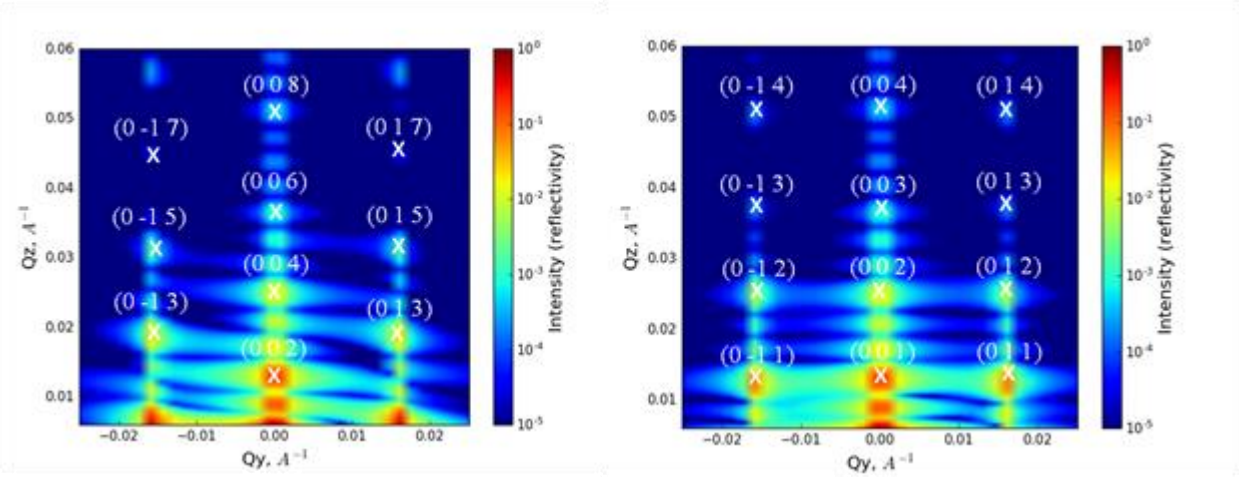

Fig. 5-4. *Results of simulations of full diffraction patterns using the modified kinematic approximation for a system with a silicon matrix, in the near-surface layer of which cubic nickel nanoparticles (edge length 150 Å) are distributed. Simulations for body-centered (left) and primitive (right) tetragonal Bravais lattices are presented. Miller indices of observed diffraction peaks are given. Crosses indicate theoretically calculated positions of diffraction peaks. In the diffraction pattern, oscillations from the total thickness of the modeled sample are clearly observed. Calculation time for each pattern was about 1 h (using processor Intel Core i5, 2.5 GHz).*

The results of 3D simulation of a full reflectometry experiment are given in Fig. II-2-5. At the left, the results are shown for the case when the dimensions of all cubic nanoparticles were identical, at the right − when the height of all cubic nanoparticles was the same but the sizes of the lateral cross-section were varied randomly in the range from 100 to 400 Å. It is interesting to note that for an ideal system of cubes, the extinction of the third-order reflection 03l for QY = ±0.0156 Å–1 is clearly observed (**Fig. 5-5**, left).

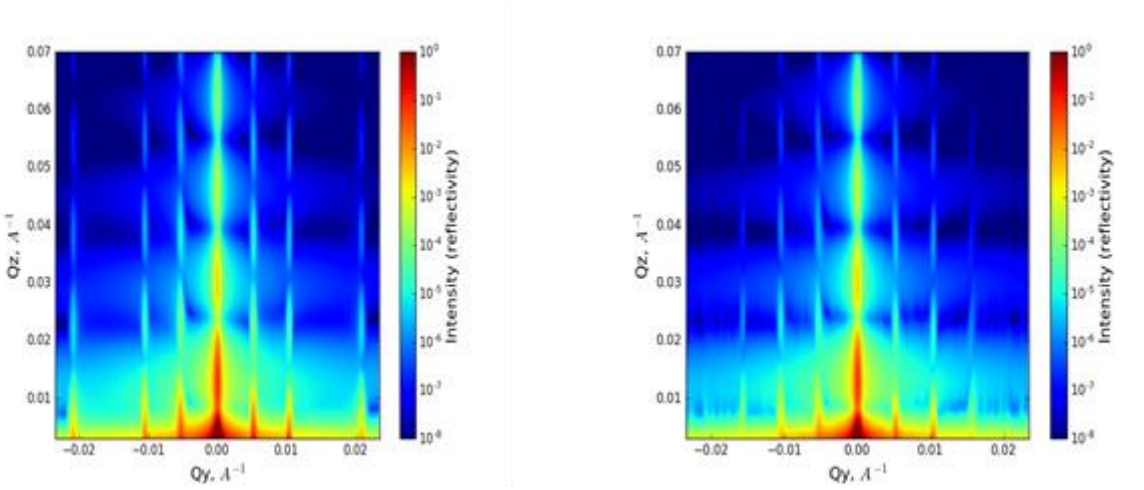

Fig. 5-5. *Simulation of a full reflectometry experiment for a system of cubic nickel nanoparticles in an organic solvent on a nickel substrate (spectrometer resolution is not taken into account).*

These extinctions can be explained by the multiplicity of lateral sizes of nanoparticles and the period of the square lattice formed by these nanoparticles. The introduction of a random distribution over lateral nanoparticle sizes results in the reappearance of this reflection, but higher-order diffraction

reflections (in this example, already the fourth-order reflections) are greatly suppressed in intensity and would be practically invisible in a real experiment.

Cryogenics and vacuum systems

Major activities in this area were carried out in accordance with the project “Development of PTH sample environment system for the DN-12 diffractometer at the IBR-2 facility” aimed at developing a cryostat for temperature and magnetic investigations of condensed matter under pressures of up to 10 GPa at the DN-12 spectrometer. A significant extension of the range of scientific problems solved by means of this diffractometer has required the construction of a cryostat with a variable temperature (in the range of 300 - 4 K) and magnetic field (0 - 4 T), which will allow us to distinguish between the effects from various types of interactions when studying complex magnetic structures, build detailed magnetic phase diagrams of magnets under study and thoroughly investigate mechanisms of magnetic phase transitions.

The magnet is a Helmholtz pair of magnets made of a high-temperature superconducting tape of the second generation YBCuO (manufactured by "SuperOx", Russia). The magnet is cooled by a closed-cycle cryocooler. The cryostat with a high-pressure cell, which in its turn is cooled by another closed-cycle cryocooler, is inserted into the center of the magnet through a horizontal shaft. The temperature of the cell is regulated by a controller in the range of (4 - 300) K.

The project is being implemented in cooperation with the National Institute of Research and Development in Electrical Engineering (ICPE-CA) Bucharest, Romania.

The following major activities have been carried out in the framework of the project:

- • Design documentation for the cryostat and magnet producing a magnetic field of 4 T was prepared.
- • Machine for HTS tape winding was developed and manufactured;
- • Cryostat for cooling the magnet was manufactured.
- • Magnet and coils were produced.
- • Horizontal cryostat for cooling high-pressure cells was manufactured and tested. This cryostat with a high-pressure cell is inserted into a magnetic field of the superconducting magnet.
- • Power source for the superconducting magnet with an operating current of up to 300 A was put into operation.
- • Preliminary tests of the cryostat with a magnet were carried out at a current of 90 A. The magnet constant was measured to be 0.0154 T/A. A magnetic field of 1.386 T was obtained. Photos of this equipment and temperature graphs of different parts of the cryostat are shown in the FLNP Annual Report for 2016. The achieved terminal temperatures of the magnet prototype (16 K), warm ends of HTS current leads (58 K), and sample (2.8 K) correspond to the design values.

In April 2017, when carrying out the start-up and adjustment work together with the Romanian colleagues, we repeated test experiments and detected the degradation of the properties of the tape in one of the magnet coils, which showed up as a decrease in the critical current value and, correspondingly, the magnetic field strength. Further studies revealed the degradation of the properties of the tape in the second coil as well.

To determine the causes of the observed effect, we carried out additional studies, which showed that the most probable reason is the discrepancy between the actual characteristics of the tape and the characteristics specified by the supplier.

When current was introduced into the magnet, it was found that at a current of 105 A, an avalanche-like increase in the potential of the coils (quenching) occurs. To identify the reasons for the growth of the potential, the magnet was dismantled, and each coil was tested separately. The coils consist of three continuous pieces of the tape connected by soldering. The resistance of each solder junction does not exceed 20 n□ at 77 K. The resistance of the junctions becomes lower with decreasing

temperature. At a current of 60 A, the potential of the coil was 4.3 mV at a temperature of 16 K and 10.8 mV at 35 K; the corresponding resistances were 70 and 180 μΩ. As can be seen, the coil resistance is three orders of magnitude greater than the resistance of the junctions, which is indicative of the absence of superconductivity along the entire length of the tape.
The quality control of HTS tapes is performed by the manufacturer by running the tape through liquid nitrogen and measuring the potential of a piece of tape about 1 m long. At this length, the potential value is close to the noise level in the measuring device (we also tested a piece of tape 75 cm long and there was no resistive component in it).
For the tape in the coil (length 750 m), the potential was found to be non-zero and was clearly detected by a microvoltmeter. The existence of the potential across the coil results in a heat release (0.75 W at a current of 75 A), so the coil quickly overheats and quenches.
Visual inspection revealed the peeling-off of the copper coating from the HTS tape (**Fig. 5-6)**. On the basis of the obtained results, it can be concluded that the HTS tape from "SuperOx" is unsuitable for manufacturing superconducting magnets.

The negotiations with the supplier in order to find out the reasons for the tape degradation and eliminate the problems have yielded no results, therefore it was decided to change the supplier of the superconducting tape and extend the project period. SuperPower Inc. (USA) was selected as a new supplier of the HTS tape, while accessories and magnet will be manufactured by the ICPE-CA Institute (Romania). At present, corresponding contracts have been concluded with these organizations. The coils made from SuperOx tape can be used in a liquid-nitrogen-cooled cryostat (temperature of about 65 K with pumping) to generate fields in the range of 0.4 to 0.8 T depending on whether one or two coils are used. It should also be noted that to install the magnet on the DN-12 diffractometer, it is necessary to upgrade the housing of the diffractometer, as well as to conduct an inspection of the existing equipment to ensure its effective operation in magnetic fields.

Fig. 5-6. *Peeling-off of the copper coating from the HTS tape.*

In 2017, the spectrometer DIN-2PI was equipped with a cryostat with a closed-cycle pulse tube cryorefrigerator. A series of tests of the cryostat were carried out to optimize its thermal performance. At the NERA spectrometer, the defective cryorefrigerator CRYOMECH PT405 was replaced with a cryorefrigerator SUMITOMO SRDK-415 with a change in the design of the thermal bridge between the sample shaft and the second stage of the cold head of the cryorefrigerator, making it possible to lower the minimum temperature at the sample position from 6 K to 5 K.
Work has been completed on the commissioning of vacuum systems of new mirror neutron guides on IBR-2 beamlines 13 and 9.

Detectors and electronics

In 2017, a new ring gas detector for small-angle thermal neutron scattering was assembled and tested with a neutron source on the RTD diffractometer (IBR-2 beamline 6a). The detector is designed for studies of biological (organic) and nanodispersed polymer objects containing functionally significant inhomogeneities of various structural complexity. A distinguishing feature of the detector is the simultaneous determination of angular and radial coordinates of detected neutrons. A photo of the detector on the test stand is shown in **Fig. 5-7.**

Fig. 5-7. *Photo of the detector on the test stand.*

The detector is divided into 9 independent equidistant coaxial rings. The cathodes of each ring are divided into 16 independent sectors forming 144 independent detector elements. The signal pickup is performed from anode wires (shared by all rings) and from each of 16 cathodes. To eliminate the effect of impulse noise and reduce the electronic noise, the preamplifiers of detector elements are arranged inside the gas volume.

Analog electronics for 144 cathode and 9 anode measuring channels have been designed, manufactured and adjusted. Digital electronics for data acquisition and accumulation are based on unified MPD modules and include 5 modules of 32-channel discriminators and an MPD32 controller. Amplitude spectra from all detector rings were obtained (**Fig. 5-8**). The commissioning on the RTD spectrometer is scheduled for early 2018.

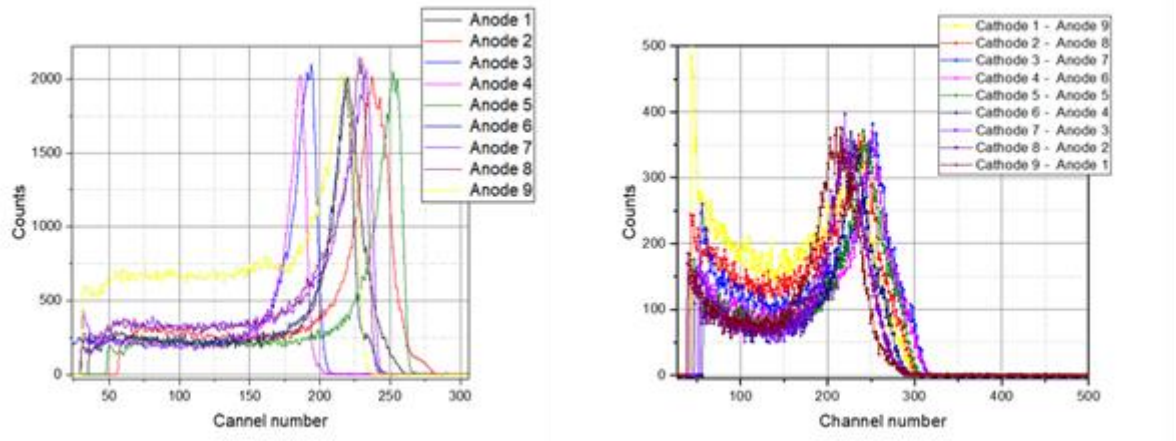

Fig. 5-8. *Amplitude spectra of a small-angle detector: from anodes (left) and from cathodes (right).*

In 2017, measurements of plasma temperature in the reaction D(d,n)3He were continued using the spectrometer based on a recoil proton telescope, which had been developed in FLNP. Measurements are performed at the National Fusion Research Institute (Daejeon, Republic of Korea) in accordance with the Protocol on Cooperation. Measurements of the background radiation were made and fast neutron spectra were measured at the KSTAR (Korean Superconducting Tokamak Advanced Research) tokamak-type nuclear fusion reactor. Photos of the telescope at the KSTAR facility are shown in **Fig. 5-9.**

Fig. 5-9. *Spectrometer on the basis of a proton recoil telescope at the KSTAR nuclear fusion reactor.*

In the framework of the collaborative work on the ESS project (Lund, Sweden), a prototype of PSD on the basis of a multiwire proportional chamber with a 10B converter has been developed and tested IBR-2 beamline 13 (**Fig. 5-10**). The coordinate resolution of the detector along the coordinate perpendicular to the anode was measured to be 0.9 mm. The ultimate goal of the work is the development of a 2D neutron PSD with a 10B converter.

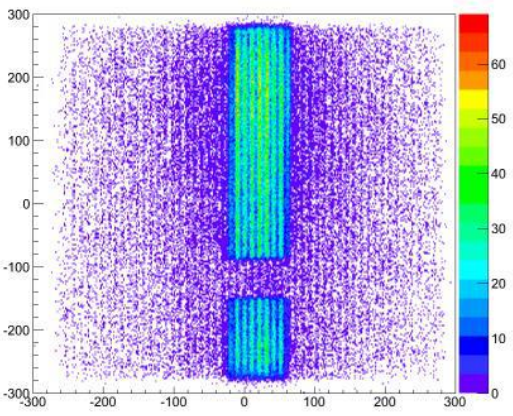

Fig. 5-10. *Coordinate spectrum obtained on IBR-2 beamline 13.*

In accordance with the technical project for the ASTRA-M detector system (modernized version of ASTRA detector) developed earlier, we continued work on the manufacturing of its main components. The installation of the system on the FSD spectrometer and first test measurements are scheduled for 2018.

The HRFD diffractometer at the IBR-2 reactor is one of three or four neutron diffraction facilities in the world which allows performing experiments at $\Delta d/d \approx 0.001$ or better. At present, the HRFD detector system comprises three detectors, two of which are placed at the scattering angles of ±152°, and the third one at 90°. The detecting elements are Li-glass scintillators. The available HRFD detectors have two disadvantages: small solid angle (~0.16 sr) and high sensitivity to gamma-ray background radiation, resulting in a relatively low data acquisition rate at a sufficiently high neutron flux at the sample position (up to 10^7 n/cm^2/s), and a high background level in the resulting diffraction spectra.

To overcome these drawbacks, the physicists submitted a request to develop a new backscattering detector with an aperture covering the scattering angles $2\theta = (133\text{-}175)^o$. For the estimated maximum (80%) of the useful detector area (technological losses may amount to up to ~ 20%) the solid angle is expected to be $\Omega \approx 1.5$ sr, which is almost an order of magnitude higher. To ensure high and ultra-high resolution, the neutron converter will be produced on the basis of a thin (~ 0.4 mm thick) ZnS(Ag)/^{6}LiF scintillator screen, wavelength-shifting fibers and photomultipliers. The production of this type of detectors has been well mastered with the detector system for the FSD spectrometer. In 2017, the detector design was developed and approved, and corresponding contracts were signed for the purchase of necessary materials (primarily scintillators and fiber optics). A schematic of the new backscattering detector is shown in **Fig. 5-11.**

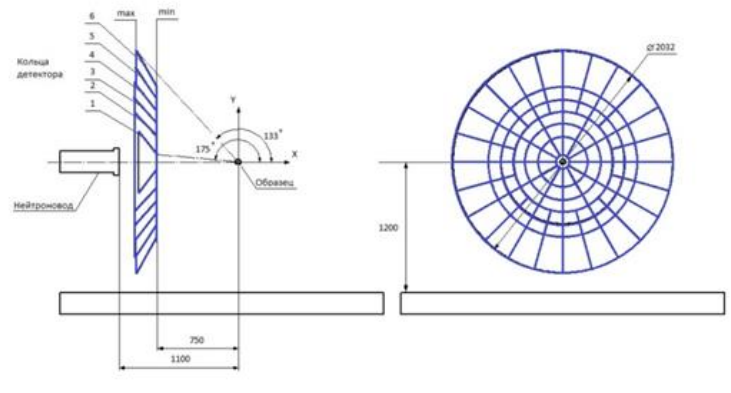

Fig. 5-11. *Schematic of the backscattering detector with a large aperture (the detector comprises 8 rings, 166 sectors, the solid angle of the detector is ΩD = 1.5-1.8 sr, the total area of the scintillator screen is 13.5 m2).*

All the detectors described above are equipped with the unified blocks of analog and digital electronics and software developed in FLNP. The digital data acquisition systems consist of two basic electronic modules, (De-Li-DAQ11,2 and MPD), one of which processes and accumulates data from one- and two-dimensional PSD, and another – from an array of point detectors (gas and scintillation counters). All parameters of the modules are programmed. New systems allow one to work both in the histogram mode and in the mode of accumulation of raw data – ListMode (with subsequent off-line processing).
In 2017, work continued on the development of electronics for detector systems. Test programs for accumulating data using multichannel digitizers were written, and 2D coordinate spectra from a neutron source were obtained. For the FSD diffractometer, an MPD accumulation system supplemented with a digital filtering module to select signals from scintillation detectors was developed and implemented.
At the requests of the researchers, measurements of neutron beam profiles on beamlines 10 and 13 of the IBR-2 reactor were performed using a monitor PSD.
In the framework of the development of the infrastructure of the Detector group, we prepared a technical design specification and signed a contract for the modernization of the clean room for assembling detectors in order to increase its area and enhance its purity class, which will allow us to work with detectors of larger sizes. The installation of climate equipment is scheduled for 2018.

A new mobile gas-filling unit designed to fill detectors with a gas mixture was developed. The unit has small dimensions and makes it possible to refill detectors directly in the IBR-2 experimental halls.

Upgrade of control systems, actuators and sample temperature control systems on IBR-2 spectrometers

During the reporting period a large amount of work has been carried out to upgrade the actuators of the IBR-2 spectrometers, neutron beam choppers, sample temperature control systems, as well as control systems of these devices. Below are a few examples of these devices.
Due to the adopted architecture of control systems for the actuators of spectrometers, the number of devices for an experimental setup can be increased without any problems in the following way:

- new mechanism is assigned the next number (up to 32);
- "2*OSM42" module is installed in 3U frame at a current of the mechanism stepper motor of less than 4.2 A; each installed module increases the number of control channels in the system by 2;
- "OSM88" module is installed in 3U frame at a current of the mechanism stepper motor of less than 8.8 A;
- if the number of control channels exceeds 32, then the control system is duplicated, and the possible number of control channels increases by another 32;
- parameters of new devices are specified in the system software;
- incorporation of one new control channel into the system takes no more than 2 days.

Following this procedure, the control system of the FSS spectrometer was created. It comprises 6 control channels and 5 modules controlling actuators of the instrument devices including:

- Huber goniometer for sample positioning (coordinates x, y, z; rotation around vertical axis);
- device for positioning Fourier chopper stator.

Two Huber goniometer devices were included into the number of actuators for the REMUR spectrometer, which control the horizontal movement (±30 mm) and inclination (±10^{o}) of the sample.
At the SKAT and NERA spectrometers, control systems for experimental setups were upgraded. Control systems of current sources (3 sources with USB interface and 4 sources with control from a programmable source of 0-10 V) were put into operation at the REMUR spectrometer.
On some IBR-2 spectrometers, there is a need for the development of small-size choppers (with their possible use in a vacuum) and corresponding control systems. One of the possible options is

to use stepper motors for this purpose. We developed an electronic module and programs for controlling the stepper motor for the chopper prototype.The results of tests of the prototype showed a principal possibility of precise control over the rotation speed of a disk with a diameter of 60 cm and a weight of 5-10 kg.
In the framework of modernization of temperature control systems, the replacement of Eurotherm temperature controllers with Lake Shore controllers was completed.
Temperature control systems based on closed cycle cold heads, as well as air and vacuum ovens were put into operation on IBR-2 beamlines 5, 6a, 6b.

Software and computer infrastructure

The main focus of the development of Sonix+ software package was on further improvement of the complex, its extension with new components, development of data visualization tools and enhancement of reliability. Among the most important activities were the following:

- development of a new version of the script interpreter module that extends the possibility of direct use of mathematical multidimensional data analysis software packages in the script (Numerical Python, etc.);
- supplementation of a basic set of widgets and improvement of GUI programs – Svetofor program for controlling and monitoring control signals and others;
- development of a new version of SpectraViewer in cooperation with the NICM Department. In this version it is intended to include visualization of spectra in Q space, as well as other useful options. **Figure 5-13** shows an example of the graph used to search for a reflected beam when tuning reflectometers.

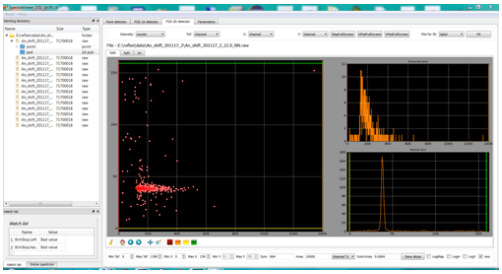

Fig. 5-13. New mode of SpectraViewer program to facilitate visual search of the reflected beam when tuning reflectometers.

A Sonix+ version for the FSS diffractometer has been prepared for practical testing and its trial operation has started.

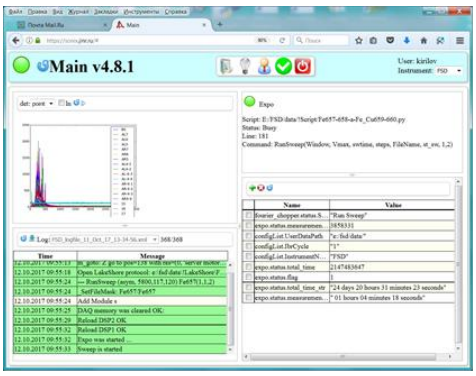

Fig. 5-14. Home page of WebSonix service using the example of FSD spectrometer.

An improved version of WebSonix 4.8 (**Fig. 5-14**) for remote control over experiments, was developed and put into operation. We added an online spectrum visualization page as well as e-mail notification on the termination of the experiment. At present, eight spectrometers (YuMO, HRFD, FSD, SKAT, NERA, EPSILON, DIN-2PI, REFLEX) have been connected to this service.

The adaptation and debugging of the Journal program on the GRAINS and HRFD spectrometers are in progress. The program is designed to automatically record measurement results and search for data by individual parameters (user name, measurement time, etc.).
Programs for monitoring the state of the CM-201 cold moderator and a new graphical interface were developed.
The development of software tools for debugging and testing digital electronics for data acquisition systems was continued.

The outdated network switches in buildings 42 and 42a were upgraded to provide a data rate of 1 Gbit/s for all end users in the offices of physicists and Directorate of the Laboratory. In the FLNP local area network the number of WiFi access points in buildings 42 and 117 was increased. Six worn-out and outdated network printers were replaced with new models (HP LaserJet M607 dp).

6. NEUTRON SOURCES

THE IBR-2 PULSED REACTOR

In 2017, the activities on the research nuclear facility IBR-2 (RNF IBR-2) were carried out in accordance with the objectives of the theme "Development of the IBR-2 Facility with a Complex of Cryogenic Neutron Moderators"
In 2017, the IBR-2 research nuclear facility was operated in a nominal on-power mode under Rostekhnadzor license valid until 30.09.2022.

Table 6-1 presents data on the IBR-2 operation for physics experiment in 2017.

Table 6-1. *data on the IBR-2 operation for physics experiments.*

№ cycle	Period	Reactor operation for physics experiments, hr	Moderator type
1	16.01-28.01	264	water
2	08.02-18.02	230	cryogenic
3	13.03-28.03	336	water
4	04.04-14.04	238	cryogenic
5	15.05-26.05	264	water
6	26.09	4	water
7	09.10-27.10	432	water
8	14.11-25.11	247	cryogenic
9	04.12-23.12	456	water
TOTAL		**2471**	

On September 26, 2017 in the 6th cycle the reactor for physical experiments was operated for 4 hours and interrupted by the activation of the safety system because of the 1DNOK pump shutdown caused by a contact failure in the block-contact group 2L of the contactor KT 7023BC of the pump control scheme. In accordance with the FLNP Order № 105 issued on 06.10.2017 the IBR-2 operation in the 6th cycle was suspended, as well as changes were proposed in the duration of the 7th and the 9th cycles. Due to multiple power supply failures in May 2016 caused by voltage drops, cycle №5 of IBR-2 operation for physical experiments was terminated before the scheduled date with a loss of about 130 hours of experimental beam time.

IREN FACILITY

The IREN (**I**ntense **R**esonance **N**eutron **S**ource) is a complex of electrophysical and technological equipment that comprises a travelling-wave linear electron accelerator LUE-200 of 10-cm frequency range (2856 MHz) and a non-multiplying neutron-producing target. The realization of the IREN project is conducted in several stages. The physical startup of the IREN facility with the LUE-200 accelerator comprising one accelerating section was conducted in 2009-2010. The first stage of the accelerator has operated for experiments for several thousand hours at a repetition rate of 10 - 25 Hz providing a pulsed electron beam with a current of 1.5 - 2.0 A, pulse width of 100 ns and energy of 30 – 35 MeV (spectrum maximum). The maximum values for the integral neutron yield obtained at a repetition rate of 25 Hz, are close to $(3\div5)\cdot10^{10}$ n/s.

In 2016, the second accelerating section with a TN2129 klystron and modulator of 180 MW/180 kW was installed and put into operation. As a result of the startup of the second section, the energy of the accelerated beam was increased: the position of the spectrum maximum shifted to 52 ± 54 MeV, and the maximum electron energy reached 60 MeV. The estimates of the integral neutron yield from the W-target based on the measurement of the neutron flux density, show a 3-4-

fold increase in the integral neutron yield as compared to that of the first stage. In 2017, the second stage of the LUE-200 accelerator operated for experiments for 1049 hours at a repetition rate of 20-25 Hz.

EG-5 ACCELERATOR

In 2017, the EG-5 electrostatic accelerator operated for 515 hours. The elemental depth profiles of near-surface layers in various samples were studied using a variety of nuclear-physical analytical techniques including Rutherford backscattering (RBS), elastic recoil detection (ERD) and particle induced X-ray emission (PIXE).

In cooperation with the Lebedev Physical Institute of the Russian Academy of Sciences the process of accumulation and redistribution of deuterium and hydrogen atoms in the assemblies of two high-purity zirconium and titanium foils under high-temperature pulsed action of deuterium plasma at the PF-4 plasma focus setup was studied. Using analytical methods, namely Rutherford Backscattering Spectrometry (***RBS***) and Elastic Recoil Detection (***ERD***), it was found that the redistribution of implanted deuterium and hydrogen gas impurities in the assemblies of irradiated foils occurs to great depths that far exceed the ranges of deuterium ions. The observed phenomenon can be explained by the redistribution of the implanted deuterium and hydrogen under the influence of powerful shock waves formed in the metal foil under the action of high-temperature pulsed plasma.

In cooperation with Maria Curie-Skłodowska University (Lublin, Poland), a large amount of research has been conducted on the effect of heavy ion implantation on the optical properties and chemical composition of near-surface layers of GaAs crystals. The investigation of the complex dielectric function in the near-surface layers was carried out using the ellipsometry technique. The chemical composition of the surface layers was studied using the X-Ray Photoelectron Spectroscopy (XPS) technique. The investigation of the real and imaginary parts of the dielectric function and of the atomic and chemical composition was performed near the surface of GaAs crystals implanted with indium ions at an energy of 250 keV and a dose of $3 \cdot 10^{16}$ cm^{-2}. The influence of heat treatment in the temperature range 400°C-900°C on the structure and optical properties of GaAs crystals implanted with indium ions was also investigated. A series of studies was made of the effect of implantation of Ne, Ar, Kr, Xe ions at an energy of 100 keV and doses from $1 \cdot 10^{12}$ cm^{-2} to $3 \cdot 10^{15}$ cm^{-2} on the change in the diele The effect of fluence and the mass of implanted ions on the optical properties and chemical composition of the near-surface layers of implanted GaAs(100) crystals was studied as well. Depth ctric function and atomic composition in the surface layer of GaAs crystals.

The effect of fluence and the mass of implanted ions on the optical properties and chemical composition of the near-surface layers of implanted GaAs(100) crystals was studied as well. Depth profiles of heavy elements in these studies were measured using the RBS technique. To study the oxygen content in the surface layers subjected to heavy ion implantation, the resonant scattering of helium ions with an energy of 3,045 MeV by oxygen atoms (NRA technique) was used, which ensured a high accuracy in measuring depth profiles of oxygen in the samples under study.

In cooperation with the Institute of Electrical Engineering of the Slovak Academy of Sciences we investigated the structural, magnetic and electrical properties of La0.67Sr0.33MnO3 epitaxial films grown on (001) SrTiO3 crystalline substrates. Depth profiles of various elements in silicon carbide samples prepared by Plasma Enhanced Chemical Vapour Deposition (PECVD) were studied using RBS and ERD techniques. The characteristics of these samples ensured their use for various applications, such as the absorption of electromagnetic energy in the spectral region of 0.1 - 2.0 THz, the creation of transparent photocathodes by depositing a film on a quartz glass substrate, as well as providing the possibility of using layered structures in the aggressive environment.

PUBLISHED PAPERS

DEPARTMENT OF NEUTRON INVESTIGATION OF CONDENSED MATTER

Atomic and magnetic structures (diffraction)

1. Balagurov Anatoly M., Igor S. Golovin, Ivan A. Bobrikov, Valeria V. Palacheva, Sergej V. Sumnikov, Victor B. Zlokazov “Comparative study of structural phase transitions in bulk and powdered Fe-27Ga alloy by real-time neutron thermodiffractometry” J. Appl. Cryst. 50 (2017) 198-210.
2. Bobrikov I.A., N.Yu. Samoylova, S.V. Sumnikov, O.Yu. Ivanshina, R.N. Vasin, A.I. Beskrovnyi, A.M. Balagurov “In-situ time-of-fight neutron diffraction study of the structure evolution of electrode materials in commercial battery with LiNi0.8Co0.15Al0.05O2 cathode” Journal of Power Sources, 372 (2017) 74-81.
3. Bobrikov I.A., N.Yu. Samoylova, S.V. Sumnikov, O.Yu. Ivanshina, R.N. Vasin, A.I. Beskrovnyi, A.M. Balagurov, In-situ time-of-flight neutron diffraction study of the structure evolution of electrode materials in a commercial battery with Journal of Power Sources 372 (2017) 74–81
4. Burzo E., P. Vlaic, D.P. Kozlenko, S.E. Kichanov, A.V. Rutkauskas, B.N. Savenko «Crystal structure and magnetic behaviour of $DyCo_2$ compound at high pressures», Journal of Alloys and Compounds, 724, 1184-1191 (2017).
5. CIRSTEA Cristiana Diana, Marcela MIHAI, Vasile CIRSTEA , Delia PATROI, Haritina CHIVU, Florina RADULESCU, Violeta TSAKIRIS, Otilia CULICOV and Anatol Mihail BALAGUROV “PHASE RELATIONS IN THE NiTiCu SHAPE MEMORY MATERIALS USED IN MEDICINE APPLICATIONS” Rev. Roum. Chim. 62 (6-7) (2017) 539-544.
6. Dang NT, DP Kozlenko, SE Kichanov, SG Jabarov, AI Mammadov, RZ Mekhtieva, TL Phan, VG Smotrakov, VV Eremkin, BN Savenko “Revealing the Formation Mechanism and Effect of Pressure on the Magnetic Order of Multiferroic BiMn2O5 Through Neutron Powder Diffraction”, Journal of Electronic Materials, 46, 6, 3373-3380 (2017).
7. Efimov V., V. Sikolenko, E. Efimova, I.O. Troyanchuk, D. Karpinsky, ,S.I. Tiutiunnikov, B.N. Savenko, D. Novoselov, D. Prabhakaran Anomalous behavior of displacement correlation function and strain in lanthanum cobalt oxide analyzed both from X-ray powder diffraction and EXAFS data Powder Diffraction 32 (2017), S151-S154.
8. Efimova E.A., V.V. Sikolenko, D.V. Karpinsky, I.O. Troyanchuk, S. Pascarelli, C. Ritter, M. Feygenson, S.I. Tiutiunnikov, and V. Efimov. A combined diffraction and EXAFS study of $LaCoO_3$ and $La_{0.5}Sr_{0.5}Co_{0.75}Nb_{0.25}O_3$ powders. Powder Diffraction 32 (2017), S52-S55.
9. Fedorov Victor, Arseniy Berezner, Tatiana Pluzhnikova, Anatolyi Beskrovnyi, Investigation of Inhomogeneous Deformation in Band Amorphous Alloys at Constant Heating Rate, AIP Conference Proceedings 1899, 030001 (2017); View online: https://doi.org/10.1063/1.5009846 View Table of Contents: http://aip.scitation.org/toc/apc/1899/1 Published by the American Institute of Physics
10. Golosova NO, DP Kozlenko, LS Dubrovinsky, V Cerantola, M Bykov, E Bykova, SE Kichanov, EV Lukin, BN Savenko, AV Ponomareva, IA Abrikosov “Magnetic and structural properties of FeCO3 at high pressures”, Physical Review B, 96, 13, 134405 (2017).
11. Golosova NO, DP Kozlenko, SE Kichanov, EV Lukin, H-P Liermann, KV Glazyrin, BN Savenko “Structural and magnetic properties of Cr2O3 at high pressure”, Journal of Alloys and Compounds, 722, 1, 593-598 (2017).
12. Golovin I.S., A.M. Balagurov, V.V. Palacheva, A. Emdadi, I.A. Bobrikov, A.Yu. Churyumov, V.V. Cheverikin, A.V. Pozdniakov, A.V. Mikhaylovskaya, S.A. Golovin “Influence of Tb on structure and properties of Fe-19%Ga and Fe-27%Ga alloys” J. of Alloys and Compounds, 707 (2017) 51-56.
13. Karpinsky D.V., I.O. Troyanchuk, M. Willinger, V.A. Khomchenko, A.N. Salak, V. Sikolenko, M.V. Silibin. Intermediate structural state in $Bi_{1-x}Pr_xFeO_3$ ceramics at the rhombohedral–orthorhombic phase boundary J. Mater. Sci. 52 (2017), 9355.
14. Kozlenko DP, K Drużbicki, SE Kichanov, EV Lukin, H-P Liermann, KV Glazyrin, BN Savenko “Anomalous lattice compression and magnetic ordering in CuO at high pressures: A structural study and first-principles calculations”, Physical Review B, 95, 5 054115 (2017).

PUBLICATIONS

15. Kozlenko DP, NM Belozerova, SS Ata-Allah, SE Kichanov, M Yehia, A Hashhash, EV Lukin, BN Savenko, “Neutron diffraction study of the pressure and temperature dependence of the crystal and magnetic structures of Zn0.3Cu0.7Fe1.5Ga0.5O4 polycrystalline ferrite”, Journal of Magnetism and Magnetic Materials, 449, 44-48 (2018).
16. Kozlenko DP, NT Dang, TL Phan, SE Kichanov, LH Khiem, SG Jabarov, TA Tran, TV Manh, AT Le, TK Nguyen, BN Savenko “The structural, magnetic and vibrational properties of Ti-doped BaMnO3”, Journal of Alloys and Compounds, 695, 2539-2548 (2017).
17. Kurlov A.S., A.I. Gusev, A.A. Rempel, V.S. Kuznetsov, I.A. Bobrikov, A.M. Balagurov “Evolution of microstructure of niobium carbide NbC0.77 powders” Wiley Online Library, Crystal Research & Technology, 1700061 (2017) 1700061 (1-7).
18. Ovsyannikov SV, Bykova E, Pakhomova A, Kozlenko DP, Bykov M, Kichanov SE, Morozova NV, Korobeinikov IV, Wilhelm F, Rogalev A, Tsirlin AA, Kurnosov AV, Zainulin YG, Kadyrova NI, Tyutyunnik AP, Dubrovinsky L. “Structural and Magnetic Transitions in CaCo3V4O12 Perovskite at Extreme Conditions”, Inorganic Chemistry, 56 (11), pp 6251–6263 (2007).
19. Palacheva V.V., A. Emdadi, F. Emeis, I.A. Bobrikov, A.M. Balagurov, S.V. Divinski, G. Wilde, I.S. Golovin “Phase transitions as a tool for tailoring magnetostriction in intrinsic Fe-Ga composites” Acta Materialia 130 (2017) 229-239. ИФ = 5.058.
20. Pashchenko A.V., V. P. Pashchenko, V. K. Prokopenko, V. A. Turchenko, Yu. F. Revenko, A.S. Mazur, V. Ya. Sycheva, N. A. Liedienov, V. G. Pitsyuga, G. G. Levchenko, Role of Structure Imperfection in the Formation of the Magnetotransport Properties of Rare-Earth Manganites with a Perovskite Structure, Journal of Experimental and Theoretical Physics – 2017. – Vol. 124, No. 1. – P. 100–113.
21. Salamatin DA, VA Sidorov, SE Kichanov, DP Kozlenko, LN Fomicheva, AV Nikolaev, OL Makarova, AV Tsvyashchenko “Effect of high pressure on charge density wave formation and magnetic structure in the cubic high-pressure phase of TbGe 2.85”, Physical Review B, 94, 21, 214435 (2017).
22. Sikolenko V., E. Efimova, A. Franz, C. Ritter, I.O. Troyanchuk, D. Karpinsky, I. Zubavichus, A. Veligzhanin, S.I. Tiutiunnikov, A. Sazonov, E. Efimov X-ray absorption spectroscopy and neutron diffraction study of the perovskite-type rare-earth cobaltites Physica B in press, [doi: 10.1016/j.physb.2017.09.104].
23. Sikolenko V.V., S.L.Molodtsov, M.Izquierdo, I.O.Troyanchuk, D.Karpinsky, S.I.Tiutiunnikov, E.Efimova, D.Prabhakaran, D.Novoselov, V.Efimov Correlated oxygen displacements and phonon mode changes in $LaCoO_3$ single crystal Physica B in press, Available online, [doi: 10.1016/j.physb.2017.10.031].
24. Troyanchuk I.O., D.V. Karpinsky, M.V. Bushinsky, V.A. Sirenko, V.V. Sikolenko, A. Franz Antiferromagnet-ferromagnet transition in $La_{1-x}Sr_xMn_{0.5}Ni_{0.5}O_3 (0<x<0.2)$ ceramics. Low Temperature Physics 43 (2017), 1219.
25. Troyanchuk I.O., D.V. Karpinsky, M.V. Bushinsky, V.V. Sikolenko, S.A. Gavrilov, M.V. Silibin Magnetic and magnetoresistance properties of $La_{0.7}Sr_{0.3}(Mn,Co)O_3$. Physica B 524 (2017), 22-26.
26. Troyanchuk I.O., M.V. Bushinsky, D.V. Karpinsky, V.V. Sikolenko, A.N. Chobot, N.V. Tereshko, O.S. Mantytskaya, S. Schorr Magnetic phase transformations and magnetotransport phenomena in $La_{0.7}Sr_{0.3}Mn_{1-x}Co_xO_3$ pervoskite compounds JETP 125 (2017), 290-297.
27. Troyanchuk I.O., M.V.Bushinsky, A.N.Chobot, N.V.Tereshko, O.S.Mantytskaya, E.A.Efimova, V.V.Sikolenko, V.M.Dobryanski. Magnetic Phase Transitions in $Ln_{1-x}Sr_xCo_{0.5}Mn_{0.5}O_3$ (Ln=La, Pr, Nd and Eu) Physics of the Solid State 59 (2017), 728-732.
28. Troyanchuk I.O., N.V. Tereshko, M.V. Silibin, S.A. Gavrilov, K.N. Nekludov, V. Sikolenko, S.Schorr, H. Szymczak. Magnetic Ordering in Manganites Doped by Ti and Al Ceramics International 43 (2017), 187-191.
29. Trukhanov A.V., S. V. Trukhanov, V. G. Kostishin, L. V. Panina, M. M. Salem, I. S. Kazakevich, V. A. Turchenko, V. V. Kochervinskii, D. A. Krivcheny, Multiferroic Properties and Structural Features of M-Type Al-Substituted Barium Hexaferrites, Physics of the Solid State. – 2017. – V. 59, No. 4. – P. 737–745.
30. Trukhanov A.V., S. V. Trukhanov, V. G. Kostishyn, L. V. Panina, I. S. Kazakevich, An. V. Trukhanov,V. O. Natarov, D. N. Chitanov, V. A. Turchenko, V. V. Oleynik,E. S. Yakovenko, L. Yu. Macuy, E. L. Trukhanova, Microwave properties of the Ga-substituted $BaFe_{12}O_{19}$ hexaferrites, Materials Research Express – 2017. – V.4, № 7. – P. 076106 (1-6).

31. Trukhanov A.V., S.V. Trukhanov, L.V. Panina, V.G. Kostishyn, D.N. Chitanov, Il.S. Kazakevich, A.V. Trukhanov, V.A. Turchenko, M.M. Salem, Strong corelation between magnetic and electrical subsystems in diamagnetically substituted hexaferrites ceramics, Ceramics International. – 2017. – V.43. – P.5635–5641.
32. Trukhanov A.V., S.V. Trukhanov, L.V. Panina, V.G. Kostishyn, I.S. Kazakevich, An.V. Trukhanov, E.L. Trukhanova, V.O. Natarov, V.A. Turchenko, M.M. Salem, A.M. Balagurov “Evolution of structure and magnetic properties for BaFe11.9Al0.1O19 hexaferrite in a wide temperature range” J. Magnetism and Magnetic Materials 426 (2017) 487–496.
33. Trukhanov S. V., A. V. Trukhanov, V. G. Kostishyn, L. V. Panina, An. V. Trukhanov, V. A. Turchenko, D. I. Tishkevich, E. L. Trukhanova, O. S. Yakovenko, L. Yu. Matzui, Investigation into the structural features and microwave absorption of doped barium hexaferrites, Dalton Transactions – 2017. – V.46. – P.9010 – 9021.
34. Trukhanov S.V., A.V. Trukhanov, V.G. Kostishyn , L.V. Panina, An.V. Trukhanov, V.A. Turchenko, D.I. Tishkevich, E.L. Trukhanova, V.V. Oleynik, O.S. Yakovenko, L.Yu. Matzui, D.A. Vinnik, Magnetic, dielectric and microwave properties of the $BaFe_{12-x}Ga_xO_{19}$ (x < 1.2) solid solutions at room temperature, Journal of Magnetism and Magnetic Materials. – 2017. – V. 442. – P. 300–310.
35. Trukhanov S.V., A.V. Trukhanov, V.G. Kostishyn, L.V. Panina, An.V. Trukhanov,V.A. Turchenko, D.I. Tishkevich, E.L. Trukhanova, O.S. Yakovenko, L. Yu Matzui, D.A. Vinnik, D.V. Karpinsky, Effect of gallium doping on electromagnetic properties of barium hexaferrite, Journal of Physics and Chemistry of Solids. – 2017. – V. 111. – P.142–152.
36. Trukhanov S.V., A.V. Trukhanov, V.G. Kostishyn, L.V. Panina, V.A. Turchenko, I.S. Kazakevich, An.V. Trukhanov, E.L. Trukhanova, V.O. Natarov, A.M. Balagurov “Thermal evolution of exchange interactions in lightly doped barium hexaferrites” J. Magnetism and Magnetic Materials 426 (2017) 554–562.
37. Trukhanov S.V., A.V. Trukhanov, V.O. Turchenko, I.S. Kazakevich, V.G. Kostishin, L.V. Panina, I.S. Kazakevich, A.M. Balagurov “Magnetic Ordering in BaFe11.9In0.1O19 Hexaferrite” Journal of Low Temperature Physics 186(1-2) (2017), pp. 44-62.
38. Valkov S., D. Neov, R. Bezdushnyi, A. Beskrovnyi, P. Petrov, Study of the microstructure, crystallographic structure and thermal stability of Al-Ti-Nb alloys produced by selective electron beam alloying, submitted to Journal of Surface Investigation: X-ray, Synchrotron and Neutron Techniques.
39. Waliszewski J., K. Rećko Magnetization distribution in some noncollinear systems (Phase Transition under review).
40. Бобриков И.А., Н.Ю. Самойлова, Д.А. Балагуров, О.Ю. Иваньшина, О.А. Дрожжин, А.М. Балагуров “Анализ структурных трансформаций в литий-ионном аккумуляторе с помощью дифракции нейтронов” Электрохимия, 2017, том 53 (2), с. 198–207. Bobrikov I.A., Samoylova N.Yu, Balagurov D.A., Ivanshina O.Yu,Drozhzhin O.A., Balagurov A.M. “Neutron diffraction analysis of structural transformations in lithium-Ion batteries” Russian Journal of Electrochemistry 53(2) (2017) 178-186.
41. Леденев Н.А., А.В. Пащенко, В.П. Пащенко, В.К. Прокопенко, Д.Д. Татарчук, Ю.Ф. Ревенко, В.А. Турченко, В.В. Бурховецкий, В.Я. Сычева, А.Г. Сильчева, Ю.В. Диденко, Г.Г. Левченко, Влияние ионов K+ и сверхстехиометрического марганца на дефектность структуры, магнитотранспортные и диэлектрические свойства магниторезистивной керамики La0.7Ca0.3–xKxMn1+xO3–δ, Физика низких температур – 2017. – Т. 43, № 9 – С. 1342–1353.
42. Сумин В.В. , Балагуров А.М., Бокучава Г., Васин Р.Н., Козлов П.А., Папушкин И.В., Скоробогатых В.Н., Томчук А.В., Торок Д. Изучение распада мартенсита в ферритно-мартенситных сталях методами рассеяния нейтронов. ФТТ (2017) принята в печать.
43. Турченко В.А., Н.А. Каланда, Л.В. Ковалев, В.Г. Симкин, А.М. Балагуров “Влияние концентрации ионов Sr на кристаллическую и магнитную структуру двойных перовскитов Ba2-xSrxFeMoO6 (x = 0–1.6)” Кристаллография 62 (2017) 33-42. “The influence of the concentration of Sr ions on the crystal and magnetic structures of Ba2 – xSrxFeMoO6 double perovskites (x = 0–1.6)” Crystallography Reports 62(1) (2017) 40-49.

PUBLICATIONS

Nanostructured materials (small-angle scattering and diffraction)

44. Andronache C., M. Balasoiu and D. Racolta, “Magnetic Interaction Between Iron Particles in Lithium-Phosphate Systems”, Russian Journal of Physical Chemistry A, 2017, 91(13) (2017) 198–201.
45. Belozerova N. M.; S. E. Kichanov; D. P. Kozlenko; O. Kaman; Z. Jirák “Core-Shell Magnetic Structure of La1–xSrxMnO 3+δ Nanocrystallites”, IEEE Transactions on Magnetics, 53, 11, p.1 (2017).
46. Bica Ioan, Maria Balasoiu, Madalin Bunoiu, “Elements of Materials Technology in DC plasma”, ISBN 978-5-94836-485-8, Technosphera JSC Publishing House, Moscow, 2017, 445 p.
47. Doroshkevich A.S., A I Lyubchyk, A K Islamov, V A Turchenko, V A Glazunova, T Yu Zelenyak, V V Burkhovetskiy, A V Shylo, M. Balasoiu, A V Saprykina, S Ohmura, O S Lygina, S I Lyubchyk, T E Konstantinova, M V Lakusta, V I Bodnarchuk, S B Lyubchyk, Yu Yu Bacherikov, Ye Aliyeva, Kh T Kholmurodov, “Nonequilibrium chemo-electronic conversion of water on the nanosized YSZ: experiment and Molecular Dynamics modelling problem formulation”, Journal of Physics: Conf. Series 848 012021(9) (2017).
48. Dragolici A.C., M Balasoiu, O L Orelovich, L Ionascu, M Nicu, D V Soloviov, A I Kuklin, E I Lizunov, F Dragolici,” CEM V based special cementitious materials investigated by means of SANS method. Preliminary results”, IOP Conf. Series: Journal of Physics: Conf. Series 848 012024(6) (2017).
49. Gurin V.S., G.E. Rachkovskaya, G.B. Zakharevich, S.E. Kichanov “SANS AND WXRD STUDY OF PbSe-DOPED SILICATE GLASSES”, Book: Physics, Chemistry and Application of Nanostructures: Reviews and Short Notes to Nanomeeting-2017, p. 136-140 (2017).
50. Loiko, P. A., Rachkovskaya, G. E., Skoptsov, N. A., Arzumanyan, G. M., Kulik, M., Kuklin, A. I., ... & Mateos, X. (2017). Mechanisms of Up-Conversion Luminescence in Glass-Ceramics Containing Er: PbF2 Nanocrystals. Journal of Applied Spectroscopy, 1-8.
51. Sergeenkov S., C. Stan, C.P. Cristescu, M. Balasoiu, N.S. Perov, C. Furtado, “Evidence forfield induced proximity type behavior in based ferromagnetic nanofluid”, Philosophical Magazine Letters 97(7) 2017 (287-293)
52. Дорошкевич А.С., А.И. Логунов , А.В. Шило , А.И. Любчик , А.К. Кириллов , Г.А. Троицкий, Т.А. Василенко , Т.Ю. Зеленяк , Ю.Ю. Бачериков , В.А. Глазунова , В.В. Бурховецкий , Д.А. Суворов , А.Х. Исламов , В.С. Дорошкевич , Х.Т. Холмуродов , Э.Б. Аскеров, А.И. Мададзада , Maria Balasoiu, Valer Almasan , А.А. Набиев , Т.Е. Константинова Комплексное исследование ВГД-уплотненной наноструктурированной системы на основе ZrO2 в аспекте сенсорных применений, Физика и техника высоких давлений 2017, том 27, № 3.
53. Дорошкевич А.С., Линник Д.С. , Гашимова В.Р. , Шило А.В., Любчик А.И. , Зеленяк Т.Ю., Аскеров Э.Б, и др. Хемоэлектронная конверсия на поверхности диоксид-циркониевых наночастиц в матрице сетчатого эпоксидного полимера. Химико-биологические науки 2017 Том 2 р 338-340.
54. Дорошкевич А.С., Э.Б. Аскеров, А.А. Набиев, А.И. Мададзада, Я. Алиева, А.Х. Исламов, Т.Ю. Зеленяк, А.И. Любчик, В.В. Бурховецкий, В.А. Глазунова, Л.В. Лоладзе, В.С. Дорошкевич, А.В Шило, С.А. Синякина, А.В.Сапрыкина, П.П. Гладышев, Х.Т. Холмуродов, М. Балашою Электрические свойства гидратированных нанопорошковых систем на основе диоксида циркония // Труды научного семинара памяти И.Л. Ходаковского, Дубна, 6-7 апреля 2017г, С.70-75.
55. Курлов А.С., А.И. Гусев, В.С. Кузнецов, И.А. Бобриков, А.М. Балагуров, А.А. Рempель “Времяпролетная нейтронография нанокристаллических порошков нестехиометрического карбида ниобия NbC0.77” ФТТ 59 (3) (2017) 588-593. A.S. Kurlov, A.I. Gusev, V.S. Kuznetsov, I.A. Bobrikov, A.M. Balagurov, A.A. Rempel “Time-of-Flight Neutron Diffraction of Nanocrystalline Powders of Nonstoichiometric Niobium Carbide NbC0.77” Physics of Solid State, 59 (3) (2017) 607-612.

Soft matter, liquids (small angle scattering and diffraction)

56. Artikulnyi A.P., Petrenko V.I., Bulavin L.A., Ivankov O.I., Avdeev M.V., Impact of poly (ethylene glycol) on the structure and interaction parameters of aqueous micellar solutions of anionic surfactant. Romanian Reports in Physics (2017), accepted.
57. Balasoiu M., O.I. Ivankov, Yu.L. Raikher, A. Rogachev, M. Bunoiu (Eds.), “3rd International

Summer School and Worshop Complex and Magnetic soft matter systems: Physico-Mechanical Properties and Structure", Book of Abstracts, ISBN 978-5-9530-0472-5, JINR Publishing House, 2017, 75 p.

58. Balasoiu M., O.Ivankov, D. Soloviov, S. Lysenko, A.-M. Balasoiu-Gaina, C. Stan, N. Lupu, D. Creanga, A. Kuklin, „Structural analysis of aqueous ferrofluids with cobalt ferrite particles stabilized with lauric acid and sodium n-dodecyl sulphate", Journal of Physics: Conf. Series 848 012026(6) (2017).
59. Balasoiu M., S.V. Kozhevnikov, Yu. V. Nikitenko, G.E. Iacobescu, M. Bunoiu, I. Bica, „Silicone rubber based magnetorheological elastomer: magnetic structure tested by means of neutron depolarization and magnetic force microscopy methods", Journal of Physics: Conf. Series 848 012016(9) (2017).
60. Balasoiu M., V.T. Lebedev, Yu. L. Raikher, I. Bica, M. Bunoiu, "The implicit effect of texturizing field on the elastic properties of magnetic elastomers revealed by SANS", Journal of Magnetism and Magnetic Materials 431 126-129 (2017).
61. Balasoiu Maria, Rodica Vladoiu, Oleksandr I. Ivankov (Eds.), "2nd Workshop on Condensed Matter Research by Means of Neutron Scattering Methods", 14-16 July 2017, Constanta, Romania, Book of Abstracts, ISBN 978-5-9530-0474-9, JINR Publishing House, 2017, 53 p.
62. Balasoiu-Gaina A-M, M Balasoiu, O Ivankov, D Soloviov, S Lysenko, C Stan, N Lupu, D Creanga and A Kuklin. Structural analysis of aqueous ferrofluids with cobalt ferrite particles stabilized with lauric acid and sodium n-dodecyl sulphate. Journal of Physics: Conference Series, 848,1, 012026.
63. Balejčíková L., V.I.Petrenko, M.V.Avdeev, V.M.Garamus, L.Almásy, P.Kopčanský. Small-angle scattering on magnetoferritin nanoparticles. J. Phys.: Confer.Series 848 (2017) 012011. doi:10.1088/1742-6596/848/1/012011
64. Balejcíková L., V.M.Garamus, M.V.Avdeev, V.I.Petrenko, L.Almásy, P.Kopcansky. The effect of solution pH on the structural stability of magnetoferritin. Coll. Surf. B 156 (2017) 375–381. http://dx.doi.org/10.1016/j.colsurfb.2017.05.036.
65. Boikova, A. S., Dyakova, Y. A., Ilina, K. B., Konarev, P. V., Kryukova, A. E., Kuklin, A. I., Marchenkova, M. A., Nabatov, B. V., Blagov, A. E., Pisarevsky, Y. V. & Kovalchuk, M. V. (2017). Octamer formation in lysozyme solutions at the initial crystallization stage detected by small-angle neutron scattering. Acta Cryst. D73, 591-599.
66. Bulavin L., Y. Prylutskyy, O. Kyzyma, M. Evstigneev, U. Ritter, P. Scharff. Chapter: Self-organization of pristine C60 fullerene and its complexes with chemotherapy drugs in aqueous solution as promising anticancer agents. Book Physics of Liquid Matter: Modern Problems. (2017) in press.
67. Bunoiu M., J. Neamțu, L.Chirigiu, M. Bălășoiu, G. Pascu, I.Bica, L.M.E.Chirigiu, „Hybrid Magnetorheological Elastomers: Effects of the magnetic field on some electrical properties", Applied Surface Science 424 (2017) 282-289.
68. Cherny, A. Y., Anitas, E. M., Osipov, V. A., & Kuklin, A. I. (2017). Scattering from surface fractals in terms of composing mass fractals. Journal of Applied Crystallography, 50(3), 919-931.
69. Cherny, A. Y., Anitas, E. M., Osipov, V. A., & Kuklin, A. I. (2017). Small-angle scattering from the Cantor surface fractal on the plane and the Koch snowflake. Physical Chemistry Chemical Physics. Phys. Chem. Chem. Phys., 2017, 19, 2261-2268.
70. Chilom C.G., D.M. Găzdaru, M. Bălăşoiu, M. Bacalum, S.V. Stolyar, A.I. Popescu, „Biomedical Application of Biogenic Ferrihydrite Nanoparticles", Romanian Journal of Physics 62(3-4) (1-13) (2017)
71. Davide Barreca, Giuseppina Lagana, Giovanni Toscano, Pietro Calandra, Mikhail A. Kiselev, Domenico Lombardo, Ersilia Bellocco. The interaction and binding of flavonoids to human serum albumin modify its conformation, stability and resistance against aggregation and oxidative injuries. Biochimica et Biophysica Acta 1861 (2017) 3531-3539.
72. Egorov V V, Ya A Zabrodskaya, D V Lebedev, A N Gorshkov and A I Kuklin. Structural features of the ionic self-complementary amyloidogenic peptide. Journal of Physics: Conference Series, 848,1, 012022.
73. Gdovinova V., N.Tomasovicova, I.Batko, M.Batkova, L.Balejcikova, V.M.Garamus, V.I.Petrenko, M.V.Avdeev, P.Kopcansky. Interaction of magnetic nanoparticles with lysozyme amyloid fibrils. JMMM 431 (2017) 8-11. http://dx.doi.org/10.1016/j.jmmm.2016.09.035
74. Golub, M., Combet, S., Wieland, D. C. F., Soloviov, D., Kuklin, A., Lokstein, H., ... & Pieper, J. (2017). Solution structure and excitation

PUBLICATIONS

energy transfer in phycobiliproteins of Acaryochloris marina investigated by small angle scattering. Biochimica et Biophysica Acta (BBA)-Bioenergetics, 1858(4), 318-324.

75. Gorshkova, Yu. E., Kuklin, A. I., & Gordeliy, V. I. (2017). Structure and phase transitions of DMPC multilamellar vesicles in the presence of Ca2+ ions. Journal of Surface Investigation: X-ray, Synchrotron and Neutron Techniques, 11(1), 27-37.
76. Gorshkova, Yu.E., Ivankov, O.I. Structure and phase transitions of the multilamellar DMPC membranes in presence of the DMSO and DESO sulfoxides, 2017 IOP Conf. Series: Journal of Physics: Conf. Series 848 (2017) 012014.
77. Gruzinov A.Yu., A.V. Zabelin, M.A. Kiselev. Short periodicity phase based on ceramide [AP] in the model lipid membranes of stratum corneum does not change during hydration. Chemistry and Physics of Lipids 202 (2017) 1–5.
78. Jargalan N., T.V. Tropin, M.V. Avdeev, V.L. Aksenov, D. Sangaa. The kinetics of dissolution and cluster formation of fullerene in polar and low polar solutions. Solid State Phenomena (2017) in press.
79. K. Ludzik , K. Kustrzepa,M. Kowalewicz-Kulbat, B. Kontek, R. Kontek, M. Jozwiak, D. Lulo “Antimicrobial and cytotoxic properties of bisquaternary ammonium bromides with different spacer chain length” Journal of Surfactants and Detergents, 2017.
80. Kholmurodov Kh., E Dushanov, M Khusenov, Kh Kahmonov, T Zelenyak, A Doroshkevich and S Majumder Molecular dynamics studies on the interaction and encapsulation processes of the nucleotide and peptide chains inside of a carbon nanotube matrix with inclusion of gold nanoparticles. IOP Conf. Series: Journal of Physics: Conf. Series. 2017, 848, 012012.
81. Kholmurodov Kh.T. (Ed), Computer Design for New Drugs and Materials. Molecular Dynamics of Nanoscale Phenomena, ISBN: 978-1-53612-082-0, Nova Science Publishers, New York (2017), 231 p.
82. Kiselev Mikhail A., Domenico Lombardo. Structural characterization in mixed lipid membrane systems by neutron and X-ray scattering. BBA 1861 (2017) 3700-3717.
83. Kubovcikova M., I.V.Gapon, V.Zavisova, M.Koneracka, V.I.Petrenko, O.Soltwedel, L.Almasy, M.V.Avdeev, P.Kopcansky. On the adsorption properties of magnetic fluids: impact of bulk structure. JMMM 427 (2017) 67–70. http://dx.doi.org/10.1016/j.jmmm.2016.10.104.
84. Kučerka N., E Dushanov, K T Kholmurodov, J Katsaras and D Uhríková. Lipid membranes loaded with Ca2+ and Zn2+ cations. IOP Conf. Series: Journal of Physics: Conf. Series. 2017, 848, 012008.
85. Kučerka N., E. Dushanov, Kh. Kholmurodov, J. Katsaras, and D. Uhríková. Calcium and Zinc Differentially Affect the Structure of Lipid Membranes. Langmuir. 2017, 33 (12), pp 3134–3141.
86. Kučerka N., E. Dushanov, Kh.T. Kholmurodov, J. Katsaras, D. Uhríková. Cation-Containing Lipid Membranes - Experiment and Simulations. European Pharmaceutical Journal (2017).
87. Kuklin A I, A V Rogachev, D V Soloviov , O I Ivankov, Yu S Kovalev, P K Utrobin, S A Kutuzov, A G Soloviev , M I Rulev and V I Gordeliy. Neutronographic investigations of supramolecular structures on upgraded small-angle spectrometer YuMO. IOP Conf. Series: Journal of Physics: Conf. Series 848 (2017),1, 012010.
88. Kulvelis, Y.V., S.S. Ivanchev, O.N. Primachenko, V.T. Lebedev, E.A. Marinenko, I.N. Ivanova, A.I. Kuklin, O.I. Ivankov,D.V. Soloviov, Structure and property optimization of perfluorinated short side chain membranes for hydrogen fuel cells using orientational stretching. RSC Advances, 2016. 6(110): p. 108864-108875.
89. Ludzik K., A. Kacperska, K.Kustrzepa, R.Dychto “Interactions between sodium dodecylsulphate and didodecyldimethylammonium bromides vesicles in aqueous solutions” Journal of Molecular Liquids 2017, 240, 273-279.
90. Lynchak O.V., Yu I. Prylutskyy, V. K. Rybalchenko, O. A. Kyzyma, D. Soloviov, V. V. Kostjukov, M. P. Evstigneev, U. Ritter and P. Scharff. Comparative Analysis of the Antineoplastic Activity of C60 Fullerene with 5-Fluorouracil and Pyrrole Derivative In Vivo. Nanoscale Research Letters, 2017, 12:8.
91. Molcan M., V.I.Petrenko, M.V.Avdeev, O.I.Ivankov, V.M.Garamus, A.Skumiel, A.Jozefczak, M.Kubovcikova, P.Kopcansky, M.Timko. Structure characterization of the magnetosome solutions for hyperthermia study. J. Mol. Liq. 235 (2017) 11–16. http://dx.doi.org/10.1016/j.molliq.2016.12.054.
92. Molchanov V S, V A Pletneva, A I Kuklin and O E Philippova. Nanocomposite composed of charged wormlike micelles and magnetic particles. Journal of Physics: Conference Series,

848,1, 012013.

93. Nabiyev A.A., A.Kh. Islamov, A.M. Maharramov, M.A. Nuriyev, R.S Ismayilova, A.S. Doroshkevic, A. Pawlukojc, V.A. Turchenko, M.İ. Rulev, V. Almasan, A.I. Kuklin, Structural Studies of dielectric HDPE+ZrO2 polymer nanocomposites, IOP Conf. Series: Journal of Physics: Conf. Series 2017 accepted
94. Nabiyev A.A., A.Kh. Islamov, A.M. Maharramov, R.S. Ismayilova, M.N. Mirzayev, A.S. Doroshkevic, V.A. Turchenko, M.I. Rulev, A.I. Kuklin, A Study of Structural and Thermal Properties of HDPE+ZrO2 Nanocomposites by X-Ray Diffraction (XRD) And Differential Thermal Analysis (DTA), American İnstitute of Physics (AIP) Conference Series 2017 accepted.
95. Nabiyev A.A., A.Kh. Islamov, A.M. Maharramov, R.S.Ismayilova, M.N. Mirzayev, A.S. Doroshkevic, V.A. Turchenko, M.I. Rulev, A.I. Kuklin, A Study of Structural and Thermal Properties of HDPE+ZrO2 Nanocomposites by X-Ray Diffraction (XRD) and Differential Thermal Analysis (DTA), Conference Proceedings Modern Trends In Physics, 2017, Baku, 43-45
96. Nagorna T.V., Kyzyma O.A, Chudoba D, Nagornyi A.V. Temporal solvatochromic effect in ternary C70/toluene/N-methyl-2-pyrrolidone solution. J. Mol. liq., 2017, 235, 111-114.
97. Nagornyi A.V., V.I.Petrenko, M.V.Avdeev, O.V.Yelenich, S.O.Solopan, A.G.Belous, A.Yu.Gruzinov, O.I.Ivankov, L.A.Bulavin. Structural aspects of magnetic fluid stabilization in aqueous agarose solutions. JMMM 431 (2017) 16–19. http://dx.doi.org/10.1016/j.jmmm.2016.10.018
98. Nikolaev, M., Round, E., Gushchin, I., Polovinkin, V., Balandin, T., Kuzmichev, P., ... & Bernhard, F. (2017). Integral Membrane Proteins Can Be Crystallized Directly from Nanodiscs. Crystal Growth & Design, 17(3), 945-948.
99. Petrenko V.I., A.V.Nagornyi, I.V.Gapon, L.Vekas, V.M.Garamus, L.Almasy, A.V.Feoktystov, M.V.Avdeev. Magnetic fluids: structural aspects by scattering techniques. Modern Problems of Molecular Physics. Selected Reviews Springer Proceedings in Physics (eds. Leonid Bulavin and Alexander Chalyi) (2017) in press.
100. Petrenko V.I., I.V. Gapon, A.A. Rulev, E.E. Ushakova, E.Yu. Kataev, L.V. Yashina, D.M. Itkis, M.V. Avdeev, Studies of electrochemical interfaces by TOF neutron reflectometry at the IBR-2 reactor, Journal of Physics: Conf. Series. (2017) accepted.
101. Petrenko V.I., O.P.Artykulnyi, L.A.Bulavin, L.Almásy, V.M.Garamus, O.I.Ivankov, N.A.Grigoryeva, L.Vekas, P.Kopcansky, M.V.Avdeev. On the impact of surfactant type on the structure of aqueous ferrofluids. Colloids Surf. A (2017), in press. https://doi.org/10.1016/j.colsurfa.2017.03.054.
102. Prylutska S., R. Panchuk, G. Gołuński, L. Skivka, Yu. Prylutskyy, V. Hurmach, N. Skorokhyd, A. Borowik, A. Woziwodzka, J. Piosik, O. Kyzyma, V. Garamus, L. Bulavin, M. Evstigneev, A. Buchelnikov, R. Stoika, W. Berger, U. Ritter, P. Scharff. C60 fullerene enhances cisplatin anticancer activity and overcomes tumor cells drug resistance. Nano Res., 2017, 10 (2), 652-671.
103. Prylutskyy Yu.I., I.V. Vereshchaka, A.V. Maznychenko, N.V. Bulgakova, O.O. Gonchar, O.A. Kyzyma, U. Ritter, P. Scharff, D.M. Nozdrenko, I.V. Mischenko. C60 fullerene as promising therapeutic agent for correcting and preventing skeletal muscle fatigue. J. Nanobiotechnol., 2017, 15:8.
104. Rajnak M., M.Timko, P.Kopcansky, K.Paulovicova, J.Tothova, J.Kurimsky, B.Dolnik, R.Cimbala, M.V.Avdeev, V.I.Petrenko, A.Feoktystov. Structure and viscosity of a transformer oil-based ferrofluid under an external electric field. JMMM 431 (2017) 99-102. http://dx.doi.org/10.1016/j.jmmm.2016.10.008
105. Rećko K., J. Waliszewski, U. Klekotka, D. Soloviov, G. Ostapczuk, D. Satuła, M. Biernacka, M. Balasoiu, A. Basa, B. Kalska-Szostko, K. Szymański, „Phase composition and magnetism of sol-gel synthesized Ga-Fe-O nanograins" Phase Transitions (ID: 1409351 DOI:10.1080/01411594.2017.1409351)
106. Ryzhykau Y., Nikolaev M., Zabelskii D., Kuklin A., Gordeliy V. Trimers of dimers of SRII/HtrII full complex. Small angle scattering structural investigation // The FEBS Journal. 2017. V. 284. Suppl. 1. P. 154.
107. Shibaev A V and A I Kuklin and O E Philippova. Effect of polymer on the arrangement of mixed anionic/cationic wormlike surfactant micelles revealed by SANS. Journal of Physics: Conference Series, 848,1, 012006.
108. Shibaev A V, A V Makarov, A L Aleshina, A V Rogachev, A I Kuklin and O E Philippova. Structure and oil responsiveness of viscoelastic fluids based on mixed anionic/cationic wormlike surfactant micelles. Journal of Physics: Conference Series, 848,1, 012019.

PUBLICATIONS

109. Shibaev, A. V., Abrashitova, K. A., Kuklin, A. I., Orekhov, A. S., Vasiliev, A. L., Iliopoulos, I., & Philippova, O. E. (2016). Viscoelastic Synergy and Microstructure Formation in Aqueous Mixtures of Nonionic Hydrophilic Polymer and Charged Wormlike Surfactant Micelles. Macromolecules. Macromolecules Macromolecules 2017, 50, 339−348.
110. Stan C., M. Balasoiu, D. Buzatu and C.P. Cristescu „Multifractal analysis of CoFe2O4/lauric acid/DDS-Na/H2O ferrofluid from TEM measurements", Journal of Computational and Theoretical Nanoscience, 14(4) 2030-2034(2017).
111. Tomchuk O.V. , Avdeev M.V., Bulavin L.A., Ryukhtin V.V., Ivankov O.I., Aksenov V.L., Nagornyi A.V. Study of tetraethoxysilane clusters in basic ethanol/water solutions by SANS contrast variation. Romanian Reports in Physics (2017) accepted.
112. Tomobe K., Yamamoto E, Kholmurodov K, Yasuoka K. Water permeation through the internal water pathway in activated GPCR rhodopsin. PLoS ONE 2017, 12(5): e0176876.
113. Tropin T.V., J.W.P. Schmelzer, V.L. Aksenov. On the possibility of modeling of kinetics of glass transition of polymers in a wide range of cooling and heating rates. Journal of Molecular Liquids, 2017, V. 235, pp. 172-177.
114. Uhríková, D., J. Teixeira, L. Hubčík, A. Búcsi, T. Kondela, T. Murugova,O.I. Ivankov, Lipid based drug delivery systems: Kinetics by SANS. Journal of Physics: Conference Series, 2017. 848(1): p. 012007.
115. Veligzhanin A.A., D.I. Frey, A.V. Shulenina, A.Yu. Gruzinov, Ya.V. Zubavichus, M.V. Avdeev, Characterization of aggregate state of polydisperse ferrofluids: some aspects of anisotropy analysis of 2D SAXS in magnetic field, JMMM (2017) in press.
116. Vlasov A. V., Yu. S. Kovalev, P. K. Utrobin, Yu. L. Ryzhykau, F. V. Frolov, E. V. Zinovev, A. V. Rogachev, A. I. Kuklin, V. I. Gordeliy. Photo-voltage of highly-oriented bacteriorhodopsin in purple membranes: Possibilities for bio solar cells. OPTOELECTRONICS AND ADVANCED MATERIALS – RAPID COMMUNICATIONS Vol. 11, No. 1-2, January-February 2017, p. 65 – 67.
117. Vlasov A., Ryzhykau Y., Gordeliy V., Kuklin A.Spinach ATP-synthases form dimers in nanodiscs. Small-angle X-ray and neutron scattering investigations // The FEBS Journal. 2017. V. 284. Suppl. 1. P. 87.
118. Vul A.Ya., E.D. Eidelman, A.E. Aleksenskiy, A.V. Shvidchenko, A.T. Dideikin, V.S. Yuferev, V.T. Lebedev, Yu.V. Kul'velis, M.V. Avdeev, Transition sol-gel in nanodiamond hydrosols, Carbon, 114 (2017) 242e249.
119. Аксенов В.Л., Т.В. Тропин, Ю.В.П. Шмельцер. Кинетические уравнения для описания перехода жидкость-стекло в полимерах. Теоретическая и математическая физика (2017) принята в печать.
120. Артикульный А.П., Петренко В.И., Булавин Л.А., Алмаши Л., Григорьева Н.А., Авдеев М.В., Аксенов В.Л., Влияние полиэтиленгликоля на структуру мицеллярных растворов олеата натрия в воде по данным малоуглового рассеяния нейтронов, Кристаллография (2017) принята в печать.
121. Булавин Л.А., Т.В. Нагорная, Е.А. Кизима, Д. Худоба, А.И. Иваньков, А.В. Нагорный, М.В. Авдеев, Кластерообразование фуллеренов в жидкостной системе С70/N-метил-2-пирролидон/толуол. Украинский физический журнал (2017) подана.
122. Горшкова Ю.Е. "Слияние фосфатидилхолиновых мембран индуцируемое диметилсульфоксидом и диэтилсульфоксидом", Поверхность. Рентгеновские, синхротронные и нейтронные исследования, 2017, (послано в печать).
123. Киселев М.А., Е. В. Земляная, А. Ю. Грузинов, Е. И. Жабицкая, О. М. Ипатова, В. Л. Аксенов. Анализ везикулярной структуры наночастиц фосфолипидной системы транспорта лекарств на основе данных МУРР. Препринт ОИЯИ Р3-2017-32, направлено в "Кристаллографию".
124. Киселев М.А., Е.В. Земляная. Дегидратация межмембранного пространства в многослойных везикулах дипальмитоилфосфатидилхолина под действием диметилсульфоксида. Нейтронные и синхротронные исследования. Кристаллография том 62, № 5, (2017) с. 795–799.
125. Маслова В.А., М.А. Киселев. Структура мицелл холата натрия. Препринт ОИЯИ Р3-2016-81. Принята к публикации в "Кристаллографии" 2017.
126. Нагорная Т.В., Е. А. Кизима, Л. А. Булавин, Д. Худоба, В. М. Гарамус, М. В. Авдеев, В. Л. Аксенов, Особенности кластеризации фуллеренов С60 в смеси толуол/N-метил-2-пирролидон. Кристаллография (2017) принята в печать.
127. Нагорный А. В., М. В. Авдеев, А. В. Еленич, С А. Солопан, А.Г. Белоус, А.В. Шуленина,

В.А. Турченко, Д.В. Соловьев, Л.А. Булавин, В. Л. Аксенов, Структурные особенности композиционных магнитных наночастиц Fe3O4/CoFe2O4 по данным рассеяния рентгеновских лучей и нейтронов, Кристаллография (2017), принята в печать.

128. Тропин Т.В., В.Л. Аксенов. Теоретическое исследование эффекта разбавления полярного раствора фуллеренов водой. Письма в ЖЭТФ (2017) направлена.
129. Тропин Т.В., М.В. Авдеев, В.Л. Аксенов. Моделирование эволюции функций распределения кластеров по размерам в полярных растворах фуллерена С60. Кристаллография (2017) принята в печать.

Thin films (reflectometry, polarized neutrons)

130. Avdeev M.V., A.A.Rulev, V.I.Bodnarchuk, E.E.Ushakova, V.I.Petrenko, I.V.Gapon, O.V.Tomchuk, V.A.Matveev, N.A.Pleshanov, E.Yu.Kataev, L.V.Yashina, D.M.Itkis. Monitoring of lithium plating by neutron reflectometry. Applied Surface Science 424 (2017) 378-382. http://dx.doi.org/10.1016/j.apsusc.2017.01.290
131. Gapon I.V., V.I. Petrenko, L.A. Bulavin, M. Balasoiu, M. Kubovcikova, V. Zavisova, M. Koneracka, P. Kopcansky, M.V. Avdeev, “Structure analysis of aqueous ferrofluids at interface with silicon: neutron reflectometry data”, Journal of Physics: Conf. Series, 848 012015(5) (2017).
132. Kulik M., E.B Asgerov, D. Kołodyńska, A. Bayramov, K. Pyszniak, A.P Kobzev Optical and nuclear study of near surface layers implanted GaAs, International Conference Modern Trends in Physics 20–22 April 2017, Baku. Pp 65-71.
133. Mateescu A.O., Mateescu, G., Balasoiu, M., Pompilian, G.O., Lungu, M., “Coating multilayer material with improved tribological properties obtained by magnetron sputtering”, IOP Conference Series: Materials Science and Engineering, 174(1) (2017) 012059.
134. Жакетов В.Д., Ю.В. Никитенко, Ф. Раду, А.В. Петренко, А. Чик, М.М. Борисов, Э.Х. Мухамеджанов, В.Л. Аксёнов, Магнетизм в структурах с ферромагнитными и сверхпроводящими слоями, ЖЭТФ, 2017, том. 151, Вып. 1, стр. 132-150.
135. Жакетов В.Д., Ю.В. Никитенко, А.В. Петренко, Ф. Раду, А. Чик, В.Л. Аксёнов, Релаксация магнитного состояния ферромагнитно-сверхпроводящей слоистой структуры, ЖЭТФ, 2017, том 152, вып. 2(8) стр. 1-16.
136. Федоров В.А., А.Д. Березнер, А.И. Бескровный, Д.С.Неов, Т.Н,Фурсова, А.В. Павликов, А.В. Баженов, Структура и свойства пленок SiOx, полученных химическим травлением лент аморфного сплава, напрвлена в ФТТ (2017).
137. Петренко В.И., Е.Н. Косячкин, Л.А. Булавин, М.В. Авдеев, Об усилении эффекта адсорбционного слоя на границе раздела «металлический электрод – жидкий электролит» в экспериментах по зеркальному отражению в рефлектометрии тепловых нейтронов, Поверхность. Рентгеновские, синхротронные и нейтронные исследования (2017), принята в печать.
138. Боднарчук В.И., П. Петров, Д.П. Козленко, Д. Дечев, Н. Иванов, И. Мартев, И.А. Касаткин, «Исследование свойств многослойных нанопокрытий TiN/WN, полученных методом магнетронного распыления», Поверхность, № 2, 2017, с. 23.

Atomic and magnetic dynamics (inelastic neutron scattering)

139. Bilski P., K. Drużbicki, J. Jenczyk, J. Mielcarek, J. Wąsicki, 2017, Molecular and Vibrational Dynamics in the Cholesterol-Lowering Agent Lovastatin: Solid-State NMR, Inelastic Neutron Scattering, and Periodic DFT Study, J. Phys. Chem. B, Volume 121, Issue 13, pp 2776-2787.
140. Drużbicki K.; R. S. Pinna; S. Rudic; M. Jura; G. Gorini; F. Fernandez-Alonso, 2016 'Cation Dynamics and Framework Flexibility in the Low-temperature Phase of Methylammonium Lead Iodide – The Need for a New Model', J. Phys. Chem. Lett. , Volume 7, pp 4701-4709.
141. Goremychkin E.A., Y.N. Pokotilovski, 2017, Neutron lifetime and density of states of fluoropolymers at low temperatures, JETP Letters Volume 105, Issue 8, pp 548-551.
142. Kiwilsza A., B. Milanowski, K. Drużbicki, J. Jenczyk, M. Jarek, J. Mielcarek, J. Lulek, A. Pajzderska, J. Wasicki, 2017, Molecular dynamics and the dissolution rate of nifedipine encapsulated in mesoporous silica,

PUBLICATIONS

Microporous and Mesoporous Materials, Volume 250, pp 186–194.

143. Klyushina E. S., B. Lake, A.T.M.N. Islam, J. T. Park, A. Schneidewind, T. Guidi, E. A. Goremychkin, B. Klemke,1 and M. Mansson, Investigation of spin-1 honeycomb antiferromagnet $BaNi_2V_2O_8$ with planar XY-type anisotropy, Phys. Rev. B accepted, in press.
144. Krzystyniak M., K. Drużbicki, G. Romanelli, M. J. Gutmann, S. Rudić, S. Imberti, F. Fernandez-Alonso, 2017, Nuclear dynamics and phase polymorphism in solid formic acid' Phys. Chem. Chem. Phys., Volume 19, pp 9064-9074.
145. Laine M., N.A. Barbosa, A. Kochel, B. Osiecka, G. Szewczyk, T. Sarna, P. Ziółkowski, R. Wieczorek, A. Filarowski, 2017, Synthesis, structural, spectroscopic, computational and cytotoxic studies of BODIPY dyes. Sens. Actuators B , Volume 238, pp 548-555.
146. Premužić D., A. Filarowski, M. Hołyńska, 2017, Structure and properties of a new rigid tripodal oxime ligand. J. Mol. Struct., Volume 1136, pp 100-106

Applied studies (texture, stresses, geological materials)

147. Altangerel B., Scheffzuek, Ch. & Sangaa, D. (2016) Structure Investigation of a Quartz and Onyx Sample from the Mongolian Noyon Region using the Neutron Time-Of-Flight Strain Diffractometer EPSILON. In: Davaa, Sureen & Odmaa Sambuu (Eds.): 6th International Conference on Contemporary Physics, ICCP-VI, Ulaan Baatar (Mongolia), June 7-10, 2016. Dedicated to the 60th anniversary of the Joint Institute for Nuclear Research Dubna, Mongolian J. Phys. 2, 442-448.
148. Baczmanski A., Wronski, S., Gadalinska, E., Zhao, Y., Le Joncour, L., Braham, C., Buslaps, T. & Scheffzuek, Ch. & Kot, P. (2017): Diffraction methods and scale transition model used to study evolution of intergranular stress and micro-damage phenomenon during elasto-plastic deformation. Submitted to Materials Research Forum LLC.
149. Bokuchava Gizo, Peter Petrov, Gancho Genchev, Nikolay Doynov, Ralf Ossenbrink, Vesselin Michailov, "Residual stress analysis in welded joints by numerical simulation and high resolution neutron diffraction", Romanian Reports in Physics, 2017 (accepted).
150. Bokuchava Gizo, Yulia Gorshkova, Ricardo Fernandez, Gaspar Gonzalez, Giovanni Bruno, "Characterization of precipitation in 2000 series aluminium alloys using neutron diffraction, SANS and SEM methods", Romanian Reports in Physics, 2017 (accepted).
151. Gadalinska E., Baczmanski, A., Wróbel, M., Wronski, S., Wronski, M., Wawszczak, R., Braham, C., Zhao, Y., Le Joncour, L. Buslaps, T. & Scheffzuek, Ch. (2016) The Role of Intergranular Stresses in Plastic Deformation Studied Using a Diffraction and Self-Consistent Model. Materials Research Forum LLC, Materials Research Proceedings 2, 551-556. [doi: http://dx.doi.org/10.21741/9781945291173-93].
152. Gadalinska E., Baczmanski, A., Wronski, S., Wróbel, M., Wierzbanowski, K., Lodini, A., Klosek, V., Buslaps, T. & Scheffzuek, Ch. (2017): Neutron and Synchrotron diffraction study of elastoplastic behaviour of Al/SiCp metal matrix composite. Materials Science Forum 905, 66-73. [doi: 10.4028/www.scientific.net/MSF.905.66].
153. Genchev Gancho, Nikolay Doynov, Ralf Ossenbrink, Vesselin Michailov, Gizo Bokuchava, Peter Petrov, "Residual stresses formation in multi-pass weldment: A numerical and experimental study", Journal of Constructional Steel Research, 2017, V. 138, pp. 633–641. https://doi.org/10.1016/j.jcsr.2017.08.017
154. Gizo Bokuchava, Yulia Gorshkova, Ricardo Fernandez, Gaspar Gonzalez, Giovanni Bruno, "Characterization of precipitation in 2000 series aluminium alloys using neutron diffraction, SANS and SEM methods", Romanian Reports in Physics, 2017, (accepted).
155. Ivankina T.I., I.Yu. Zel, T. Lokajicek, H. Kern, K.V. Lobanov, A.V. Zharikov, "Elastic anisotropy of layered rocks: ultrasonic measurements of biotite gneiss versus texture-based theoretical predictions (effective media modeling)", Tectonophysics, 2017, V. 712-713, pp. 82-94.
156. Keppler R., Behrmann, J.H. & Stipp, M. (2017). Textures of eclogites and blueschists from Syros island, Greece: Inferences for elastic anisotropy of subducted oceanic crust. J. Geophys. Res. 122 (7), 5306-5324. [doi: 10.1002/2017JB014181].
157. Kichanov S.E., I.A. Saprykina, D.P. Kozlenko "Old Russian treasures meet with neutrons in Dubna", International NR Newsletter, №12, p.12-13 (2017).

158. Kichanov S.E., K.M. Nazarov, D.P. Kozlenko, I.A. Saprykina, E.V. Lukin, B.N. Savenko “Analysis of the internal structure of ancient copper coins by neutron tomography”, Journal of Surface Investigation: X-ray, Synchrotron and Neutron Techniques, 11, 3, 585-589 (2017).
159. Kichanov S. E., D. P. Kozlenko, I. A. Saprykina, E. V. Lukin, A. V. Rutkauskas, K. M. Nazarov, B. N. Savenko “A Study of the Archeological Objects by Means of a Neutron Tomography Method” JINR NEWS, 1, 20-23 (2017).
160. Kossak-Glowczewski J., Froitzheim, N., Nagel, T.J., Pleuger, J., Keppler, R., Leiss, B. & Regent, V. (2017). Along-strike shear-sense reversal in the Vals-Scaradra Shear Zone at the front of the Adula Nappe (Central Alps, Switzerland).Swiss J. Geosci. 110 (2), 677-697. [doi: 10.1007/s00015-017-0270-7].
161. Lychagina T., Zisman, A., Yashina, E. & Nikolayev, D. (2017): Directly verifiable neutron diffraction technique to determine retained austenite in steel. Adv. Eng. Mater. 1700559, [doi: 10.1002/adem.201700559].
162. Papushkin I.V., D. Kaisheva, G.D. Bokuchava, P. Petrov, “Study of residual stresses in CT test specimens welded by electron beam”, Journal of Physics: Conference Series, 2017, http://conferenceseries.iop.org (in print).
163. Petrov P., G. Bokuchava, I. Papushkin, G. Genchev, N. Doynov, V. Michailov, M. Ormanova, “Neutron diffraction studies of laser welding residual stresses”, Proceedings of SPIE, Vol. 10226, 102260D (January 5, 2017). http://dx.doi.org/10.1117/12.2261802.
164. Scheffzuek Ch., Mueller, B.I.R., Breuer, S., Altangerel B. & Schilling, F.R. (2016): Applied Strain Investigation on Sandstone Samples Using Neutron Time-of-Flight Diffraction at the Strain Diffractometer EPSILON, IBR-2M Dubna. In: Davaa, Sureen & Odmaa Sambuu (Eds.): 6th International Conference on Contemporary Physics, ICCP-VI, Ulaan Baatar (Mongolia), June 7-10, 2016. Dedicated to the 60th anniversary of the Joint Institute for Nuclear Research Dubna, Mongolian J. Phys. 2, 427-434.
165. Wronski M., Baczmanski, A., Wierzbanowski, K., Wronski, S., Scheffzuek, Ch. & Kot, P. (2017). Investigation of lattice strain of Mg-alloy and Al/SiC using in situ TOF neutron diffraction. Submitted to Materials Research Forum LLC.
166. Бокучава Г.Д., Ю.Е. Горшкова, И.В. Папушкин, С.В. Гук, Р. Кавалла, “Исследование пластически деформированных TRIP-композитов методами нейтронной дифракции и малоуглового рассеяния нейтронов”, Поверхность. Рентгеновские, синхротронные и нейтронные исследования, 2018, № 3 (принято в печать).
167. Круглов А.А., Г.Д. Бокучава, И.В. Папушкин, "Нейтронная фурье-стресс-дифрактометрия по времени пролета на реакторе ИБР-2 для решения материаловедческих задач", Сборник материалов IV Международной конференции "Многомасштабное моделирование структур, строение вещества, наноматериалы и нанотехнологии (MMSN-4)", 18 – 21 сентября 2017 г., г. Тула, Россия, Изд-во ТГПУ им. Л.Н. Толстого, с. 54-59. ISBN 978-5-9500383-7-2. http://cheb.tsput.ru/conf/international/MMSN-2017/.
168. Сумин В.В. , Васин Р.Н., Исламов А.Х., Папушкин И.В., Томчук А.В. Изучение порошков ДУО-сталей методом нейтронографии. ФТТ (2017) принята в печать.
169. Сумин В.В., А.М. Балагуров, Г.Д. Бокучава, Р.Н. Васин, П.А. Козлов, И.В. Папушкин, В.Н. Скоробогатых, А.В. Томчук, Д. Торок, “Изучение распада мартенсита в ферритно-мартенситных сталях методами рассеяния нейтронов”, Письма в ЭЧАЯ, 2017. (принято в печать).
170. Цуканов В.В., Зиза, А.И., Михайлов, М.С., Николаев, Д.И. & Лычагина, Т.А. Исследование превращений остаточного аустенита при отпуске высокопрочной стали Cr-Ni-Mo-V композиции (подано в журнал “Письма о материалах”), 2017.

Instruments and Methods

171. Alekseev I.V., E.A. Goremychkin, N.A. Gundorin, A.V. Petrenko, I.L. Sashin, 2017,On a neutron detector based on $TlInSe_2$ crystals intercalated with a lithium isotope.

PUBLICATIONS

Semiconductors, Volume 51, Issue 6, pp. 740-744.

172. Avdeev M.V., Bobrikov I.A., Petrenko V.I., Characterization of Battery Materials: Neutron Methods, In Electrochemical Storage Materials – From Crystallography to Manufacturing Technology, Eds. D.C. Meyer, T. Leisegang, H. Stöcker, DeGruyter Publishing, 2017, in press.
173. Bodnarchuk V., V. Sadilov, S. Manoshin, R.V. Erhan, A. Ioffe, «Expected performance of time-gradient magnetic field SESANS diffractometer at pulsed reactor IBR-2», Journal of Physics: Conf. Series 862 (2017) 012003.
174. Kichanov S.E. “The first steps in neutron tomography processing: a freeware solution for newbies”, International NR Newsletter, №12, p.13-17 (2017).
175. Kozhevnikov S.V., F. Ott, E.M. Semenova, Neutron Zeeman beam-splitting method for the investigation of magnetic nanostructures, Physica B 508 (2017) 12-21.
176. Kozhevnikov S.V., T. Keller, Yu.N. Khaydukov, F. Ott, F. Radu, Characterization methods for neutron channeling in planar waveguides, Nucl. Instr. and Meth. A 875 (2017) 177-184.
177. Soloviev A G, T M Solovjeva, O I Ivankov, D V Soloviov, AV Rogachev and A I Kuklin. SAS program for two-detector system: seamless curve from both detectors. IOP Conf. Series: Journal of Physics: Conf. Series 848,1, (2017) 012020. doi :10.1088/1742-6596/848/1/012020
178. Авдеев М.В., В.И.Боднарчук, В.И.Петренко, И.В.Гапон, А.В.Томчук, А.В.Нагорный, В.А.Ульянов, Л.А.Булавин, В.Л.Аксенов. Нейтронный времяпролетный рефлектометр “ГРЭИНС” с горизонтальной плоскостью образца на реакторе ИБР-2: возможности и перспективы. Кристаллография 62(6) (2017) 1014–1021. DOI:10.7868/S0023476117060029 / M.V. Avdeev, V.I.Bodnarchuk, V.I.Petrenko, I.V.Gapon, O.V.Tomchuk, A.V.Nagorny, V.A.Ulyanov, L.A.Bulavin, V.L.Aksenov. Neutron time-of-flight reflectometer GRAINS with horizontal sample plane at the IBR-2 reactor: possibilities and prospects. Crystallography reports 62(6) (2017) 1002-1008. DOI:10.1134/S1063774517060025.
179. Авдеев М.В., Р.А. Еремин, В.И. Боднарчук, И.В. Гапон, В.И. Петренко, Р.В. Эрхан, А.В. Чураков, Д.П. Козленко, Концепция малоуглового дифрактометра в классической конфигурации на холодном замедлителе реактора ИБР-2, Поверхность. Рентгеновские, синхротронные и нейтронные исследования (2017) принята в печать.
180. Аксенов В.Л., А.М. Балагуров, Ю.Н. Пепелышев, А.Д. Рогов “Высокопоточный источник нейтронов на основе каскадного бустера” Вопросы атомной науки и техники. Серия: Физика атомных реакторов. 2017, вып. 2, с. 4-24.
181. Балагуров А.М. “Дифракция нейтронов для решения структурных задач” LAMBERT Academic Publishing, Saarbruken, 2017, 282 стр.
182. Бокучава Г.Д., И.В. Папушкин, “Нейтронная стресс-дифрактометрия по времени пролета”, Поверхность. Рентгеновские, синхротронные и нейтронные исследования, 2018, № 2 (принято в печать).
183. Злоказов В.Б., Д.А. Балагуров, И.А. Бобриков, Н.Ю. Самойлова, А.М. Балагуров “Визуализация и анализ больших массивов нейтронных дифракционных данных, измеренных в реальном времени” Поверхность, 2 (2017) 5-15. V. B. Zlokazov, D. A. Balagurov, I. A. Bobrikov*, N. Yu. Samoylova, and A. M. Balagurov “Visualization and Analysis Of Large Neutron Diffraction Data Arrays Measured in Real Time” J. Surf. Invest. 11 (1) (2017) 169-178.
184. Кожевников С.В., В.Д. Жакетов, Ю.Н. Хайдуков, Ф. Отт, Ф. Раду, Каналирование нейтронов в плоском волноводе, ЖЭТФ, том 152, вып. 6 (2017). doi: 10.7868/S0044451017120000.
185. Кожевников С.В., В.К. Игнатович, Ф. Раду, Применение зеемановского пространственного расщепления пучка в рефлектометрии поляризованных нейтронов. Поверхность. Рентгеновские, синхротронные и нейтронные исследования (2018), принято в печать.
186. Кожевников С.В., Ф. Отт, Ф. Раду, Нейтронные методы исследования магнитных плёнок, ЭЧАЯ, том 49, вып. 2 (2018), принято в печать.
187. Кожевников С.В., Ю.Н. Хайдуков, Ф. Отт, Ф. Раду, Каналирование нейтронов в потенциальной яме плоского волновода, ЖЭТФ (2018), направлено в журнал.
188. Эм В. Т., А. М. Балагуров, В. П. Глазков, И. Д. Карпов, P. Mikula, Н. Ф. Мирон, В. А. Соменков, В. В. Сумин, J. Saroun, М. Н. Шушунов “Двухкристальный монохроматор для нейтронной стресс-дифрактометрии” ПТЭ, 2017, т.4, с. 75-81.

Patents

189. Никитенко Ю.В., В.Д. Жакетов. Способ определения пространственных профилей ядерного и магнитного потенциалов взаимодействия поляризованных нейтронов со слоистой структурой. Подана заявка.

SECTOR OF RAMAN SPECTROSCOPY

190. Arzumanyan G.M., Kuznetsov E.A., Sarakovskis A., KriekeG., “Near-infrared-to-blue up-conversion luminescence in transparent Eu3+/Yb3+ doped oxyfluoride phosphors”, J. Mat. Sc. Eng-B, 2017, 7(2), pp. 71-76.
191. Arzumanyan G.M., Doroshkevich N.V., Mamatkulov K.Z., et al., “Phospholipid detection by surface-enhanced Raman scatteringusing silvered porous silicon substrates”,, J. PSS-A, 2017, 214(8), pp. 1600915 (1-6).
192. LoikoP.A., RachkovskayaG.E., Skoptsov N.A., Arzumanyan G.M., et al., “Photoluminescence of transparent glass-ceramics based on ZnO nanocrystals and co-doped with Eu3+, Yb3+ ions”,J. Appl. Spectr., 2017, 84(1), pp. 172-1–172-8.
193. ЯкимчукД.В., КанюковЕ.Ю., ДемьяновС.Е., БундюковаВ.Е., АрзуманянГ.М. идр., «Зависимость сигнала гигантского комбинационного рассеяния света от формы серебряных наноструктур, выращенных в порах SiO2/n-Si-шаблона», Приборы и методы измерений, 2017, 8(3), стр. 228-235б
194. Arzumanyan G.M., Mamatkulov K.Z., Fabelinsky V.I., et al., “Surface Enhanced micro-CARS from Gold Nanoparticle-Immobilized Organic at a Nanostructured CeO2/Al Film”, Technical Digest/ProceedingsInt. Conf. ECONOS,2-5 April, 2017,pp. 73-74.
195. Kaniukov E.Yu., Yakimchuk D.V., Arzumanyan G.M., et al., “Growth mechanisms of spatially separated copperdendrites in pores of a SiO2 template”, Philosophical Magazine, 2017, 97(26), pp. 2268-2283.
196. Arzumanyan G.M., Kuznetsov E.A., Alekseeva, et al, “Synthesis, structure and optical properties of glass-ceramics based on ZnO nanocrystals and codoped with Er3+ and Yb3+ ions”, Physics, Chemistry and Application of Nanostructures, World Scientific, Chapter · June 2017, pp.369-372.

DEPARTMENT OF IBR-2 SPECTROMETERS COMPLEX

197. Булавин М.В., Шариковый холодный замедлитель нейтронов реактора ИБР-2: некоторые аспекты создания и применения, автореферат дисс. канд. физ.-мат. наук: 01.04.01, Объединенный институт ядерных исследований, Дубна, 2017, 149 с.
198. Bulavin M.V., Kazakov A.V., Shabalin.E.P., To theory of pneumotransport of beads of cold neutron moderator of the IBR-2 reactor. Physics of particles and nuclei letters, 2017, Vol. 14, №3, 520–532.
199. Bolshakova I., Bulavin M., Kargin N., Kost Ya., Kuech T., Kulikov S., Radishevskiy M., Shurygin F., Strikhanov M., Vasil’evskii I. and Vasyliev A., Metal Hall sensors for the new generation fusion reactors of DEMO scale. Nuclear Fusion 57(11), June 2017, pp. 1-5.
200. Булавин М.В., Еник Т.Л., Куликов С.А., Рябухин О.В., Хатченко Е.Ю.,Радиационное окрашивание уральских топазов с использованием электронного и нейтронного излучений, Научный журнал Физика, по материалам XII Иссык-Кульской международной школы-конференции «Радиационная физика твердого тела», SCORPh-2017 – №1, 2017 – с. 55-57
201. Афанасьев С.В., Булавин М.В., Верхоглядов А.Е., Замятин Н.И., Кулагин Е.Н., Шафроновская А.И., Некоторые физические характеристики нейтронного

PUBLICATIONS

потока на пучке №3 ИБР-2 на значительном удалении от реактора Сообщение ОИЯИ Р3-2017-55, 2017.
202. Aksenov V.L., Ananiev V.D., Komyshev G.G., Rogov A.D., Shabalin E.P. On the Limit of Neutron Fluxes in the Fission-Based Pulsed Neutron Sources, Physics of Particles and Nuclei Lett. V, 14. № 5, p. 788 (2017).
203. Аксенов В.Л., Комышев Г.Г., Рогов А.Д, Шабалин Е.П, Высокопоточный импульсный исследовательский реактор на основе нептуния, Сообщение ОИЯИ Р13-2017-57, Дубна, 2017. Направлено в журнал Атомная энергия.
204. Рзянин М.В., Шабалин Е.П., Динамика импульсов мощности в исследовательском реакторе с нептуниевым ядерным топливом. Сообщение ОИЯИ Р13-2017-69. Направлено в журнал Атомная энергия.
205. Белушкин А. В., Маношин С.А., Моделирование отражения нейтронов от поверхности наноструктуированных объектов в модифицированном кинематическом приближении. Поверхность. Рентгеновские, синхротронные и нейтронные исследования, Принято к публикации, Сентябрь, 2017.
206. Belushkin A., Manoshin S., Some peculiarities for grazing incidence neutron diffraction from 3D near-surface nanostructures. Physica E, 2017, vol. 89 , pp. 93–99, DOI: 10.1016/j.physe.2017.02.010,
207. Bodnarchuk V., Erhan R., Ioffe A., Manoshin S., Sadilov V., Expected performance of time-gradient magnetic field SESANS diffractometer at pulsed reactor IBR-2. Journal of Physics: Conf. Series 862, 2017, 012003, DOI:10.1088/1742-6596/862/1/012003,
208. Кирилов А.С. "Новые версии программ юстировки и визуализации спектров для рефлектометров реактора ИБР-2". Письма в ЭЧАЯ. 2016, Т.13, № 1(199). С. 208-219.
209. Bogdzel A.A., Churakov A.V., Farkas G., Hervoches Ch., Litvinenko E.I., Lukas P., Pilch J., Ryukhtin V., Saroun J., Strunz P., Zhuravlev V.V. Upgrade of detectors of neutron instruments at Neutron Physics Laboratory in Řež, Nucl. Instrum. Methods Phys. Res. Sect. A 841(2017) 5-11.

NUCLEAR PHYSICS DEPARTMENT

Experimental investigations

210. Balibrea-Correa J., E Mendoza E., D Cano-Ott D., et al., Measurement of the neutron capture cross section of the fissile isotope 235U with the CERN n_TOF total absorption calorimeter and a fission tagging based on micromegas detectors, EPJ Web of Conferences
211. Barbagallo M., Colonna N., Aberle O., et al., 7Be (n, α) and 7Be (n, p) cross-section measurement for the cosmological lithium problem at the n_TOF facility at CERN, EPJ Web of Conferences 146, 01012
212. Chen Y.H., Tassan-Got L., Audouin L., et al., Characterization of the nTOF EAR-2 neutron beam, EPJ Web of Conferences 146, 03020
213. Dupont E., Otuka N., Cabellos O., et al., Dissemination of data measured at the CERN n_TOF facility, EPJ Web of Conferences 146, 07002
214. Gandhi A., D. N. Grozdanov, F. A. Aliyev, W. Dongming, N. A. Fedorov, Yu. N. Kopatch, V.R. Skoy, V.M. Bystritsky, I. N. Ruskov, C. Hramco, E. P. Bogolyubov, Yu. N. Barmakov, V. Kumar, V. Mishra, N. K. Rai, and A. Kumar, “TANGRA: Tagged Neutrons and Gamma Rays”, Proceedings of the DAE Symp. on Nucl. Phys. 62 (2017) http://sympnp.org/proceedings/62/G42.pdf
215. Gledenov Yu.M., Nesvizhevsky V.V., Sedyshev P.V., Shul’gina E.V., Szalanski P., Vesna V.A. First observation of P-odd asymmetry of α-particle emission in the 10B(n,α)7Li nuclear reaction. Physics Letters B 769 (2017) 111-116. (IF 4.807)
216. Gledenov Yu., Zhang G., Gonchigdorj K., Sedysheva M., Krupa L., Enkhbold S., Chuprakov I., Wang Z., Fan X., Zhang L. and Bai H. “Cross sections of the 144Sm(n,α)141Nd and 66Zn(n,α)63Ni reactions at 4.0, 5.0 and 6.0 MeV”. EPJ Web of Conferences 146, 11033 (2017)
217. Goremychkin E. A. and Yu.N. Pokotilovski, “Neutron lifetime and density of states of fluoropolymers at low temperatures”,Письма в ЖЭТФ, 105 (2017) 523-524; JETP Lett. 105 (2017)

218. Gunsing F., Aberle O., Andrzejewski J., et al., The measurement programme at the neutron time-of-flight facility n_TOF at CERN, EPJ Web of Conferences 146, 11002
219. Ruskov I., Kopatch Y., Bystritsky V., Skoy V., Shvetsov V., et al., TANGRA – an experimental setup for basic and applied nuclear research by means of 14.1 MeV neutrons, EPJ Web of Conferences. https://www.epj-conferences.org/articles/epjconf/pdf/2017/15/epjconf-nd2016_03024.pdf
220. Fry J., Alarcon R., Allen R. et al. (79 authors, including Sharapov E. I.), Status of the NPDGamma experiment, Hyperfine Interactions, v. 238:11 (2017).
221. Hickerson K. P., Sun X., Bagdasarova Y. et al. (43 authors, including Sharapov E.I.) First direct constraints on Fierz interference in free neutron beta-decay, Physical Review C 96, 042501(R) (2017).
222. Khuukhenkhuu G., Munkhsaikhan J., Odsuren M., Galsandamdin, Gledenov Yu.M., Sansarbayar E., Sedysheva M.V. " Alfa-cluster formation factor in (n,α) reaction cross sections". In: Proc. of the 24 International Seminar on Interaction of Neutron with Nuclei (ISINN-23), Dubna, 2017, E3-2017-8, pp. 166-174.
223. Mastromarco M., Barbagallo M., Vermeulen M.J.,et al., The 236U neutron capture cross-section measured at the n_TOF CERN facility, EPJ Web of Conferences 146, 11054
224. Mendoza E., Cano-Ott D., Altstad S. et al., Measurement of the 241Am neutron capture cross section at the n_TOF facility at CERN, EPJ Web of Conferences 146, 11022
225. Mingrone F., Altstadt S., Andrzejewski J.,et al., High precision measurement of the radiative capture cross section of 238U at the n_TOF CERN facility, EPJ Web of Conferences 146, 11028, Phys. Rev., C 95, 034604
226. Morris C.L., Adamek E.R., Broussard L.J. et al. (32 authors, including Sharapov E. I.), A new method for measuring the neutron life time using in situ neutron detector, Review of Scientific Instruments, v.88 (2017), 053508.
227. Fedorov N.A., Grozdanov D.N., Bystritskiy V.M., Kopach Yu.N., et al. "Measurements of the gamma-quanta angular distributions emitted from neutron inelastic scattering on 28Si", EPJ Web of Conferences (ожидается публикация)
228. Oprea C., A. Oprea, V. Macocian, S. Filip. Isomeric States Produced in Nuclear Reactions on Indium. Proceedings of XXIV International Seminar on Interaction of Neutrons with Nuclei (ISINN24) Dubna, Russia, May 24-27, 2016 Dubna: JINR, E3-2017-8, p. 437-443 (2017)
229. Pattie R. W. Jr., Callahan N. B., Cude-Woods C. et al. (38 authors, including Sharapov E.I.) Measurement of the neutron lifetime using an asymmetric magnetogravitational trap and in situ detection, ArXiv:1707-01817 [nucl-exp] (2017).
230. Sabaté-Gilarte M., Barbagallo M., Colonna N. et al., High-accuracy determination of the neutron flux in the new experimental area n_TOF-EAR2 at CERN, The European Physical Journal A 53 (10), 210
231. Sabaté-Gilarte M., Praena J., Porras I. et al., The 33S (n, α) 30Si cross section measurement at n_TOF-EAR2 (CERN): From 0.01 eV to the resonance region, EPJ Web of Conferences 146, 08004
232. Seestrom S.J., Adamek , Barlow D. et al. (34 authors, including E. I. Sharapov), Total Cross Sections for Ultracold Neutrons Scattering from Gases, Physical Review C 95, 015501 (2017).
233. Stamatopoulos A., Tsinganis A., Colonna N., et al., Measurement of the 240Pu (n, f) cross-section at the CERN n_TOF facility: First results from experimental area II (EAR-2), EPJ Web of Conferences 146, 04030
234. Tagliente G., Andrzejewski J., Heinitz S., et al., Recent results in nuclear astrophysics at the n_TOF facility at CERN, PoS, 161
235. Bystritsky V.M., Kopatch Yu.N., Skoy V.R., Ruskov I.N., et al., "Romashka" and "Romasha" gamma-ray spectrometers", Proceedings of the DAE Symp. on Nucl. Phys. 62 (2017) http://sympnp.org/proceedings/62/G9.pdf
236. Wang Zhimin, Bai Huaiyong, Zhang Luyu,Jiang Haoyu, Lu Yi Chen Jinxiang, Zhang Guohui, Gledenov Yu. M.,, Sedysheva M. V., Khuukhenkhuu G. "Cross section measurement for the 10B(n,t2α) three-body reactions at 4.0, 4.5 and 5.0 MeV. I. Prediction of the

PUBLICATIONS

experimental spectrum". Physical Review C96, 044620 (2017). (IF 3.82)

237. Wang Zhimin, Bai Huaiyong, Zhang Luyu,Jiang Haoyu, Lu Yi Chen Jinxiang, Zhang Guohui, Gledenov Yu. M.,, Sedysheva M. V., Khuukhenkhuu G. "Cross section measurement for the 10B(n,t2α) three-body reactions at 4.0, 4.5 and 5.0 MeV. II. Experimental setup and results". Physical Review C96, 044621 (2017). (IF 3.82)
238. Wright T., Guerrerro C., Billowes J., et al. (The n_TOF Collaboration), The 33S(n,α)30Si cross section measurement at n_TOF-EAR2 (CERN): From 0.01 eV to the resonance region, Phys. Rev. C 96, 064601
239. Kopatch Yu., Chietera A., Stuttgé L., et al., Angular Correlations in the Prompt Neutron Emission in Spontaneous Fission of 252Cf, EPJ Web of Conferences 146, 04017 (2017), https://www.epj-conferences.org/articles/epjconf/pdf/2017/15/epjconf-nd2016_04017.pdf
240. Zeinalov Sh.S., Sedyshev P.V., Shvetsov V.N., Sidorova O.V. Prompt fission neutron investigation in 235U(nth,f) reaction, EPJ Web of Conferences 146,04022 (2017), ND2016.
241. Грозданов Д. Н., Федоров Н. А., Быстрицкий В. М., et al., "Измерение угловых распределений гамма-квантов в реакциях неупругого рассеяния Нейтронов с энергией 14.1 МэВ на ядрах углерода и кислорода, Известия Российской академии наук. Серия Физическая (ожидается публикация).
242. Джилавян Л.З., Покотиловский Ю.Н., «Модельное описание фотоядерного 13C(γ,p)12B активационного детектирования углерода»,Письма в ЭЧАЯ, 14 (2017) 1-8. (L.Z. Dzhilavyan, Yu.N. Pokotilovski, "Model description of photonuclear 13C(γ,p)12B activation detection of carbon", PEPAN Lett. 14 (2017) 726-731).
243. Sadigov A, Suleymanov S, Ahmadov F, et al., A micropixel avalanche phototransistor for time of flight measurements, Nuclear Instruments and Methods in Physics Research Section A., volume 845, 2017, pp. 621-622
244. Ahmadov F, Ahmadov G, Guliyev E, Madatov R, et al., New gamma detector modules based on micropixel avalanche photodiode, Journal of Instrumentation, volume 12, 2017
245. Ahmadov F., Ahmadov G., Sadigov A.,Sadygov Z., Madatov R., Suleymanov S., Akberov R., Zerrouk F., New phoswich detector based on MAPD and LFS & p-terphenyl scintillator, Functional materials, Vol.24, No.3, 2017.
246. Ahmadov G.S., Ahmadov F.I., Kopatch Yu.N., Telezhnikov S.A., Nuriyev S.M., Sadigov A.Z., Sadygov Z.Y., Suleymanov S.S., Heydarov N., Valiyev R., Nazarov M., Akbarov R., Madatov R., Garibov A.A., A Position Sensitive Alpha Particle Detector Based on a LYSO Crystal and a Micro-Pixel Avalanche Photodiode, ISINN-24 proceedings, 2017
247. Tsulaia, I.M. Salamatin, K.M. Salamatin, D.B. Berikov, Yu.D. Mareev, A.P. Sirotin // Fundamental Interactions & Neutrons, Nuclear Structure, Ultracold Neutrons, Related Topics: Proceedings of the XXIV International Seminar on Interaction of Neutrons with Nuclei (Dubna, Russia, May 24–27, 2016). Dubna : JINR, 2017. – p.315-325.

Theoretical investigations

248. Игнатович В.К. «Респектабельные фундаментальные псевдонауки.» Теоретические и Практические Вопросы Современной Науки, ISSN:2411-1899, Изд:Евразийское Научное Объединение, 2017, №7(19), стр. 11-14.
249. Ignatovich V.K. "On respectable pseudoscience of "weak measurements" and others.» International science project №7, 35-45 (2017)
250. Игнатович В.К. «Интерференционный метод исследования свойств волнового пакета нейтрона», Эффективные исследования Современности, ISSN:2411-1899, Изд:Евразийское Научное Объединение, 2017, №10(2), стр. 1-10.
251. Игнатович В.К. «Сингулярные связанные состояния атома водорода» Теоретические и Практические Вопросы Современной Науки, ISSN:2411-1899,

Изд:Евразийское Научное Объединение, 2017, №11 (23).

252. Игнатович В.К. «Ложность ЭПР парадокса и всех последующих развитий его» Первый независимый научный вестник. № 22 (2017).

253. Ignatovich V. K. “There is no photon spin hall effect at an interface between two isotropic media.” East European Science Journal n. 23 (2017).

Applied research

254. Gorelova S.V., Frontasyeva M.V.. The use of higher plants in biomonitoring and environmental bioremediation. Chapter of the Book. Phytoremediation: Management of Environmental Contaminants, Volume 5 (Ansari A.A., Gill S.S., Gill R., Lanza G., and Newman L., eds.). P. 103-155. New York: Springer, 2017.

255. Бондаренко Г.Г., Волобуев И.В., Ерискин А.А., Кобзев А.П., Никулин В.Я., Перегудова Е.Н., Силин П.В., И.В. Боровицкая. Распределение дейтерия и водорода в Zr - и Ti – сборках фольг при воздействии импульсной дейтериевой высокотемпературной плазмы. Металлы. 2017, №5, с.64 – 69. IP 0.43

256. Spankova M., Strbik V., Chromik S., Zheng D.N., Li J., Machajdik D., Kobzev A.P., Plecenik T. and Sojkova M. Characterization of Epitaxial LSMO Films Grown on STO Substrates. Acta Physica Polonica A, 2017, Volume 131, Issue 4, pp. 848-850. IP 0.469.

257. Lazo P., Steinnes E.. Qarri F., et al., Origin and spatial distribution of metals in moss samples in Albania: A hotspot of heavy metal contamination in Europe. Chemosphere, 190, 2017, http://authors.elsevier.com/sd/article/S0045653 51731559X. IF: 4.208.

258. Nickel S., Schröder W., Schmalfuss R., et al. Modelling and mapping heavy metal and nitrogen concentrations in moss in 2010 throughout Europe by applying Random Forests models. Atmospheric Environment, Vol. 156, 2017, p. 146-159. https://doi.org/10.1016/j.atmosenv.2017.02.032 http://www.sciencedirect.com/science/article/pi i/S1352231017301127. IF: 3.629.

259. Stihi C., Popescu I.V., Frontasyeva M., et al.. Characterization of Heavy Metal Air Pollution in Romania Using Moss Biomonitoring, Neutron Activation Analysis, and Atomic Absorption Spectrometry. Analytical Letters, http://dx.doi.org/10.1080/00032719.2016.1 275661. IF: 1.150.

260. Ужинский А., Ососков Г., Фронтасьева М.. Управление данными мониторинга окружающей среды. Открытые системы. СУБД, Open System Publications (https://www.osp.ru/) № 4, 2017, с. 42-43, ISSN 1028-7493, https://www.osp.ru/os/2017/04/13053390/

261. Demcak S., Balintova M., Hurakova M., Frontasyeva M., Zinicovscaia I., Yushin N.. Utilization of poplar wood sawdust for heavy metals removal from model solutions. Nova Biotechnologica et Chimica, Vol. 16, No. 1, 2017, p. 26-31. DOI: 10.1515/nbec-2017-0004. IF: 1.129.

262. Milićević T., Aničić Urošević M., Vuković G., Škrivanjb S., Relić D., Frontasyeva M.V., Popović A.. Assessment of species-specific and temporal variations of major, trace and rare earth elements in vineyard ambient using moss bags. Ecotoxicology and Environmental Safety, Vol. 144, 2017, p. 208–215. IF: 3.130.

263. Vuković G., Aničić Urošević M., Škrivanj S., Vergel K., Tomašević M., Popović A.. The first survey of airborne trace elements at airport using moss bag technique. Environ Sci Pollut Res, No. 24, 2017, p. 15107-15115, DOI 10.1007/s11356-017-9140-0, IF: 2.828.

264. Badawy W.M., Ghanim E.H., Duliu O.G., Samman H.El, Frontasyeva M. V.. Major and trace element distribution in soil and sediments from the Egyptian Central Nile valley. Journal of African Earth Sciences. No. 131, 2017, p. 53-61. IF: 1.403.

265. Chmielowska-Bąk J., Arasimowicz-Jelonek M., Izbiańska K., Frontasyeva M., Zinicovscaia I., Guiance-Varela C., Deckert J.. NADPH oxidase is involved in regulation of gene expression and ROS overproduction in soybean (Glycine max) seedlings exposed to cadmium. Acta Societatis Botanicorum Poloniae. Vol. 86,

PUBLICATIONS

No. 2, pp. 17. DOI: 10.5586/asbp.355, 2017. IF: 1.213

266. Okasha A., Atta D., Badawy W.M., Frontasyeva M. V., Elhaes H. and Medhat Ibrahim. Modeling the coordination between Na, Mg, Ca, Fe, Ni, and Zn with organic acids. Journal of Computational and Theoretical Nanoscience, Vol. 14, 2017, p. 1357–1361, IF 1.343.
267. Nassar N., Kravtsova A., Frontasyeva M., Sherif M.. Neutron activation analyses used to study elemental accumulation in some marine macrophytes (Mediterranean Sea coast of Egypt). American Journal of Analytical Chemistry, Vol. 8, No. 6, 2017, p. 395-405.
268. Nekhoroshkov P., Kravtsova A., Kamnev A., Bun'kova O., Duliu O., Frontasyeva M. & Yermakov I.. Assessment of Minor and Trace Elements in Aquatic Macrophytes, Soils and Bottom Sediments Collected along Different Water Objects in the Black Sea Coastal Zone by Using Neutron Activation Analysis. American Journal of Analytical Chemistry, Vol. 8 No 4, p. 225.
269. Zinicovscaia I., Safonov A., Tregubova V., Ilin V., Frontasyeva M.V., Demina I.. Competitive bioaccumulation and biosorption of metals by bacteria Pseudomonas putida. Desalination and Water Treatment, Vol. 74, 2017, p. 149-154. doi: 10.5004/dwt.2017.20732. IF: 1.631
270. Mróz T., Szufa K., Frontasyeva M.V., Tselmovich V.A., Ostrovnaya T.M., Kornaś A., Olech M., Mietelski J.W., Brudecki K.. Determination of atmospheric deposition of trace elements across King George Island (Antarctica) using reactor neutron activation analysis and scanning electron microscopy. Environmental Science and Pollution Research. https://link.springer.com/article/10.1007%2Fs11356-017-0431-2. IF: 2.76.
271. Yusuf Abdo S., Zinicovscaia I., Duliu O.G., Frontasyeva M.V., Sherif M.M., Epithermal neutron activation analysis of major and trace elements in Red Sea scleractinian corals. Journal Radioanalytical and Nuclear Chemistry, DOI 10.1007/s10967-017-5511-8, 2017 IF: 1.282.
272. Zinicovscaia I., Duliu O.G., Culicov O., Sturza R., Bilici C., Gundorina S.. Geographical origin identification of Moldavian wines by neutron activation analysis. Food Analytical Methods, 2017, 10:3523–3530, DOI: 10.1007/s12161-017-0913-3; IF:2.092
273. Zinicovscaia I., Cepoi L., Chiriac T., Mitina T., Grozdov D., Yushin N., Culicov O.. Application of Arthrospira (spirulina) platensis biomass for silver removal from aqueous solutions. International Journal of Phytoremediation, 2017, 19(11):1053-1058, DOI: 10.1080/15226514.2017.1319332. IF: 1.77

AYSS AND FLNP FELLOWSHIPS

In 2017, within the framework of the competition of the Association of Young Scientists and Specialists of JINR, the scholarships were awarded to:

1. grant for young PhD researchers
   - **A.I. Ivankov**
   - **A.V. Nagornyi**
   - **T.V. Tropin**

2. grant for young specialists
   - **I.A. Markovnikov**
   - **K. Nazarov**
   - **N.A. Kovalenko**
   - **V.V. Shvetsov**
   - **K.I.Mikhailov**

3. grant for young researchers
   - **C. Colmon**
   - **N.M. Belozerova**
   - **K.N. Vergel**
   - **D.N. Grozdanov**
   - **I.V. Gapon**
   - **C. Hramco**

4. grant for young workers
   - **D.A. Motchev**

Since 2002, in FLNP a scholarship named after Academician of the USSR Academy of Sciences and first Director of the Laboratory of Neutron Physics **I.M. Frank** has been established in order to stimulate scientific and methodical research of young scientists.

In 2017 **I.M. Frank scholarships** were awarded to:

- In Neutron Nuclear Physics: **I. Zinicovscaia**
- In Condensed Matter Physics: **E. A.Kizima, A.V. Tomchuk, A.V. Rutkauskas**
- In Development of basic facilities: **K.A. Mukhin**

Since 2006, a scholarship has been founded to immortalize the memory of outstanding scientist, Corresponding Member of the USSR Academy of Sciences **F.L. Shapiro**. The scholarship is awarded annually to young FLNP employees in the following research directions: UCN physics; polarized neutrons; neutron spectroscopy.

In 2017 **F.L. Shapiro scholarships** were awarded to:

- In “Neutron Spectroscopy and Condensed Matter Research” **S.V. Sumnikov**
- In "Polarized Neutrons": **V.D. Zhaketov**
- "UCN Physics": **S.V. Goryunov**

FLNP SEMINARS

- Katsufumi Tomobe and Kenji Yasuoka (Keio University, Japan) *«Water behavior around biological materials: rhodopsin and monosaccharide» (09.01.2017)*
-

CONFERENCES AND MEETINGS

1. The **24th International Seminar on Interaction of Neutrons with Nuclei: Fundamental Interactions & Neutrons, Nuclear Structure, Ultracold Neutrons, Related Topics** (ISINN-25); 23 – 26.05.2017, Dubna. (hppt:\\isinn.jinr.ru).

2. The "**4rd International Conference of the Serbian Society for Ceramic Materials**"; 14-16.06.2017, Belgrade, Serbia. With the financial support of the FLNP JINR (http://ceramic-society.rs/)

3. The **International Conference on Neutron Scattering 2017** (ICNS2017), 9-13.07.2017 Daejeon, Republic of Korea. With the financial support of the FLNP JINR (http://www.icns2017.org/).

On the International Conference on Neutron Scattering 2017 (ICNS2017) held in Daejeon, Republic of Korea from 9 to 13 July 2017 a general overview of FLNP facilities as well as the results achieved in hard and soft condensed matter research utilizing various elastic and inelastic neutron scattering techniques were presented. The outreach in public relations was enforced through the gold sponsorship of JINR.

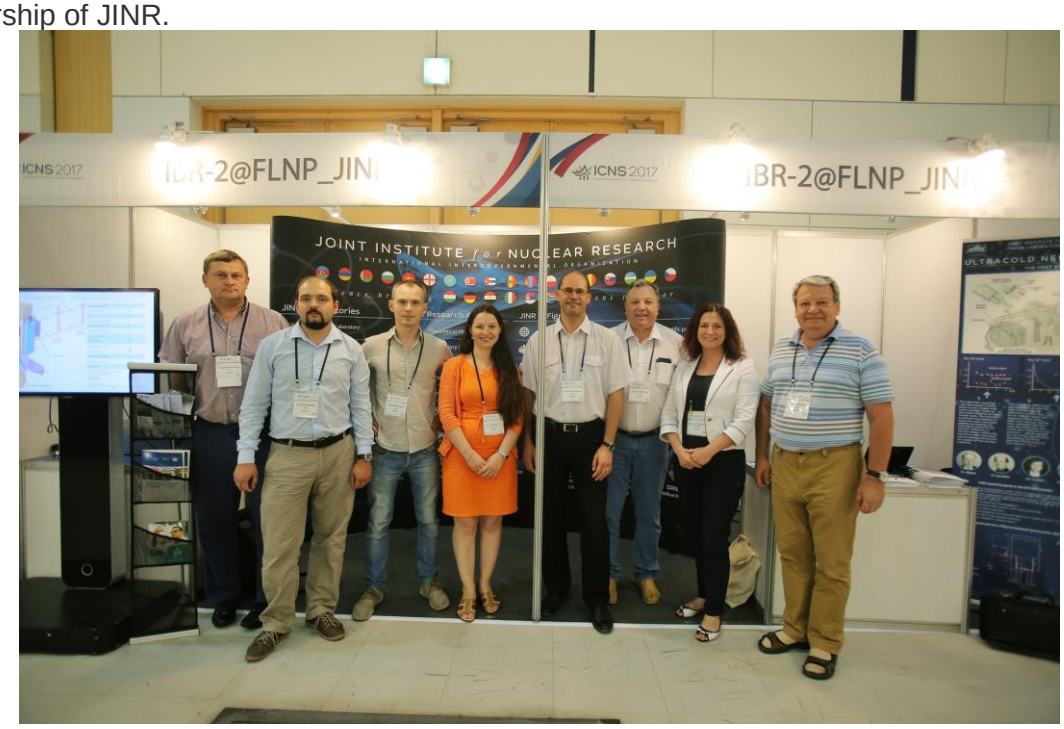

4. **International Seminar "Development of Neutron Nuclear Methods"** dedicated to the 80th Anniversary of Alexandr Strelkov, 22.09.2017, Dubna.

5. **International Conference "Condenced Matter Research at the IBR-2"**; 9-12.10.2017, Dubna(http://indico.jinr.ru/conferenceDisplay.py?confId=192).

EDUCATIONAL PROGRAM

- The FLNP successfully collaborates with the JINR University Centre in the organization of **summer practical work for students** from JINR Member States (Belarus, Czech Republic, Poland, Romania, Slovakia,) and Associated Members (Egypt, South Africa).

Lectures and excursions to the FLNP facilities were organized for **teachers of physics** from Russia and JINR Member States.

- **The VIII International School for Young Scientists and Students "Instruments and Methods of Experimental Nuclear Physics. Electronics and Automatics of Experimental Facilities"** was held on November 7-11, 2017 in Dubna. The School was organized by the Frank Laboratory of Neutron Physics with the support of the JINR Directorate. The school is aimed at young researchers, postgraduates and senior students of scientific centres and institutes of Russia and the CIS countries.

The School covers the following topics: neutron sources, neutron detectors, spectrometers, sample environment systems, electronics of detectors and data acquisition electronics, automation of experiments at spectrometers, software of spectrometers. The scientific programme of the School includes lectures on the current state of electronics and software of neutron spectrometers, instruments and methods of neutron physics experiments and practical trainings. Excursion to the main laboratory facilities will be held in the frames of the School.

VISITS AT OUR FACILITIES

- Dmitry Tayursky Vice-Rector of Kazan Federal University, Sergey Nikitin Director of the Institute of Physics (11.01.2017)
- Delegations of Bolivia composed of Vice-Minister for energy and alternative sources of energy Joaquín Rodríguez and officials of the Ministry (29.01.2017)
- Representatives of the JSC "Rosatom Overseas Ink" with Evgeny Pakermanov (20.01.2017)
- Delegation of the Republic of Paraguay headed by the Executive Secretary of the National Radiological and Nuclear Regulatory Authority Mr. Cesar Jose CARDOZO ROMAN (27.04.2017)
- Delegation of Bolivia headed by Minister of Energy Mr. Rafael ALARCON ORIHUELA (27.04.2017)

EVENTS

STRUCTURE OF LABORATORY AND SCIENTIFIC DEPARTMENTS

Directorate:	
Director	*V.N. Shvetsov*
Deputy Director	*O.A. Culicov*
Deputy Director	*E.V. Lychagin*
Deputy Director	*N. Kucerka*
Deputy Director	*S.V. Kozenkov*
Chief engineer:	*A.V. Vinogradov*
Scientific Secretary	*D.M.Chudoba*
Laboratory Scientific Leader	*V.L. Aksenov*
Advisor to Directorate	*V.D. Ananiev*
Advisor to Directorate	*L.B. Pikelner*

Reactor and Technical Departments	Head

IBR-2 reactor	Chief engineer: *A.V. Dolgikh*
Mechanical maintenance division	*A.A. Belyakov*
Electrical engineering department	*V.A. Trepalin*
Design bureau	*A.A. Kustov*
Experimental workshops	*A.N. Kuznetsov*

Scientific Departments	Head
The Division of Condensed Matter Research and Developments	*A.V. Belushkin*
Nuclear physics department	*V.N. Shvetsov*
Sector of Raman Spectroscopy	*G.M. Arzumanyan*

Administrative Services
Secretariat
Finances
Personnel

Scientific Secretary Group
Secretariat
Translation
Graphics

6.ORGANIZATION

DIVISION OF CONDENSED MATTER RESEARCH AND DEVELOPMENTS

DEPARTMENT OF NEUTRON INVESTIGATION OF CONDENSED MATTER

Sub-Division	Title	Head
Head of the Department		*D.P. Kozlenko*
Sector 1: Neutron Diffraction. Head: *G D. Bokuchava*		
Group No.1	HRFD	*A.M. Balagurov*
Group No.2	DN-2	*A.I. Beskrovnyi*
Group No.3	DN-12	*B.N. Savenko*
Group No.4	SKAT /Epsilon	*Ch. Scheffzük*
Sector 2: Neutron Optics. Head: *M.V. Avdeev*		
Group No.1	REMUR	*Yu.V. Nikitenko*
Group No.2	REFLEX	*V.I. Bodnarchuk*
Group No.3	GRAINS	*V.I. Petrenko*
Small angle scattering group		*A.I. Kuklin*
Inelastic neutron scattering group		*D. Chudoba*

DEPARTMENT OF IBR-2 SPECTROMETERS COMPLEX

Sub-Division	Title	Head
Head of the Department		*S.A. Kulikov*
Group No.1	Detectors	*A.V. Churakov*
Group No.2	Electronics	*A.A. Bogdzel*
Group No.3	Information technologies	*A.S. Kirilov*
Group No.4	Sample environment and choppers	*A.P. Sirotin*
Group No.5	Cryogenic investigations	*A.N. Chernikov*
Group No.6	Cold moderators	*M.V. Bulavin*

SECTOR OF RAMAN SPECTROSCOPY

Sub-Division	Title	Head
Head of the Sector		*G.M. Arzumanyan*
Group of biomolecular spectroscopy		
Group of luminescence and structural analysis		

NUCLEAR PHYSICS DIVISION

Sub-Division	Title	Head
Sector 1.	Investigations of neutron-nuclear interactions	*Y.N. Kopatch*
Sector 2.	Investigation of neutron fundamental properties.	*E.V. Lychagin*
Sector 3.	Neutron Activation Analysis and Applied Research:	*M.V. Frontasyeva*
IREN facility		*V.G. Pytaev*

PERSONNEL

Theme	Departments	People
-1104-	Nuclear Physics Division	122
	The Division of Condensed Matter Research and Developments	
-1121-	Department of neutron investigation of condensed matter	95
-1122-	Department of IBR-2 spectrometers complex	48
-1111-	Sector of Raman Spectroscopy	8
-1105-	IBR-2 reactor	46
	Mechanical and Technical Department	47
	Electric and Technical Department	30
	Central Experimental Workshops	36
	Nuclear Safety Group	6
	Design Bureau	5
	FLNP infrastructure:	
	Directorate	10
	Services and Management Department	24
	Scientific Secretary Group	5
	Supplies Group	4
Total		**486**

PERSONNEL FROM THE JINR MEMBER STATES (BESIDES THE RF) at December 31, 2016 (work stages longer than 4 months)

Country	People	of which young specialists (≤35 years)
Azerbaijan	9	8
Armenia	1	1
Belarus	1	1
Bulgaria	8	4
Czech Republic	2	2

6.ORGANIZATION

Georgia	2	1
Germany	1	
Kazakhstan	19	19
Moldova	1	1
Mongolia	9	9
Poland	9	2
Romania	9	3
Slovakia	2	1
Ukraine	14	11
Uzbekistan	1	1
Vietnam	4	4
TOTAL	**92**	**70**

Other 8 employes from Mongolia, Slovakia Poland and Czech Republic performed work stages of three months in FLNP.

OUR PhD STUDENTS

In 2016 28 PhD students from 10 countries conducted their experimental research at the FLNP facilities.

Name	Country	PhD student of
Alekseenok Yu.V.	Belarus	International Sakharov Environmental University
Hristozova G.	Bulgaria	Paisii Hilendarski University
Vasiliev A.	Bulgaria	Sofia University
Sanizlo A.	Hungary	Obuda University
Bagdaulet M.	Kazakhstan	Al-Farabi Kazakh National University
Muhametuli B.	Kazakhstan	Al-Farabi Kazakh National University
Hramco C.	Moldova	University of the Academy of Science of Moldova
Nyamsuren B.	Mongolia	National University of Mongolia
Luczynska K.	Poland	Institute of Nuclear Chemistry and Technology
Belozerova N.M.	Russia	JINR University centre
Zhaketov V.D.	Russia	JINR University centre
Rumyantsev I.	Russia	Ivanov State University
Rutkauskas A.V.	Russia	JINR University centre
Rizhikov Yu.L.	Russia	Moscow Institute of Physics and Technology
Vlasov A.B.	Russia	Moscow Institute of Physics and Technology

Zinovev E.V.	Russia	Moscow Institute of Physics and Technology
Husenov M.A.	Russia	Moscow State University of Technology „STANKIN“
Suminkov S.V.	Russia	Moscow State University
Khalansky D.A.	Russia	Dubna International University for nature, Society and Man
Zelenyak T.Y.	Russia	Dubna International University for nature, Society and Man
Vergel K. N.	Russia	Dubna International University for nature, Society and Man / FLNP JINR
Kravtsova A.V.	Russia	A.O. Kovalevsky Institute of biology of the Southern Seas
Nekhoroshkov P.S.	Russia	A.O. Kovalevsky Institute of biology of the Southern Seas
Gapon I.V.	Ukraine	National University of Kyiv
Nagornaya T.V.	Ukraine	National University of Kyiv
Samoylenko S.A.	Ukraine	National University of Kyiv
Husenov M.A.	Republic of Tajikistan/Russia	S.U. Umarov Physical-Technical Institute of Academy of Sciences of the Republic of Tajikistan/ Moscow State University of Technology „STANKIN“
Rakhmonov H.R	Republic of Tajikistan/Russia	S.U. Umarov Physical-Technical Institute of Academy of Sciences of the Republic of Tajikistan/ National Research Nuclear University MEPhI

In 2016, 3 PhD theses were defended using the experimental material obtained in FLNP.

7. INTERNATIONAL COOPERATION AND USER INTERACTION

INTERNATIONAL COOPERATION

In 2016 the Frank Laboratory of Neutron Physics collaborated with 270 institutions from 45 countries.

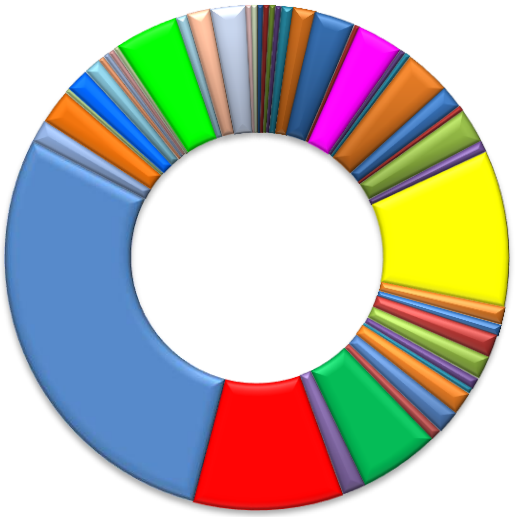

Albania, Armenia, Argentina, Australia, Austria, Azerbaijan, Belarus, Belgium, Bulgaria, China, Croatia, Czech Republic, Egypt, Finland, France, Georgia, Germany, Hungary, Italy, Japan, Kazakhstan, Latvia, Macedonia, Moldova, Mongolia, Norway, Poland, Republic of Korea, Romania, Russia, Serbia, Slovakia, Slovenia, South Africa, Switzerland, Tajikistan, Thailand, Taiwan, Turkey, Ukraine, Uzbekistan, Vietnam, USA, United Kingdom, Spain

USER INTERACTION

In 2016 were two calls for proposals for experiments at the IBR-2 reactor (01 September – 15 October 2013; Call-II: 01 March – 15 April 2014). A total of 238 proposals for conducting experiments were received from 19 different countries. The received proposals covered the broad spectrum of neutron research in physics, materials science, chemistry, geosciences, biology and applied sciences. 208 received proposals were admitted for realization.

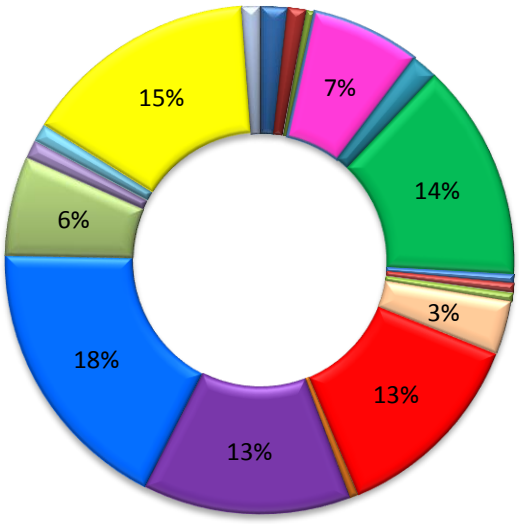

Azerbaijan, Belarus, Bulgaria, China, Czech Republic, Germany, India, Latvia, Moldova, Mongolia, Poland, Republic of Korea, Romania, Russia, Slovakia, Sweden, Taiwan, Ukraine, Vietnam

7. INTERNATIONAL COOPERATION AND USER INTERACTION

Proposal distribution by science (left) and by facilities (right).

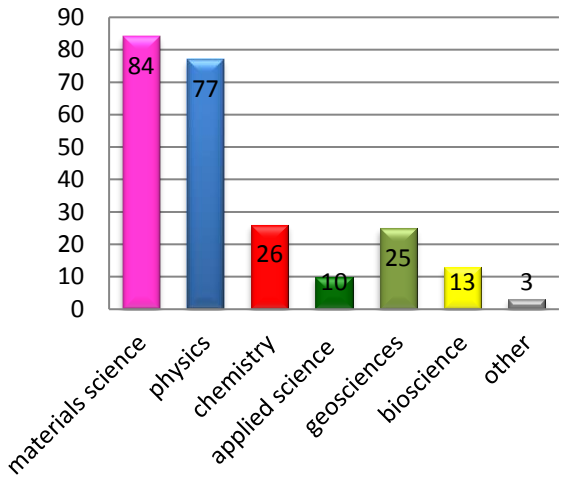

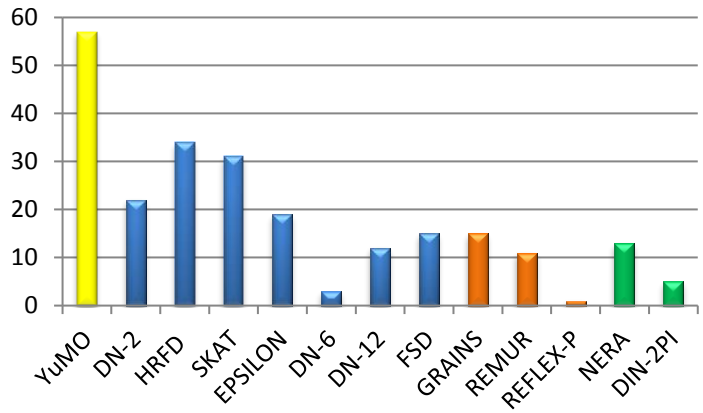

List of Visitors from the Member States or Associated Members of JINR in 2016

Country	Nr of visitors
Azerbajan	3
Armenia	2
Belarus	7
Bulgaria	7
Czech Republic	2
Egypt	6
Germany	22
Kazakhstan	2
Moldova	2
Mongolia	7
Poland	26
Romania	10
Serbia	5
Slovakia	8
Ukraine	14
RSA	2
Vietnam	2

List of Visitors from the not Member States or Associated Members of JINR in 2016

Country	Nr of visitors
Argentina	1
China	7
Croatia	2
Republic of Corea	7
Sweden	6
Taiwan	1
Tajikistan	1
USA	5

8. FLNP AND MASS-MEDIA

In the year 2016 Frank Laboratory of Neutron Physics was at center of interest of mass media in Russia and abroad

Dubna Channel
January 2016

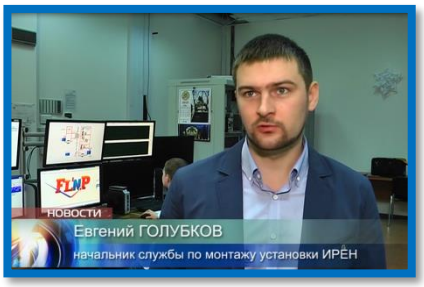


PTJ 29

LABORATORIUM FIZYKI NEUTRONOWEJ I.M. FRANKA ZIBJ W DUBNEJ I „POLSKA GRUPA NEUTRONOWA"

Frank Laboratory of Neutron Physics of JINR in Dubna and "Polish Neutron Group"

Dorota Chudoba

PTJ VOL. 59 Z. 2 2016

Postępy Fizyki Jądrowej

59 Z.2 2016

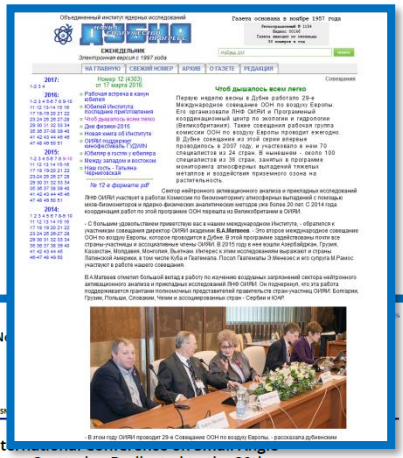
Чтоб дышалось всем легко

Dubna
March 2016

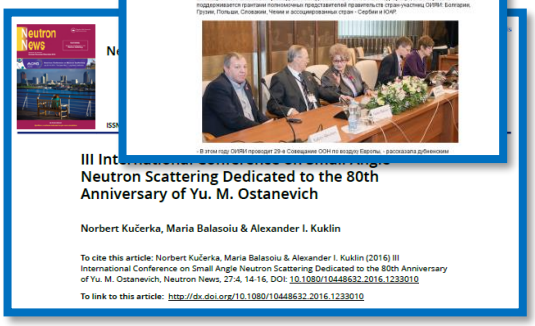

Neutron News
27 No 4 2016

III Int… Neutron Scattering Dedicated to the 80th Anniversary of Yu. M. Ostanevich

Norbert Kučerka, Maria Balasoiu & Alexander I. Kuklin

To cite this article: Norbert Kučerka, Maria Balasoiu & Alexander I. Kuklin (2016) III International Conference on Small Angle Neutron Scattering Dedicated to the 80th Anniversary of Yu. M. Ostanevich, Neutron News, 27:4, 14-16, DOI: 10.1080/10448632.2016.1233010

To link to this article: http://dx.doi.org/10.1080/10448632.2016.1233010

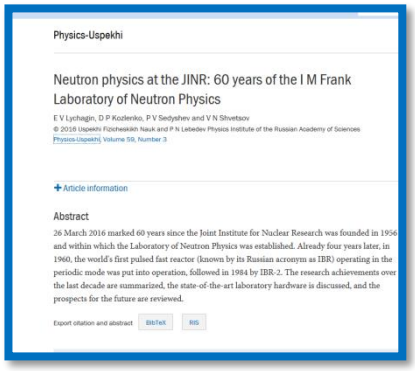
Physics-Uspekhi

Neutron physics at the JINR: 60 years of the I M Frank Laboratory of Neutron Physics

E V Lychagin, D P Kozlenko, P V Sedyshev and V N Shvetsov

© 2016 Uspekhi Fizicheskikh Nauk and P N Lebedev Physics Institute of the Russian Academy of Sciences

Physics-Uspekhi, Volume 59, Number 3

+ Article information

Abstract

26 March 2016 marked 60 years since the Joint Institute for Nuclear Research was founded in 1956 and within which the Laboratory of Neutron Physics was established. Already four years later, in 1960, the world's first pulsed fast reactor (known by its Russian acronym as IBR) operating in the periodic mode was put into operation, followed in 1984 by IBR-2. The research achievements over the last decade are summarized, the state-of-the-art laboratory hardware is discussed, and the prospects for the future are reviewed.

Export citation and abstract BibTeX RIS

Physics-Uspekhi
59 (3) 2016

PhysicsWorld
29 No5 2016

360° TV
December 2016

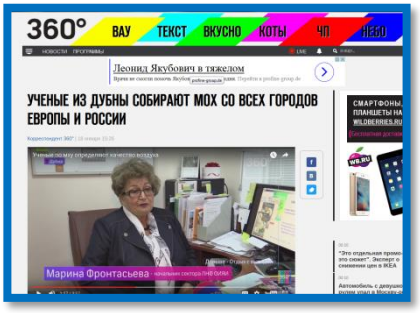

10. CONTENT